NUMERICAL PREDICTION OF FLOW CHARACTERISTICS AROUND SQUARE CYLINDERS IN TANDEM

By

Mrinal Chandra Saha

A thesis submitted to the Department of Mechanical Engineering in partial

fulfilment of the requirements for the degree of

Master of Science

in

Mechanical Engineering

March, 1992

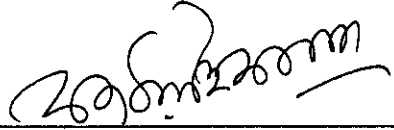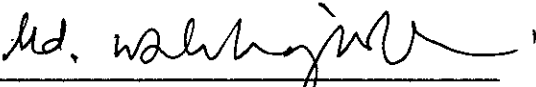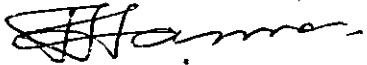BANGLADESH UNIVERSITY OF ENGINEERING AND TECHNOLOGY, DHAKA-1000
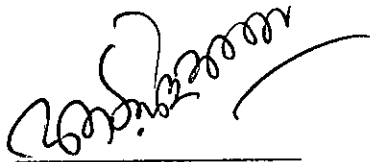
BANGLADESH

The thesis titled "NUMERICAL PREDICTION OF FLOW CHARACTERISTICS AROUND SQUARE CYLINDERS IN TANDEM", submitted by **Mrinal Chandra Saha, Roll No. 881427P, Registration No. 82352** of M.Sc. Engineering (Mechanical) has been accepted as satisfactory in partial fulfillment of the Master of Science in Engineering (Mechanical) on 25th March, 1992.

BOARD OF EXAMINERS:

1.

   Dr. A.K.M. Sadrul Islam   Chairman
   Associate Professor   (Supervisor)
   Dept. of Mechanical Engineering
   BUET, Dhaka.

2.

   Dr. Md. Wahhaj Uddin   Member
   Professor & Head   (Ex-Officio)
   Dept. of Mechanical Engineering
   BUET, Dhaka.

3.

   Dr. A.C. Mandal   Member
   Professor
   Dept. of Mechanical Engineering
   BUET, Dhaka.

4.

   Dr. J. A. Naser   Member
   Assistant Professor
   Dept. of Chemical Engineering
   BUET, Dhaka.

5.

   Dr. Abdul Hannan   Member
   Professor   (External)
   Dept. of Water Resources Engg.
   BUET, Dhaka.

CERTIFICATE OF RESEARCH

This is to certify that the work presented in this thesis is the outcome of the investigations carried out by the canditate under the supervision of Dr. A. K. M. Sadrul Islam in the Department of Mechanical Engineering of Bangladesh University of Engineering and Technology, Dhaka, Bangladesh.

Superviser

Candidate

ABSTRACT

This investigation deals with the numerical prediction of the distribution of mean pressure and wake-velocity around two square cylinders in tandem in a fluid field of Reynolds number 2.87×10^4. The prediction is based on the Navier-Strokes equations and the standard k-ϵ model of turbulence. The numerical solutions of the governing partial differential equations are obtained using TEACH-T computer code. The computer code is based on standard finite volume technique and an algorithm known as SIMPLE (Semi Implicit Method for Pressure-Linked Equations).

The tandem arrangements of the two square cylinders are studied in terms of two parameters-the spacing ratio and the size-ratio, defined respectively as L/D and d/D, in terms of notations of figure 4.1.

The predictions of the drag-coefficient as well as the distribution of the mean pressure and the velocity in a two dimensional wake are presented at various spacing-ratio of the cylinders with three different size-ratio of the rear cylinder.

A detail investigation is performed at the critical spacing, which is four times the side of the square for equal sized cylinders. Similar analysis is also performed for the tandem arrangements with two other sets of size-ratio (e.g. for d/D=0.7, 0.5) within the range of interspacing $2.0 \leq L/D \leq 5.0$. Velocity field and stream function contour are also presented here for the clear understanding of the wake and vortex shedding phenomenon.

ACKNOWLEDGEMENTS

TABLE OF CONTENTS

Page No.

LIST OF FIGURES

LIST OF SYMBOLS

Γ circulation, molecular or turbulent diffusivity of scalar

ρ density of air

C_D drag co-efficient

C_μ eddy viscosity factor

ν_t eddy (turbulent) kinematic viscosity ; $\mu_t = \nu/\rho$

μ_{eff} effective viscosity

ν free stream kinematic viscosity of air

p fluctuating component of pressure

P_o free-stream static pressure

U_o free-stream velocity

x,y cartesian co-ordinate directions

u fluctuating component of velocity in x-direction

v fluctuating component of velocity in y-direction

b half width of the wake

E integration constant

ν kinematic viscosity

P local static pressure

τ_w local wall shear stress

l length scale represents the size of the turbulent eddies

λ length scale factor (=0.005)

C_p mean pressure coefficient

U mean stream velocity

V mean normal velocity

μ molecular viscosity of air

y^+ non-dimensional distance from wall

u^+ non-dimensional axial velocity U/U_τ

σ Prandtl/Schmidt number (μ/Γ)

R_e Reynold number (U_o $\rho D/\mu$)

U_τ shear velocity

ψ stream function

τ shear stress

D size of the upstream square cylinder

d size of the downstream square cylinder

L spacing of the cylinders

S source term in conservation equation

τ_I shear stress in inertial sublayer

μt turbulent viscosity

G turbulent energy production rate

ϵ turbulent kinetic-energy dissipation rate

k turbulent kinetic-energy

I turbulent intensity

D/Dt total derivative

H total height of the computational domain

κ vonkarman constant (=0.4187)

$c_{\epsilon 1}, c_{\epsilon 2}, \sigma_\kappa, \sigma_\epsilon$ are dimensionless constants

SUBSCRIPT

i,j Tensor subscript: terms in which a subscript appears twice are summed over all value (1,2,3) of that subscript.

SUPERSCRIPT

$\bar{}$ Instantaneous value

LIST OF THE TABLE

CHAPTER-I

INTRODUCTION

1.1 General

The subject of bluff body flow is receiving a great deal of attention [8,9,17,40,44,50,52,53,59,68,77,89] * recently. This is mainly because of its importance in energy saving, for example, road vehicles must now meet stringent requirements of fuel-consumption which translates into achieving reduced aerodynamic drag. Flow past a bluff body is always associated with the separation of flow behind the body incurring large energy losses. Specially, in case of flow past rectangular and square bodies, the separation occurs at the corners of the front face leading to complex wake formation behind it.

Recent engineering problems involving wind loads on large structures like a group of skyscrapers, chimney, towers, bridges, oil rigs or marine structures requiring investigation of flow patterns and aerodynamic characteristics. Large structures must also be designed so as to avoid potentially disastrous wind-induced large-amplitude oscillations. The occurrences of certain disastrous collapse of suspension bridges and damage of buildings due to wind effects at different places also prove that wind loading on buildings and structures should not be treated as minor criteria for design purposes. Inspite of the importance of bluff-body flows, relatively little is known about them.

---

* numbers in parenthesis refer to serial number of references on page 120

A number of numerical and experimental studies of flow around circular cylinder [1,9,52,78,82,88], some experimental studies of flow around square and rectangular cylinders at high Reynolds number [28,35,45,54,56,57,61,65,67,69,76,83,86], and computer simulation of flow at low Reynolds number around square or rectangular cylinders [12,14,66] are reported in the literature. Recently some works have been conducted for multiple obstacles of various arrangements [4,6,26,29,32,33,34,35,37,49,64,80,81,90,91] of which a little number of experimental studies of flow around tandem arrangements of square cylinders are reported [29,49,80,81]. To the authors knowledge, no numerical prediction is yet reported in the literature on the study of flow characteristics around square cylinders in tandem.

1.2   Nature of Wind Loading

The effect of wind on buildings and other structures may be treated as static or dynamic loading. Other effects of winds like noise, fire hazard, predestrains´ discomfort, etc. are not usually considered in the structural design.

The static effects refer to the steady (time-average) forces and pressures tending to give the structure a steady displacement. On the other hand, dynamic effect has the tendency to set the structures oscillating. A steady wind load on buildings and structures is very difficult to achieve because wind loads are always associated with varying speeds and direction of winds.

When a building is very stiff the dynamic response of the structure may be neglected and only the static loads may be considered. This is because the natural frequency of an extremely stiff building is too high to be excited by wind.

1.3   Relevance of this study in Bangladesh

Bangladesh is a land-hungry country. The urban population of this country is increasing at a very fast rate, making the housing problem worse everyday. One possible solution of this housing problem is to construct multistoried buildings. The need to build in highly windy sites or the need to locate a number of tall buildings close together will undoubtedly pose problems not yet encountered by the architects and town-planners. Hence the knowledge of wind loading on a single or a group of buildings is essential for economic design. Apart from wind loading, concentration of high rise buildings in a locality may lead to environmental problems like unpleasant feeling of on people at ground level and stagnant-air, damage to doors and windows in and near passages. Hence now-a-days both wind loading and environmental problem are considered as important design criteria.

Investigations of real flow around buildings is an impossible task. But the two-dimensional flow around a square cylinder can be taken to approximate the flow around a square-shaped building. So, in designing a building, knowledge of the effect of wind loading on a single building is sufficient. But for a group of buildings, knowledge of single building is not sufficient. Because, the

interference of the neighboring buildings in a group makes the nature of wind loadings different from that on an isolated building.

The problems of predicting the flow patterns around scattered bluff bodies can be coped with by understanding the nature of flow on multiple bluff bodies in close proximity in wind tunnel.

While numerous investigations are made on the flow past single obstacle of various shapes, only a few studies are reported on the flow around complex configuration of multiple obstacles. For understanding wind load pattern on an obstacle in a group of nearby obstacles, the present investigation of pressure distributions around square cylinders in tandem arrangements with various spacing-ratios as well as size-ratios is undertaken.

1.4 Importance of Numerical Investigation

Due to development of high speed personal computer with large memory, recently Engineers and Town Planners have started emphasizing numerical simulation over experimental investigation. Experiments with either model or prototype are both costly and time consuming. For the present study of square cylinders in tandem, full-scale experiments will not only be complex and costly but would be extremely difficult as it would require monitoring pressure distributions on the group of building, simultaneously and instantaneously, because of variation of speed and direction of wind with time. The real flow around buildings is very complex and the formulation of

mathematical model to predict the flow is almost impossible. Thus, model study is a must. Since experimental model study is costly, the present investigation emphasize on numerical model study.

1.5   Aim of the Study

The main aim of the study is to observe the surrounding flow in case of more than one bluff body placed in a uniform flow. It is obvious that the surrounding flow would be different from the case of single body, because there would be interference in the flow by one body on the other depending on the spacings of the bodies.

The present study takes into account the fundamental nature continued to the investigation of aerodynamic forces and pressure distribution on the body. The present study is an attempt to give an understanding about the variation of wind load pattern imposed on a cylinder due to the change in side dimension of the downstream cylinder with varying the spacings between the cylinders. The study is performed with a view to meet the above mentioned requirements. The prime objectives of the study are:

1.   To predict the pressure distribution around single square cylinder and compare with the experimental results.

2.   To predict the pressure distribution around tandem square cylinders and observe the effects of transverse spacing of the cylinders and as well as sizes of the rear cylinder.

3. To compare the difference in wind effects for various spacing-ratio and size-ratio of the square cylinders.

4. To predict the drag coefficient.

5. To study the mean velocity distribution in the wake behind the square cylinders arranged in tandem.

1.6 Scope of Study

The present study covers the numerical investigations of the distributions of mean pressure around square cylinders, isolated and in tandem with varying spacings. It also includes the mean velocity profiles in the wake of these cylinders in isolation and in tandem.

1.6.1 Order of presentation

The contents of this presentation are divided into several chapters. Chapter-II containing a brief description of the findings of several researchers in the field of flow around single and multiple bodies. Notable contributions are those of Bearman [8], Bearman et al [4,6], Lee [45], Nakamura et al [60,61,62], Vickery [83], Parkinson et al [68], Barriga et al [7], Igarashi [32,34], Igarashi et al [33] and Zdravkovich [90,91]. Findings of several other researchers are also included in this chapter. In chapter-III, mainly an account of the mathematical model is presented. It further includes the partial differential equations ensuing conservation of mass, momentum, turbulence model and boundary conditions. A complete outline of FDM (Finite Difference Method) is

also presented here. Chapter-IV contents the numerical solution-method of the present study, including the discretisation procedure, method of calculation and computational details. In chapter-V, the analysis of the present prediction and the available experimental results are presented. The results are presented in graphical form. In few cases the existing experimental and numerical results of different researchers are compared with those of the present study.

Finally, the conclusions drawn from the present investigation are given in chapter-VI. This chapter also includes suggestions for further research in this field.

CHAPTER-II

REVIEW OF LITERATURES

2.1 General

With the increasing importance of bluff body aerodynamics, over the past few decades, an enormous increase in research works concerning laboratory simulations, full-scale measurements and more recently, numerical calculations and theoretical prediction for flow over a wide variety of bluff bodies is observed. It is true that researchers from all over the world have contributed greatly to the knowledge of flow over bluff bodies but the major part of the reported works are of the fundamental nature involving the flow over a single body and little about multiple bodies. A number of experiments and numerical simulations were carried out by several researchers and the effects of flow chacteristics around square, rectangular and circular cylinders in tandem were investigated. A brief description of some of the research works related to the present study is given below.

2.2   Literature concerning single obstacle

BEARMAN AND TRUEMAN [4] investigated the base surface pressure coefficient and drag coefficient of rectangular cylinder with one face normal to the flow. It was found that the drag co-efficient was maximum (about 2.94) when d/h = 0.62, where d is the section depth and h is section width normal to the wind direction. By introducing a splitter plate into the wake it was observed that the increased drag effect was completely eliminated. This finding

demonstrated that the high drag is associated with the regular shedding of vortices. It was also observed that the further the vortices away from the body, the higher the base pressure. It was suggested that for higher values of d/h (>0.6) the vortices were forced to form further downstream because of the influence of the trailing edge corners.

BOSTOCK AND MAIR [5] studied the pressure distributions and forces on rectangular and D-shaped cylinders placed in two dimensional flow at Reynolds number 1.9×10^5. It was found that for rectangular cylinders a maximum drag co-efficient is obtained for d/h=0.67. Reattachments of the boundary layers on the sides of the cylinders occurred only for d/h<0.35.

BARRIGA, CROWE AND ROBERSON [7] studied the effects of angle of attack, turbulence intensity and scale on the pressure distribution of a single square cylinder placed in a turbulent cross flow. They found that when the square cylinder was positioned in a cross flow with one face normal to the flow direction, only drag force was produced; but in the same flow a negative lift force was developed at small positive angle of attack, the magnitude of which depended on the turbulence characteristics of the cross flow. It was suggested that the negative lateral force on the square cylinder oriented at a small positive angle of attack was due to the relatively large negative pressure coefficient in the seperated zone on the windward side wall. It was also concluded that the effect of turbulence intensity was to decrease the pressure near the front corner of the windward side wall and promote flow reattachment near the rear, giving rise to very significant increase in

aerodynamic moment.

DAVIS AND MOORE [12] carried out a numerical study of vortex shedding from rectangular cylinders. Numerical solutions for two-dimensional time dependent flow about rectangles in infinite domains using QUIKTEST method proposed by Leonard [47] for time dependent-convection dominated flows was reported. This scheme utilizes quadratic UPWIND differencing in one dimension in a manner similar to the QUICK method for two-dimensional steady flows (Leonard et al [46]). The initiation and subsequent development of the vortex shedding phenomena was investigated for Reynolds number varying from 100 to 2800. It was found that the properties of these vortices were strongly dependent on the Reynolds number. Lift and drag coefficients were also found to be influenced by Reynolds number. The computer simulation described in the paper was carried out on a UNIVAC 1108.

HUA [24] made measurements of fluctuating lift and the oscillating amplitude on a square cylinder in a wind tunnel test. It was represented that the wind pressure distributions and the lift force on the stationary cylinder normal to the wind was proportional to the square of its amplitude.

LEE [45] made an elaborate study of the effect of turbulence on the surface pressure field of a square prism. Various turbulent intensities were produced by placing different square mesh grids upstream of the model. The measurements of the mean and fluctuating pressures on a square cylinder placed in a two-dimensional uniform and turbulent flow was presented. It was

observed that the addition of turbulence to the flow raised the base pressure and reduced the drag of the cylinder. It was suggested that this phenomena was attributable to the manner in which the increased turbulence intensity thickens the shear layers, which causes them to reattach intermittently to the rear of the side faces. The subsequent deflection of the shear layers cause the vortex formation region to move downstream, thus raising the base pressure. The strength of the vortex shedding was shown to be reduced as the intensity of the incident turbulence was increased. Measurement of drag at various angle of attack (0 to 45°) showed that with increase in turbulence level the minimum drag occurred at smaller values of angle of attack.

NAKAMURA AND OHYA [60] studied the effects of turbulence on the mean flow past square rods. Measurements were made on square rods with different lengths with their square face normal to the flow to investigate the effects of turbulence intensity and scale on the mean flow characteristics. The turbulence intensity varied from 3.5% to 13% and the length to size ratio of d/h of the rods ranged from 0.1 to 2.0 where d was the length of the rod. It was found out that there were two main effects of turbulence on the mean flow past a three-dimensional sharp edged bluff body. Small-scale turbulence increased the growth rate of the shear layer, while large-scale turbulence enhanced the roll up of the shear layer. The consequences of these depended on the shape of the bluff body. For a square plate, both small and large-scale turbulence reduced the size of the base cavity. As the length of the square rod was measured beyond the critical (0.6 times the height), the shear layer-

edge direct interaction controlled the near wake, eventually leading to flow reattachment the effect of small-scale turbulence was to promote the shear-layer direct interaction.

NAKAMURA AND OHYA [61] attempted to study the vortex shedding from square prisms placed normal to smooth and turbulent approaching flows. Flow visualization and the measurement of the velocity and pressure for the flow past prisms of variable length-to-size ratios (i.e., d/h=0.1 (square plate), 0.05, 1.0 (cube) and 2.0 where h is the size of the square cross section and d is the prism length) with Reynolds number of Re=(0.5-14.7)x10° in terms of h was made. It was found that square prisms shed vortices in one of the two fixed wake planes which were parallel with the plate sides. The plane of shedding was switched irregularly from one to the other. It was further showed that the vortex shedding from a square prism with d/h= 0.5 and a cube was similar, while for a square prism with d/h= 2.0, no such vortex shedding was observed.

NAKAMURA AND MATSUKAWA [62] experimentally investigated the vortex excitation of rectangular cylinders with a long side normal to the flow in a mode of lateral translation using free and forced oscillation methods. The rectangular cylinders had side ratio of 0.2, 0.4 and 0.6. The forced oscillation experiments included measurements of the fluctuating lift-force at amplitudes upto 10% of the length of the long side. The results of the measurement of the mean base pressure, the fluctuating lift-force and the velocity fluctuation in the near wake was presented.It was found that the vortex excitation of a rectangular cylinder was strongly dependent on the

side ratio. It was concluded that the critical change of the mean base pressure of an oscillating rectangular cylinder with increasing side ratio was closely correlated with the vortex excitation characteristics.

OKAJIMA [65] conducted experiments in a wind tunnel and in a water tank on the vortex shedding frequencies of various rectangular cylinders. The results showed how the strouhal number (St=fd/U, where f is the frequency of vortex shedding) varied with width to height ratio of the cylinder for Reynolds number between 70 and 2×10^4. It was found that there existed a certain range of Reynolds number for the cylinders with the width to height ratios of 2 and 3 where flow pattern abruptly changed with a sudden discontinuity in strouhal number. For Reynolds number below this region, the flow separated at the leading edges, reattached on either the upper or lower surfaces of the cylinder during a period of vortex shedding. Again for Reynolds number beyond it the flow fully detached itself from the cylinder.

OKAJIMA [66] carried out numerical simulation of flow around rectangular cylinders in the range of low Reynolds number of 150 to 800 by a finite difference method (FDM) and flows at high Reynolds number by a discrete vortex method (DVM). The results simulated by FDM successfully indicated the existence of the critical range of Reynolds number where the value of the strouhal number changes, accompanied with a drastic change of flow pattern. At high Reynolds number, the flows around rectangular cylinders with different side ratios from 0.6 to 8 was computed by DVM and succeeded in a simulation of the phenomenon that the value of strouhal number abruptly changes when

the side ratio of a model is 2.8 or 6, as the critical value. The computed results of the flow pattern, base pressure, drag force and strouhal number showed a good agreement with the experimental ones.

ROBERSON, LIN AND RUTHERFORD [74] carried out experiments on circular cylinders, spool shaped bodies, cup-shaped bodies, square rods and rectangular rods to observe the effect of turbulence on the drag of these bodies. For square rods with their axes parallel to the flow direction it was found that drag co-efficient decreased approximately 25% when the turbulence intensity increased from 1% to 10%. Two rectangular rods were used; one had a square cross-section and the other had a length (in the free stream direction) to breadth ratio to two (L/B = 2). The drag was measured with the axes of the rectangular rods oriented normal to the free stream direction. It was noted that on the sides of the square rod the pressure change with a change in turbulence intensity was about the same as for the rear face; but for the rectangular rod, the change in pressure on the sides was large, but small on the rear face. It was concluded that bodies which have shapes such that reattachment of the flow is not a factor experience an increase in drag co-efficient with increased turbulence intensity. On the other hand bodies for which reattachment or near reattachment of flow occurs with increased turbulence may experience either a decrease or increase in drag co-efficient with increased turbulence intensity depending upon the shape of the body.

ROBERSON, CROWE AND TSENG [75] measured pressure distribution on rectangular rods placed in a cross flow with the rods oriented at small angles of attack with respect to the wind direction. The Reynolds number based on the minimum dimension of the rod was 4×10^4 and the turbulence intensity of the cross flow ranged between 1% and 10%. It was concluded that the free stream turbulence had a significant effect on the pressure distribution about bodies of rectangular cross-section. With small angle of attack these bodies had a significantly lower pressure on their windward side wall than did the same bodies with zero angle of attack. To study the pressure distribution on bodies that more nearly represent building configurations, tests were made on bodies of square cross-section placed on the floor of the wind tunnel. It was found that decreasing relative height of the body had an attenuating effect on the negative pressure on the windward side wall and it also increased the critical angle of attack.

SAKAMOTO AND ARIE [79] collected experimental data on the vortex shedding frequency behind a vertical rectangular prism and vertical circular cylinder attached to a plane wall and immersed in a turbulent boundary layer. It was tried to investigate the effect of aspect ratio (height/width) of these bodies and boundarylayer characteristics on the vortex shedding frequency. Measurements revealed that two types of vortex were performed behind the body, depending on the aspect ratio; they were the arch type vortex and the karman type of vortex. The arch type vortex appeared at an aspect ratio less than 2.0 and 2.5 for rectangular and circular cylinders respectively. The karman type of vortex appeared for the aspect ratio greater than the above

values. The whole experiment was conducted at a turbulent level of 0.02% and free stream velocity of 20 m/s. The aspect ratio was varied between 0.5 to 8

VICKERY [83] carried out an experimental investigation of fluctuating lift and drag on a long square cylinder. It was attempted to establish a correlation between the lift and the distribution of fluctuating pressure on a cross-section of the cylinder. It was found that the magnitude of the fluctuating lift was considerably greater than that for a circular cross-section. It was also reported that the presence of large scale turbulence in the stream had a remarkable influence on both the steady and the fluctuating forces. At small angle of attack (less than 10°) turbulence caused a reduction in base pressure and a decrease in fluctuating lift of about 50%.

2.3 Literature concerning multiple obstacles

BEARMAN AND WADCOCK [6] described how the flows around two circular cylinders, displaced in a plane normal to the free stream, interact as the two bodies are brought close together. Surface pressure measurements at a Reynolds number of 2.5×10^4 based on the diameter (D) of the single cylinder, showed the presence of mean repulsive force between the cylinders. At gaps between 0.1 diameter and one diameter a marked asymmetry in the flow was observed with the two cylinders experiencing different drags and base pressures. The base pressure was found to change from one steady value to another or simply fluctuate between the two extremes. It was also showed how mutual interference influenced the formation of vortex streets from the two

cylinders.

HAYASHI, SAKURAI AND OHYA [27] made an experimental investigation into the wake characteristics of a group of flat plates, consisting of two, three or four plates placed side by side normal to the flow direction. It was found that when the ratio of the split width to the plate width (split ratio) of a row of flat plates was less than about 2, the flows through the gaps were biased either upward or downward in a single way, leading to multiple flow patterns for a single split ratio value. The plates on the biased side showed high drag and regular vortex shedding, while those on the unbiased side showed the opposite. It was suggested that the origin of biasing was strongly related to the vortex shedding of each plates of a row. The experiment was conducted for Reynolds number of $(1.3-1.9) \times 10^4$.

IGARASHI [32] reported on the characteristics of flow around two circular cylinders of different diameters arranged in tandem. The Reynolds number defined by the diameter of the first cylinder was varied in the range of 1.3×10^4 to 5.8×10^4 and the longitudinal spacing between the axis of the cylinders in the interval of 0.9 diameter to 4.0 diameter. The reattachment of seperated shear layers from the first cylinder, jump phenomena and the bistable flow at the critical region for the cases of cylinders with equal and unequal diameters were discussed.

IGARASHI AND SUZUKI [33] conducted experimental investigation on the characteristics of the flow around three circular cylinders arranged in line.

There were three cases concerned with the behavior of the shear layers separated from the first cylinders on the downstream ones, the first was a case without reattachment, the second was one with reattachment and the third was one rolling up in the front region of the downstream cylinder.

IGARASHI [34] experimental investigation was carried out on the characteristics of the flow around four circular cylinders arranged in line. Concerning the behavior of the shear layers separated from the first cylinder to the downstream ones, the flow patterns were classified according to the longitudinal spacing between the axis of the cylinders and Reynolds number. Flow characteristics of these pattern was elucidated. The Reynolds numbers corresponding to the reattachments of the shear layers into the second cylinder were obtained. The flow characteristics around the downstream cylinders changed drastically in this transition region. Thereby, a bistable flow and a hysterisis phenomenon emerged.

KOEING AND ROSHKO [39] described an experimental investigation of the shielding effects of various disks placed co-axially upstream of an axisymmetric flat faced cylinder. For certain combinations of the diameter and gap ratios it was observed a considerable decrease in the drag of such a system. By flow visualization technique it was also showed that for such optimum shielding the upstream surface which separated from the disk reattached smoothly onto the front edge on the downstream cylinder.

LEUTHEUSSER [41] made wind tunnel tests of a typical building configurations.

The experiment was conducted on four models each with different height and cross-section. It was found that the static wind loadings on each of the buildings in free standing condition and as a member of a group of buildings. It was concluded that the wind loading of a building was less severe when it formed a part of a group than when it was free standing.

LUO AND TENG [49] reported on the measurements of aerodynamic forces on a square cylinder which was downstream to an identical cylinder. The experiment was carried out for both tandem and staggered arrangements of the cylinders. It was showed that when the two cylinders were in tandem formation a critical spacing equal to about four times the side length D of the square cylinder existed. It was also found that when the two cylinders were in staggered formation, the lift force that act on the downstream cylinder can be either positive or negative.

MASANORI AND SAKURAI [58] explained the wake characteristics of a group of normal flat plates, consisting of two, three or four plates placed side by side with slits in between to the normal flow direction. It was found that when the ratio of the slit width to the plate width (slit ratio) of a row of flat plate is less the flows through the gaps were biased either upward or downward in a stable way, leading to multiple, stable flow pattern for single slit ratio value. The plates on the biased side showed high drag and regular vortex shedding, while these on the unbiased side showed the opposite. It was suggested that the origin of biasing was strongly related to the vortex shedding of each plate of a row.

ZDRAVKOVICH [90] made an experimental investigation with a smoke visualization technique the laminar wake behind a group of three cylinders. The main characteristics of the interaction between the three cylinders was the appearance of the strong sinesous oscillations some distance downstream in the wake, which led to the formation of a new single vortex street. The mechanism of the formation process of the vortex street and the part played in it by the sinuous oscillations was demonstrated by the series of photographs. In an interaction between three fully developed vortex streets. Some of the rows of the vortices crossed and there was an extremely complicated rearrangements of vorticity in the wake. It was also found wakes some-times which were laminar on one side and turbulent on the other.

It is obvious from the above mentioned papers that many researchers have carried out extensive research works on both for single cylinder and for multiple cylinders with different types of flow and have presented many valuable results in this regards. But numerical study with tandem cylinders has not been made anywhere to date. So, the present investigation would definitely contribute to the idea of numerical modeling on tandem square cylinders

CHAPTER-III

MATHEMATICAL MODEL OF THE PRESENT STUDY

3.1 Governing equations

The general governing equations for conservation of mass and momentum expressed in cartesian tensor notation are [10], for conservation of mass,

$$\frac{\partial \hat{\rho}}{\partial t} + \frac{\partial (\hat{\rho}\hat{U}_i)}{\partial x_i} = 0 \qquad (3.1)$$

and for conservation of momentum,

$$\frac{\partial \hat{U}_i}{\partial t} + \hat{U}_j \frac{\partial \hat{U}_i}{\partial x_j} = -\frac{1}{\hat{\rho}}\frac{\partial \hat{P}}{\partial x_i} + \frac{1}{\hat{\rho}}\frac{\partial}{\partial x_j}(\mu\frac{\partial \hat{U}_i}{\partial x_j}) + \frac{1}{3\hat{\rho}}\frac{\partial}{\partial x_i}(\mu\frac{\partial \hat{U}_i}{\partial x_i}) \qquad (3.2)$$

where U, P, ρ are functions of time and defined as [10]

$$U = \lim_{(t_1-t_2)\rightarrow\infty}\frac{1}{(t_1-t_2)}\int_{t_2}^{t_1} \hat{U}(x_1,x_2,x_3,t)\,dt \qquad (3.3)$$

Defining $\hat{U}$= U+u and $\hat{P}$= P+p and neglecting the effect of density fluctuations, then instantaneous values of $\hat{U}$ and $\hat{P}$ may be splitted into time-averaged (U, P) and fluctuating (u, p) components. Thus, for steady flows, the partial differential equations for conservation of mass and momentum, takes the following form [10]:

Mass:

$$\frac{\partial}{\partial x_i}(\rho U_i) = 0 \qquad (3.4)$$

Momentum:

$$\frac{\partial}{\partial x_j}(U_j U_i) = -\frac{1}{\rho}\frac{\partial P}{\partial x_i} + \frac{1}{\rho}\frac{\partial}{\partial x_j}(\mu\frac{\partial U_i}{\partial x_j}) + \frac{\partial}{\partial x_j}(-\overline{u_i u_j}) \qquad (3.5)$$

For incompressible fluid where both the density ρ and viscosity coefficient μ are constant, then the momentum equation (3.5) reduces to

$$\frac{\partial}{\partial x_j}(\rho U_j U_i) = -\frac{\partial P}{\partial x_i} + \frac{\partial}{\partial x_j}(\mu\frac{\partial U_i}{\partial x_j}) + \frac{\partial}{\partial x_j}(-\rho\overline{u_i u_j}) \qquad (3.6)$$

where $-\overline{u_i u_j}$ is known as Reynolds stress

where U_i represents the mean value of velocity and u_i represents their fluctuating quantities.

In case of laminar flow, the problem is governed by (3.4) -(3.6) except the term representing the Reynolds stress. But for turbulent flow, equations (3.4)-(3.6) do not form a closed system because these equations contains unknown Reynolds stresses $-\rho\overline{u_i u_j}$: this diffusional flux plays a significant role in determining the flow behavior as the small time-scale effects are expressed

through them. Again from the experiments it was found that in turbulent flows, the magnitude of the turbulent-diffusion term is substantially greater than the laminar-diffusion term except in the immediate vicinity of solid surface [10]. Thus, the unknown correlations can not be neglected. The problem regarding unknown correlations may be solved by representing them as dependent variables. It may also be solved by specifying the correlations as function of known quantities, for example, by Prandtl mixing length for $\overline{u_i u_j}$. The above procedure of problem solver can be presented as TURBULENT MODELING.

3.2 Turbulence Model of the Present Study

There are many approaches of turbulence modeling found in the literature based on different assumptions. Two of such assumptions are known as ZERO- and ONE- equation models where the value of k is specified. But the assumptions that Reynolds shear stress is directly proportional to the square of kinetic energy and the gradient of the mean velocity, and inversely proportional to the dissipation rate is more realistic than a specified value of k [10]. Hence, TWO-equation model is used here. The model used in the present work is the standard k-ϵ model [42] in which the unknown Reynolds stresses are expressed using 'gradient transport hypothesis'[23] which assumes fluxes are assumed proportional to the gradients of mean flow properties. The constant of proportionality is μ_t, known as turbulent viscosity.

According to 'Gradient Transport Hypothesis' [23] Reynolds stresses are:-

$$-\rho\overline{u_i u_j} = \mu_t(\frac{\partial U_i}{\partial x_j} + \frac{\partial U_j}{\partial x_i}) \qquad (3.7)$$

μ_t turns out to be a function of turbulence energy k and dissipation rate $\in$ where k and $\in$ are derived from their own transport equations.

3.3 The k- and $\in$- equations

The general equation for turbulence energy k is,

$$\frac{Dk}{Dt} = \frac{1}{\rho}\frac{\partial}{\partial x_j}(\frac{\mu_{eff}}{\sigma_k}\frac{\partial k}{\partial x_j}) + \frac{\mu_t}{\rho}(\frac{\partial U_i}{\partial x_j} + \frac{\partial U_j}{\partial x_i})\frac{\partial U_i}{\partial x_j} - \varepsilon \qquad (3.8)$$

and general equation for energy dissipation rate $\in$ is,

$$\frac{D\varepsilon}{Dt} = \frac{1}{\rho}\frac{\partial}{\partial x_j}(\frac{\mu_{eff}}{\sigma_\varepsilon}\frac{\partial \varepsilon}{\partial x_j}) + \frac{C_{\varepsilon 1}\mu_t}{\rho}\frac{\varepsilon}{k}(\frac{\partial U_i}{\partial x_j} + \frac{\partial U_j}{\partial x_i})\frac{\partial U_i}{\partial x_j} - C_{\varepsilon 2}\frac{\varepsilon^2}{k} \qquad (3.9)$$

For steady turbulent flow, these equations becomes

$$\frac{\partial}{\partial x_j}(\rho U_j k) = \frac{\partial}{\partial x_j}(\frac{\mu_{eff}}{\sigma_k}\frac{\partial k}{\partial x_j}) + G - \varepsilon\rho \qquad (3.10)$$

and

$$\frac{\partial}{\partial x_j}(\rho U_j \varepsilon) = \frac{\partial}{\partial x_j}(\frac{\mu_{eff}}{\sigma_\varepsilon}\frac{\partial \varepsilon}{\partial x_j}) + \frac{C_{\varepsilon 1}\varepsilon G}{k} - \frac{\rho C_{\varepsilon 2}\varepsilon^2}{k} \qquad (3.11)$$

where

$$G = \mu_t(\frac{\partial U_i}{\partial x_j} + \frac{\partial U_j}{\partial x_i})\frac{\partial U_i}{\partial x_j} \qquad (3.12)$$

For two-dimensional plane flow, equation (3.12) can be written as:

$$G = \mu_t[\ 2\ (\frac{\partial U}{\partial x})^2 + 2(\frac{\partial V}{\partial y})^2 + (\frac{\partial U}{\partial y} + \frac{\partial V}{\partial x})^2\ ] + S_G \qquad (3.13)$$

S_G covers additional generation term whose effects are small except for flows of non-uniform properties. For the present prediction this term is omitted and S_G given by [30] is

$$S_G = -\frac{2}{3}\mu_t[\frac{\partial V}{\partial y} + \frac{\partial U}{\partial x}]^2 \qquad (3.14)$$

Where $\mu_{eff} = \mu_t + \mu$

and $\mu_t = \rho C_\mu k^2 / \varepsilon$

The value of the constants use in k-ε model [43] are,

c_μ =0.9 $c_{\varepsilon 1}$ =1.44 $c_{\varepsilon 2}$ =1.92 σ_k =1.0 σ_ε =1.3

The above coefficients can be constant in the sense that they are not changed in any one calculation and it is to be hoped that they will not vary much from one flow to another. The values shown are similar to those proposed by [36] and are those recommended by [22], and [71]. The value of c_μ is undoubtedly not constant. The stress model suggests a value of c_μ is 0.15 and consistency with the law of wall requires $c_\mu/\sigma_\epsilon=0.069$. The decay of isotropic turbulence suggests that $c_{\epsilon 2}$ has a value of around 1.8 and near - wall turbulence dictates that $(c_{\epsilon 2} - c_{\epsilon 1})$ is fixed: values of $c_{\epsilon 1}$ and $c_{\epsilon 2}$ are given below [10]:

Authors	$c_{\epsilon 1}$	$c_{\epsilon 2}$
Hanjalic and Launder [25]	1.45	2.0
Wyngaard et al [85]	1.50	2.0
Gibson and Launder [21]	1.45	1.9

3.4   Outline of FDM

Flow is assumed to be two-dimensional, steady and incompressible turbulent flow and has been computed about the primitive variables i.e. velocities (U,V) and pressure P, by solving the Navier-Strokes equations and continuity equation respectively.

3.5 Boundary conditions

At inlet of the computational domain, the assumed profiles are:

$$U = U_{in} = U_o$$

$$V = 0.0$$

$$k = k_{in} = I U_o^2$$

where I= turbulent intensity factor, and in the present study it is assumed to be 3% .

$$\epsilon = \epsilon_{in} = k^{3/2}_{in}/l$$

where l= λH and λ represents length scale factor, and its value is assumed to be 0.005.

At the outlet of the computational domain, zero gradient of stream wise velocity, k and ϵ are employed.

3.6   Wall boundary conditions

Near wall, the local Reynolds number ($R_y = y\sqrt{k}/\lambda c$, where λ is length scale factor, c is the molecular velocity and y is the distance from the wall) becomes very small and the turbulence model, which is designed for high Reynolds number, becomes inadequate. Both this fact and the steep variations of properties near walls, special formula (wall functions) and modifications are necessary. This low Reynolds number region is not solved in the computation rather bridged by the wall function. The overall modification of boundary conditions can be expressed as following.

3.6.1 The basis of wall boundary conditions

The universal velocity profile in the region near the wall is shown in figure 3.1. It is clearly indicated that the wall region is made up of three zones [23] : the viscous sublayer $(0<y^+<5)$, transition zones or buffer layer $(5<y^+<30)$ and inertial sublayer or turbulent zone $(30<y^+<400)$ where the flow is assumed to be completely turbulent but $\tau \approx \tau_w$, and the buffer zone $(5<y^+<30)$ of vigorous turbulence dynamics where the flow is neither completely dominated by viscous effect nor completely turbulent. our approach, as is indeed done in many engineering calculations , is to dispose of the "buffer" layer by defining a point $y^+ = 11.63$ (where the linear velocity profiles is the viscous sublayer meets the logarithmic velocity profile in the inertial sublayer) below which the flow is assumed to be purely viscous and above which it is purely turbulent. According to the above terminology, the boundary conditions can be used for different equations.
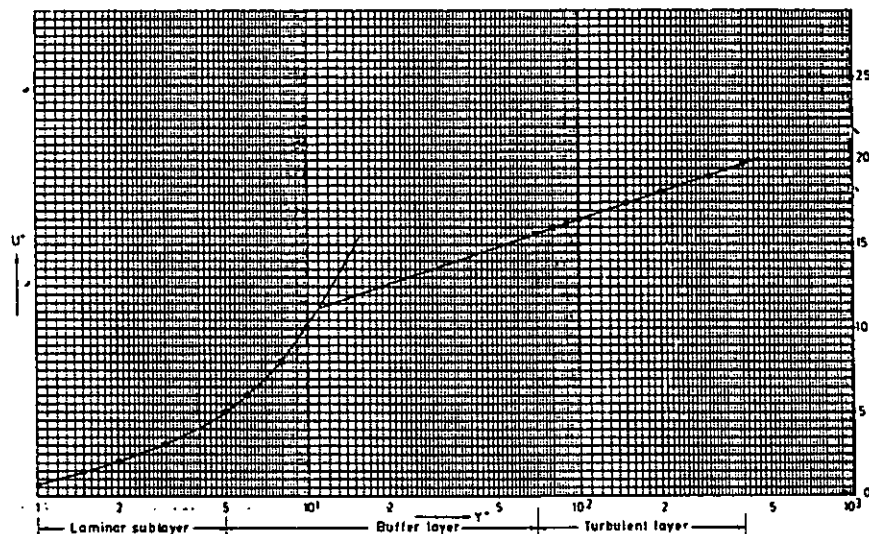

Fig. 3.1 Universal velocity profile in the region
near the wall

(a) The momentum equation can be reduced to a particularly simple non dimensional form as follows: [20]

$$\tau = (\mu + \mu t) du/dy$$

$$\tau/\tau w = (1 + \mu t/\mu) dU^+/dy^+$$

For $y^+ \leq 11.63$, $\mu t/\mu \ll 1$, $\tau \approx \tau w$, thus $U^+ = y^+$

For $y^+ > 11.63$, $\mu t/\mu \gg 1$, $\tau \approx \tau w$, and $\mu t = \rho \kappa y U_\tau$ [23]

Thus $\qquad U^+ = 1/\kappa \, \log_e(Ey^+)$

Where $\qquad y^+ = U_\tau y/\nu$

$$U^+ = U/U_\tau$$

$$U_\tau = \sqrt{(\tau w/\rho)}$$

$$\tau w = \rho c_\mu^{1/4} k^{1/2} \kappa U /[\log_e(E \, y^+)]$$

(b) The wall treatment for k- and ϵ- equations are to be formulated on the basis of local equilibrium condition that the local rate of production of turbulence is balanced by its dissipation rate ϵ.

(i) The turbulence energy equation reduces to a simple form that yields expression for both the shear stress $\tau \approx \tau w$ and the dissipation rate ϵ within the `buffer´ and viscous sublayer.

$$\text{production} \approx \text{dissipation}$$

Thus $\qquad -uv \, du/dy = \epsilon$, yielding

$$k = \tau I/\rho c_\mu^{1/2}$$

and $\in$ modified from the k-balance as

$$\int_v \in dv \approx c_\mu{}^{3/4} k^{3/2} U^+ dv/y_p, \text{ with}$$

$$U^+ = y^+ \qquad \text{for } y^+ \leq 11.63$$

$$U^+ = 1/\kappa \log_e(Ey^+) \qquad \text{for } y^+ > 11.63$$

(ii) $\in$- equation reduced to [20]

$$c_{\in 1} = c_{\in 2} - (\kappa^2/\sigma_\in c_\mu{}^{1/4})$$

thus $\qquad \sigma_\in = \kappa^2/(c_{\in 2} - c_{\in 1})c_\mu{}^{1/4}$

3.6.2 Incorporation of wall boundary condition

(a) Momentum equations:

(i) Tangential velocity:

U_p shown in figure 3.1 from usual momentum balance but due to usual shear force (F_s) expression, suppressed in FDE (Finite Difference Equation) by setting
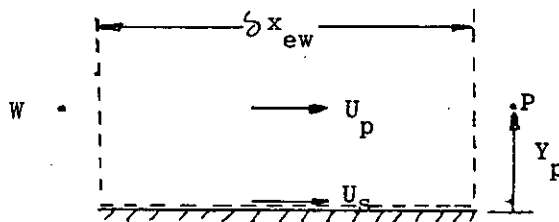
Fig. 3.1

as=0 : Then the momentum 'source' for tangential velocity component adjacent to the south wall is calculated as :

$$S_s = \tau_s \, \delta x_{ew} = - \mu_{eff} \, \delta x_{ew} \, (u_p - u_s)/ \, y_p$$

where δx_{ew} is the area of cell, y_p is the normal distance from cell centre to the wall and μ_{eff} is the effective viscosity, can be expressed as

$$\mu_{eff} = \mu \qquad\qquad\qquad \text{for } y^+ \leq 11.63$$

$$\mu_{eff} = \rho c_\mu^{1/4} \, k_{pw}^{1/2} \kappa y_p \, / \, \log_e(E \, y_p^+) \quad \text{for } y^+ > 11.63$$

with

$$y_p^+ \;= c_\mu^{1/4} \, \rho_p \, k_{pw}^{1/2} \, y_p \, /\mu$$

where $\qquad k_{pw} = (k_p + k_w)/2$

S_s is then linearised as equation

$$S = S_u + S_p \, \phi_p$$

where S_p and S_u represent the implicit and explicit contribution respectively

$$S_p = \mu_{eff} \, \delta x_{ew} \, /y_p$$

$$S_u = \mu_{eff} \, U_s \, \delta x_{ew}/y_p$$

(ii) Normal velocity: For velocities normal to a wall, no special wall treatment is necessary.

(b) Turbulence energy, k :

K_p shown in figure 3.2 from usual k-balance but used flux expression suppressed by setting as =0 , with source S_k (= $G-\rho\epsilon$) evaluated as follows:
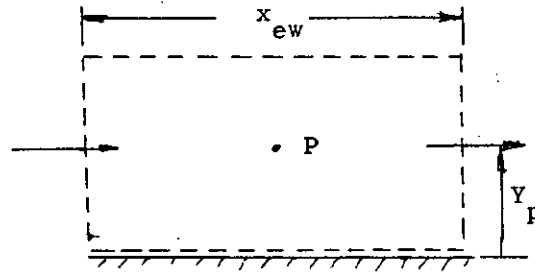
Fig. 3.2

(i) calculation of G altered by noting [20]

$$\int_v \mu_t \, (\partial U/\partial x + \partial V/\partial y)^2 \, dv \approx \tau_s \, (U_p - U_s) \, \delta v/y_p$$

and $\qquad \tau_s = \mu_{eff} \, (U_p - U_s)/ y_p$

(ii) calculation of $\rho \epsilon$ altered by noting [20]

$$\int_v \rho \epsilon \, dv \approx \rho c_\mu^{3/4} \, (k_p^{3/2} - k_s^{3/2}) \, U^+ \, \delta v/y_p$$

$$U^+ = y^+ \qquad\qquad \text{for } y^+ \leq 11.63$$

$$U^+ = 1/\kappa \, \log_e(Ey^+) \qquad \text{for } y^+ > 11.63$$

(c) **Energy Dissipation rate,ϵ :**

In wall-flows, unlike k which falls to zero at the wall, ϵ reaches its highest value (much higher than in a free stream) at the wall. This makes ϵ- balance for a cell extending upto a wall very difficult as we are ignorant on how to modify ϵ_s in such cases. It is due to this shear ignorance that we adopt a fixed value for ϵ_p (irrespective of y^+) based on 'equilibrium relations'.

$$\epsilon_p = c_\mu^{3/4} \cdot k_p^{3/2} /\kappa y_p$$

(d) Pressure correction, p :

At boundaries where the normal velocity is prescribed, the finite-difference equation for local pressure correction must be defined so that this velocity is not changed i.e. p/ is zero. This is done , for example the cell adjacent to a 'south' wall, by setting $a_s = 0$.

3.7 Boundary conditions on cylinders :

Boundary conditions around the cylinders are simply that, surface normal and tangential velocities are zero. Surface shear stress is determined as like as wall shear stress. Velocity components inside the cylinders are fixed by insertion of appropriate boundary conditions. Similar treatment is used for other properties. Since the velocities at the corners of the cylinder are undefined, the situation in these areas must be treated specially. Davis & Moore [12] calculated the convective flux across the control volume half-face at the front faces shown in figure (3.3) by (i) assuming an average normal velocity across these half-faces equal to that at the outer edge of the half face (i.e. using V_p for the normal velocity across the U-control volume and vice versa), and (ii) assuming that the fluxed quantity (U_s and V_e in figure 3.3b, 3.3c) satisfies a linear fit a+bx+cy through the nearest three non-zero nodal values of the respective velocity component. The convective flux across the rear corner half-faces is accomplished by quadratic upwinding with the addition of some linear interpolations to obtained values of the fluxed quantity at the centre of each of the half-faces. In the present study, the

convective flux across the half faces of the front and rear corners of the cylinder is accomplished by insertion of half the total convective flux across the whole control volume.
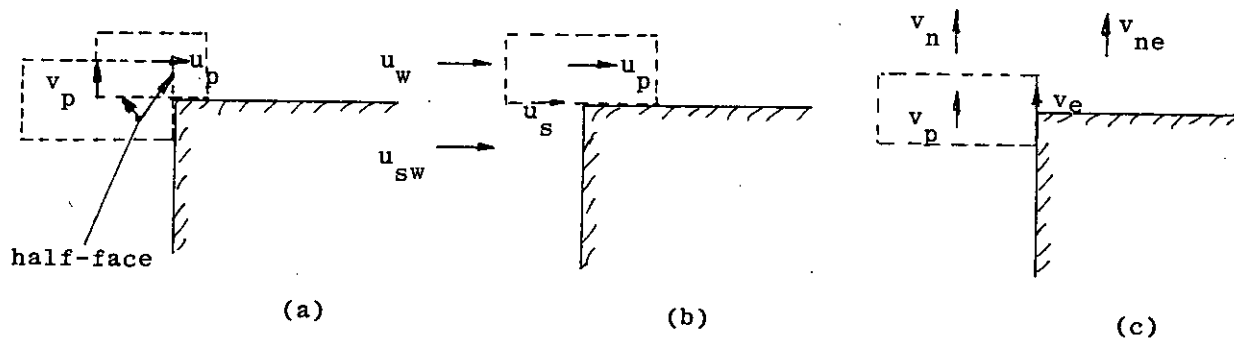

(a)   (b)   (c)

Fig. 3.3 :

CHAPTER-IV

THE NUMERICAL SOLUTION METHOD

4.1   Introduction

In this chapter the numerical procedure employed for solving the partial differential equations governing the mass, momentum etc., presented in chapter-III is discussed. The solution of the above partial differential equations are obtained by a computer code, name as TEACH-T. The discretization of momentum transport equation as well as pressure correction, as used in TEACH-T, are described in APPENDIX-A. The solution procedure starts by supplying initial guessed values of the velocity and pressure fields and then computes a converged solution by iteration. The algorithm of the solution procedure used in TEACH-T is known as SIMPLE (Semi Implicit Method for Pressure-Linked Equations), developed by Patanker [72] and described in APPENDIX-B.

4.2 The method of discretisation

An overview of the discretisation method for the numerical solution of the fluid flow problems is given by Patanker [72]. In the present study, the finite-volume approach, as described by Gosman et al [18] and others, is adopted. In this approach, the differential equations are integrated over a finite-volume and are then expressed in an algebraic form called discretisation equation. The discretised equations thus represent the conservation principles for the selected volume. In accordance with this approach, the computational domain

is here divided into a finite number of discrete volumes or 'cells' using a computational grid shown in figure 4.2. Following the well established practice of 'staggered' arrangement (Patanker [72]), the numerical solution is accomplished on a variably spaced staggered mesh in which the scalar quantities (including pressure, density, viscosity, k and $\in$) are defined at the centers and the normal velocities at cell faces shown in figure 4.3. The variable spacing is such that the mesh spacings in the x- and y- directions, Δx and Δy, are only function of x and y, respectively.

4.3 Method of numerical calculation

The partial differential equations can be expressed in standard form as:

$$\frac{\partial}{\partial x_j}(U_j \rho \phi) = \frac{\partial}{\partial x_j}(\Gamma_\phi \frac{\partial \phi}{\partial x_j}) + S_\phi \qquad (4.1)$$

Where ϕ is a variable, Sϕ is the source term and $\Gamma\phi$ is their diffusive transport coefficient. All these terms of equations (4.1) are shown in Table 4.1.

In the present study, the convective and diffusive fluxes are discretised by UPWIND differencing scheme which is very much numerically stable. The source term (right hand terms of the equation 4.1) are expressed by a linear relationship shown below :

$$-\int_v S_\phi dv = b\phi_p + c$$

where b and c is generally a function of ϕ_p.

The discretised equations are solved simultaneously using the SIMPLE algorithm of Patanker & Spalding [70] by repeated sweeps of a line-by-line application of the Tri-Diagonal Matrix Algorithm (TDMA) (Patanker [72]).

4.4 Computational details

Grid dependence test was made to determine the improved grid size of the calculation domain of the present study. The test was done at Reynolds number of 2.87×10^4 for three grid systems; (15x22), (25x40), (49x79) shown in figure 4.4. For this test, predicted U-velocity profiles at various axial locations was compared with experimental values of Hossain [29]. The predictions with 49x79 grid are in close agreement with the measurements and hence the further calculations are made with this grid. All calculations were carried out in a personal computer ACER [system 15 with INTEL 80386 microprocessor] in the Department of Mechanical Engineering of BUET, Dhaka.

4.4.1 Single cylinder

A 50mm square cylinder was used and the computational domain was divided into a large number of grids by two sets of orthogonal lines parallel to the axes x and y shown in fig. 4.2. The grid distribution in the calculation domain was non-uniform in both x and y directions. Computational meshes employed in this case was 49x79, with the first number being the number of mesh points in the

y-direction and the second in the x-direction.

4.4.2 Two cylinders in tandem

In the study of two cylinders in tandem, a 50 mm square front cylinder was used with three different sizes of the rear cylinder having size-ratio of 1.0, 0.7, 0.5. The non-uniform computational meshes employed in this arrangements was 49x85.

A wind speed of 8.61 m/s with 3% turbulence-intensity was used in this computations. Referring to the width of the front cylinder, the flow Reynolds number used in the present prediction was 2.87×10^4 .

Over the whole computational domain mesh cells are concentrated in the area near the cylinders. The mesh size of the front cylinder was 21x21 and the mesh sizes of the rear cylinders were 21x21, 15x11, 11x11 corresponding to the size-ratio of 1.0, 0.7, 0.5. The height of the computational domain selected was 457 mm in conjunction with height of the test section of the wind tunnel for Hossain [29]. The value of x_R was 650mm, large enough for flow at x=0 to remain undisturbed, while the value of x at exit from the computational domain was 5500mm. The initial conditions for the computations were uniform flow everywhere (impulsive start).

The steady state solution of equations (3.4) to (3.14) is obtained by an iterative solution procedure. Convergence of the solution was considered

satisfactory when the normalized residual mass source errors of each equation, summed over the whole calculation domain, were smaller than 5×10^{-3}. Approximately 2000 iterations were needed for the convergence of the standard k-ϵ model with under-relaxation factor of 0.2; this corresponds to approximately 6 hours of CPU time on INTEL 80386 microprocessor using 32 bit precision. In order to substantiate the behavior of flow, velocity vector and stream function plots were also obtained.

CHAPTER-V

RESULTS AND DISCUSSIONS

5.1 General

This chapter is devoted to the analysis of results obtained from the numerical prediction of flow around a single square cylinder and also around two cylinder in tandem. For cylinders in tandem, the predictions are obtained for three different size-ratios in a flow field of Reynolds number of 2.87×10^4.

Effects of interspacing between the cylinders are observed by changing the spacing-ratio. In addition, comparative study with the various research works and the present predictions are presented. The mean pressure co-efficients, C_p are calculated by the formula $(P-P_o)/(0.5\rho U_o^2)$ and the stream function ψ can be obtained by the relation : $U=\partial\psi/\partial y$ and $V=-\partial\psi/\partial x$. The mean drag forces acting on the cylinders at various L/D are calculated by integrating the pressure distributions on front and rear surfaces only and neglecting the effect of shear stress on the top and bottom surfaces.

5.2   Single cylinder

The distributions of mean pressure co-efficients, C_p is presented in fig.5.1 and are compared with those of Lee [45]; Pocha [69]; Hossain [29] and Davis & Moore [12]. The pressure distribution at the front face shows good agreement with other works. In all the cases a stagnation point is established at the middle of the front face. All other faces the results deviate considerably.

The predicted result on rear face only matches with Lee [45] whereas at the top and bottom surfaces it deviates considerably.

The predicted pressure distribution of Davis & Moore [12] shows smaller value (more negative) in top, bottom and rear faces than the present prediction although upto 1/5th portion of the bottom and rear faces along the direction of flow shows similar trend. The result deviates mainly because of (i) the corresponding Reynolds number for Davis & Moore [12] and the present is 1000 and 2.87×10^4 respectively (ii) Davis & Moore [12] used the standard QUICKEST scheme in his prediction which is second order accurate and the present prediction uses standard UPWIND scheme which is first order accurate.The velocity defect distributions in a two-dimensional wake behind a square cylinder has been shown in fig. 5.2 to examine the self-preservation of the flow. Here the predicted profiles are in close agreement with the theoretical profile as x/D decreases.

Fig. 5.3 shows the mean velocity distribution in the wake of the square cylinder. It is seen that the spread of the wake increases as distance from the body increases and the difference between the velocity in the wake and that of outside becomes smaller. The similar pattern of mean velocity distribution was observed in Hossain [29] which is logical from the view point of the energy transfer to the wake from the surroundings i.e. due to shearing action of the flowing fluid more and more fluid is entrained into the wake and thereby reduces the velocity defect.

The comparison of the predicted drag co-efficient,C_D is made with other researchers shown in Table 5.1. It is seen that C_D varies from 1.77 to 2.33 at various Reynolds number. The predicted co-efficient is 1.46 which is lower than others.

Fig. 5.4(a,b) shows the velocity field and stream function contour for single cylinder. Two symmetric vortices are found in fig 5.4(a). In fig 5.4(b) there are 20 stream function contours equally spaced from 0.0 to 1.0. Although two closed stream function contours are expected, but there is one. This is mainly because of choice of contour values.

5.3 Cylinders in tandem

5.3.1 Cylinders in tandem with size-ratio of 1.0

Fig 5.5 shows the variation of drag coefficients against spacing-ratios.In general, the present work predicts considerably lower value of C_D both for front cylinder and rear cylinder beyond L/D>4.0. No sharp changes in the value of C_D was observed while the measurements of Hossain [29], Lue & Teng [49] and Ohaya et al [67] found a critical spacing at L/D=4.0 where C_D changes sharply in both the cylinders. For L/D<4.0 the present study predicted higher value of C_D for rear cylinder and exists positive drag instead of negative drag which is found in Hossain [29]. The explanation of the above observation is that when L/D<4.0, the boundary layers that separated from the front cylinder reattached on to the rear cylinder and a region of slow moving fluid

is formed which is bounded by the shear layers and the two cylinders. The bounded region is at a pressure that is lower than the wake pressure of the rear cylinder because of shedding vortices of that cylinder and hence the latter is subjected to a negative drag force or thrust (Lue & Teng [49]).

Fig 5.6 to 5.10 shows the velocity field and stream function contour for d/D=1.0. In the velocity field two symmetric vortices are found between the cylinders and two reverse flows are found beyond rear cylinder but the present code is unable to predict above such reattachment of the separated boundary layer.

Fig 5.11 and 5.12 shows the mean pressure distribution around two tandem square cylinders for different streamwise interspacing and comparison is made with the measurements of Hossain [29]. Similar trend exists with stagnation point at the mid point on the front of the front cylinder as found by Hossain [29] and no such point is observed on the front of the rear cylinder. Instead negative pressure is observed on that surface. However, with increasing the interspacing, the C_p values on the front of the rear cylinder becomes less negative. It is observed that on the two lateral sides and rear side of the front cylinder, the pressure distributions have almost no effect on interspacing which is the reverse statement of Hossain [29].

Smaller value (more negative) of C_p- value prevails over the half portion along the direction of bottom and rear surfaces whereas uniform but greater value (less negative) prevails over the whole of the top surface. In the front

surface of the rear cylinder, the rate of increase (less negative) of C_p- value for L/D<4.0 is much lower than for L/D>4.0. In other surfaces the C_p- value becomes more negative as L/D increases.

Figs. 5.13 to 5.17 show the mean velocity distribution in the wakes behind the cylinders arranged in tandem for different interspacing. It can be seen from the figures that the velocity defect is considerably large behind front cylinder for L/D<4.0 and also there is little change in the half width. However, for L/D>4.0 the velocity defect behind front cylinder becomes smaller and gradually decreases with increasing in streamwise distance from the cylinder. The distribution of mean velocity behind the rear cylinder is similar for all interspacing.

Fig. 5.18 shows the velocity defect distribution in a two-dimensional wake behind the front cylinder for longitudinal spacing L/D=3.0 to 4.0 and is compared with Hossain [29]. It can be seen that the width of the velocity profile follows the same pattern as found by Hossain [29].

Fig. 5.19 and 5.20 shows velocity defect distribution in a two-dimensional wake behind the cylinders for longitudinal spacing of L/D>4.0 and L/D=3.0 to 5.0 respectively and comparison is made with theoretical results. It is observed from both the figures that the shape of the velocity profile is similar to that of a single cylinder.

5.3.2　Cylinders in tandem with size-ratio of 0.7

Fig 5.21 shows the variation of drag co-efficient with various interspacing of the two tandem cylinders for d/D=0.7. It is seen that for the rear cylinder there exists negative drag for L/D<3.0 and positive drag exists when L/D>3.0.

Fig 5.22 to 5.25 shows the velocity field and stream function contour for d/D=0.7 for different L/D. All cases two reverse flows are found and from velocity field it is clear that the boundary layer that separated from the front cylinder are reattached on to the rear cylinder as L/D<3.0 which covers the necessary explanations of causing negative drag force or thrust on the rear cylinder. Uniform drag coefficient exists over the whole range of L/D investigated.

Fig. 5.26 and 5.27 show pressure distribution around two tandem cylinders for d/D=0.7 within the range of 2.0≤L/D≤5.0. On the front cylinder it is clear that pressure coefficient has little effect on L/D except front face and similar trend is observed as d/D=1.0. On the otherhand, pressure coefficient on the rear cylinder has significant effect on L/D. In the front surface instead of stagnation point, negative value prevails and C_p value increases (less negative) as L/D increases.

Figs. 5.28 to 5.31 show the mean velocity distribution in the wakes behind the cylinders arranged in tandem for different interspacing. It can be seen from the figures that the velocity defect is considerably large behind the front

cylinder for L/D≤3.0 and also there is not much change in the half width. However, for L/D≥4.0 the velocity defect behind the front cylinder becomes smaller and gradually decreases with increase in longitudinal distance. For the rear cylinder, the half width increases as L/D increases although similar velocity defect exists.

Fig. 5.32 shows the dimensionless velocity defect distribution in a two-dimensional wake behind the front cylinder for longitudinal spacing L/D=2.0 to 3.0. It can be seen that the width of the velocity profile does not change upto $\Delta U/\Delta U_{max}$ equal 0.6 and after than the velocity profile changes slightly.

Figs. 5.33 and 5.34 show dimensional velocity distribution in a two-dimensional wake behind cylinders for longitudinal spacing of L/D=4.0 to 5.0 and L/D=2.0 to 5.0 respectively and comparison is made with theoretical results. It is observed from both the figures that the shape of the velocity profile is similar to that of a single cylinder.

5.3.3 Cylinders in tandem with size-ratio 0.5

Fig 5.35 shows the variation of drag co-efficient with various interspacing of the two tandem cylinders for d/D=0.5. It is seen that the rear cylinder also exist negative drag for L/D<3.0 and positive drag exists when L/D>3.0.

Figs.5.36 to 5.39 show the velocity field and stream function contour for d/D=0.5 for different L/D. In all cases two reverse flows are found and from

velocity field it is also clear that the boundary layer that separated from the front cylinder are reattached on to the rear cylinder upto L/D=3.0. The explanation of the negative drag can be easily understood from above figures. Uniform drag coefficient existsover the whole range of L/D investigated.

Fig. 5.40 and 5.41 show pressure distribution around two tandem cylinders for d/D=0.5 within the range of 2.0≤L/D≤5.0. On the front cylinder it is clear that pressure coefficient has little effect on L/D except front face and similar trend is observed as d/D=1.0. On the otherhand, pressure coefficient on the cylinder has significant effect on L/D. In the front surface instead of stagnation point, negative value prevails and C_p value increases (less negative) as L/D increases.

Figs. 5.42 to 5.45 show the mean velocity distribution in the wakes behind cylinders arranged in tandem for different interspacing. It can be seen from the figures that the velocity defect is considerably large behind the cylinder for L/D≤3.0 and also there is not much change in the half width. However, for L/D≥4.0 the velocity defect behind the front cylinder becomes smaller and gradually decreases with increase in longitudinal distance. For the rear cylinder, the half width increases as L/D increases although similar velocity defect exists.

Fig. 5.46 shows the dimensionless velocity distribution in a two-dimensional wake behind the front cylinder for longitudinal spacing L/D=2.0 to 3.0. It can be seen that the width of the velocity profile has little effect on L/D.

Fig. 5.47 and 5.48 shows dimensional velocity distribution in a two-dimensional wake behind the cylinders for longitudinal spacing of L/D=4.0 to 5.0 and L/D=2.0 to 5.0 respectively and comparison is made with theoretical results. It is observed from both the figures that the shape of the velocity profile is similar to that of a single cylinder.

5.4   Effect of the size of the rear cylinder

The present prediction is mainly concerning the effect of the size of the rear cylinder in the flow field. In this regard three different sizes of the rear cylinder with their size-ratios of 1.0, 0.7, 0.5 were considered in this prediction.

Fig. 5.49 shows the comparison of drag coefficient of the two tandem cylinders for different sizes of the rear cylinder with various streamwise interspacing investigated $2.0 \leq L/D \leq 8.0$. On the front cylinder, the size of the rear cylinder has little effect on drag coefficient throughout the interspacing investigated. On the otherhand, the rear cylinder has significant effect of the size of the cylinder itself. There exists negative drag coefficient for d/D=0.7 and 0.5 as L/D<3.0. Due to lag of experimental value, no such comments can be made about critical spacing.

CHAPTER-V

RESULTS AND DISCUSSIONS

5.1 General

This chapter is devoted to the analysis of results obtained from the numerical prediction of flow around a single square cylinder and also around two cylinder in tandem. For cylinders in tandem, the predictions are obtained for three different size-ratios in a flow field of Reynolds number of 2.87×10^4.

Effects of interspacing between the cylinders are observed by changing the spacing-ratio. In addition, comparative study with the various research works and the present predictions are presented. The mean pressure co-efficients, C_p are calculated by the formula $(P-P_0)/(0.5 \rho U_0{}^2)$ and the stream function ψ can be obtained by the relation : $U=\partial \psi/\partial y$ and $V=-\partial \psi/\partial x$. The mean drag forces acting on the cylinders at various L/D are calculated by integrating the pressure distributions on front and rear surfaces only and neglecting the effect of shear stress on the top and bottom surfaces.

5.2 Single cylinder

The distributions of mean pressure co-efficients, C_p is presented in fig.5.1 and are compared with those of Lee [45]; Pocha [69]; Hossain [29] and Davis & Moore [12]. The pressure distribution at the front face shows good agreement with other works. In all the cases a stagnation point is established at the middle of the front face. All other faces the results deviate considerably.

4. The width of the velocity profiles does not change fo[...] ratio throughout the length of velocity defect and it ass[...] [...]gular shape when L/D<4.0 for size-ratio 1.0 and L/D<3.0 for size-ratios 0.7,0.5 and the width of this profile increases as the size-ratio decreases.

8. Half width increases with increase of axial distance.

9. The formation of the wake and the vortex shedding phenomenon can be easily understood from velocity and contour plot.

6.3   Recommendations

1. The present study can be repeated using square cylinders with round corners.

2. Effect of Reynolds numbers on cylinders arranged in tandem may be investigated.

3. Further research can be carriedout for greater size-ratios.

4. Effect of turbulence intensity on cylinders may be investigated.

5. Further investigation can be carriedout by increase the number of cylinders in tandem arrangements.

6. Investigation can be improved with a modification of the wall treatment.

7. Investigation of the present study is for isotropic condition. An anisotropic condition can also be done.

8. The same problem can be solved using the code in which more accurate scheme like QUICK or QUICKEST can be used both for steady and unsteady state.
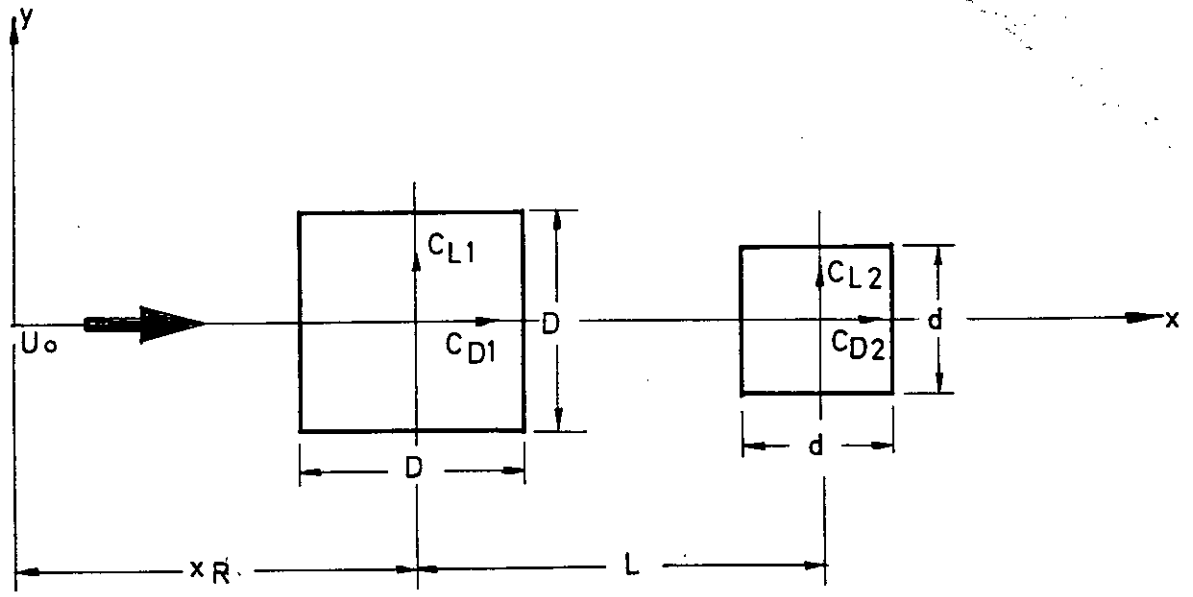
Fig. 4.1 : Tandem configuration of two square cylinder
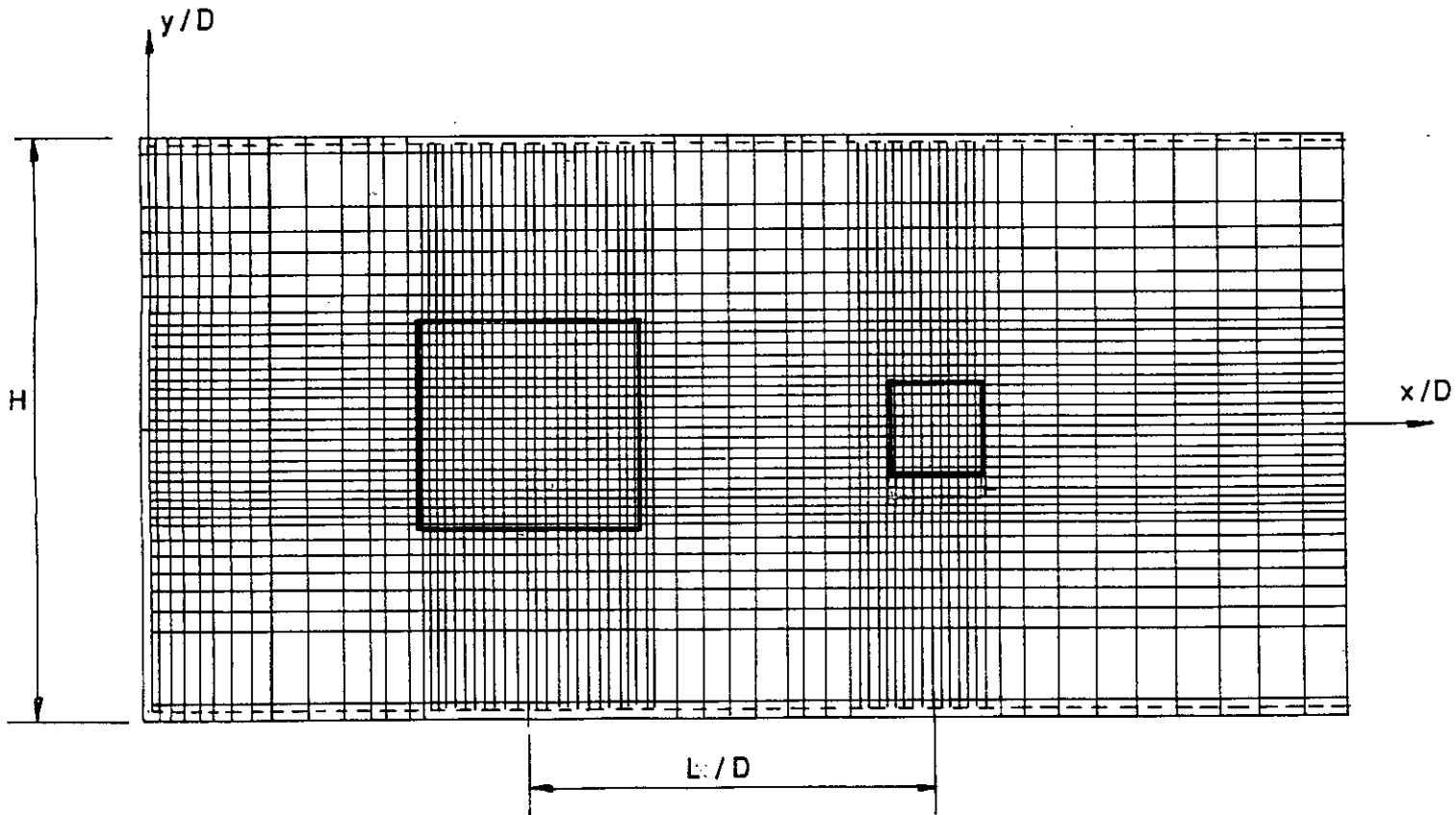
Fig. 4.2 : The non-uniform grid pattern used in this study
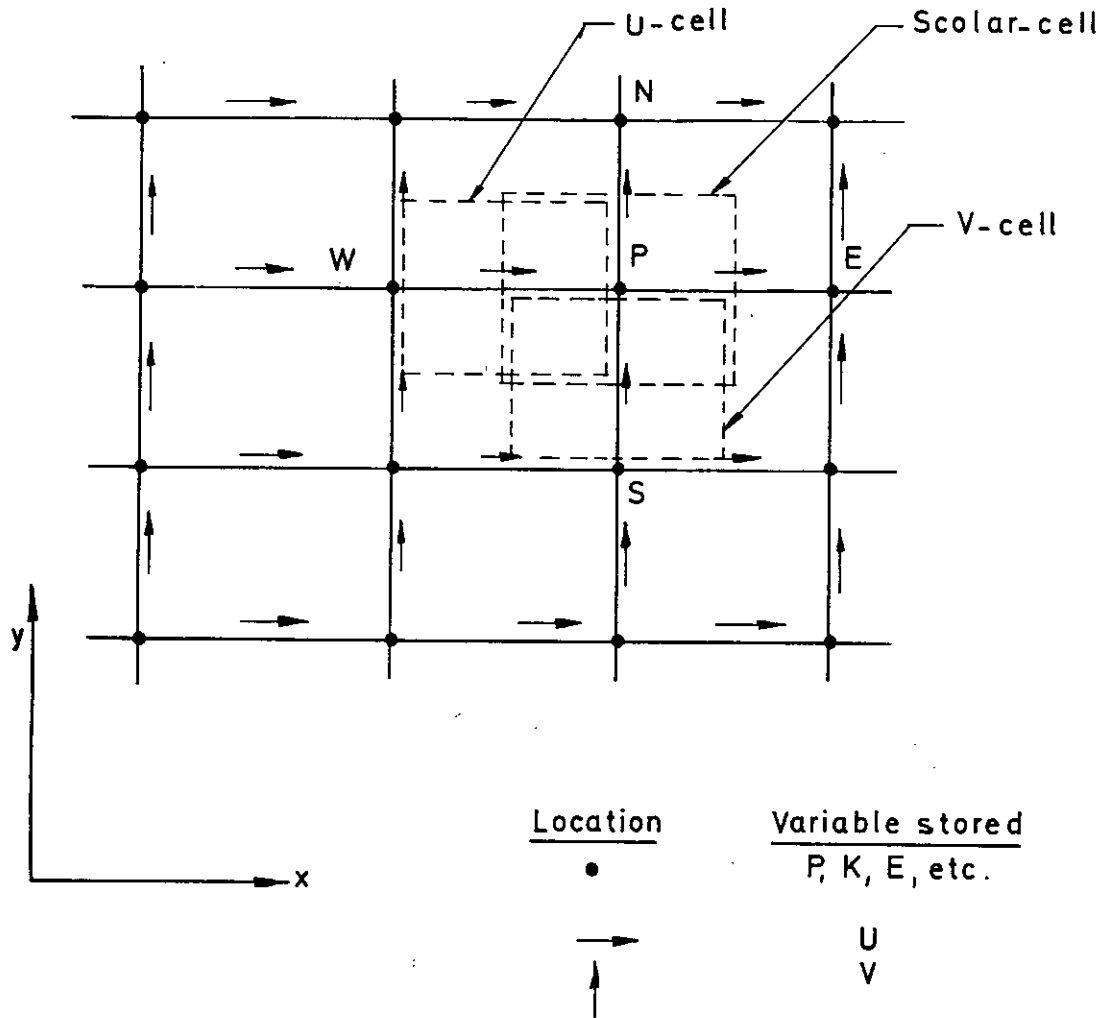
Fig. 4.3 Computational grid, location and control volumes
(cells) of scolar variables and axcial and
radial velocities.
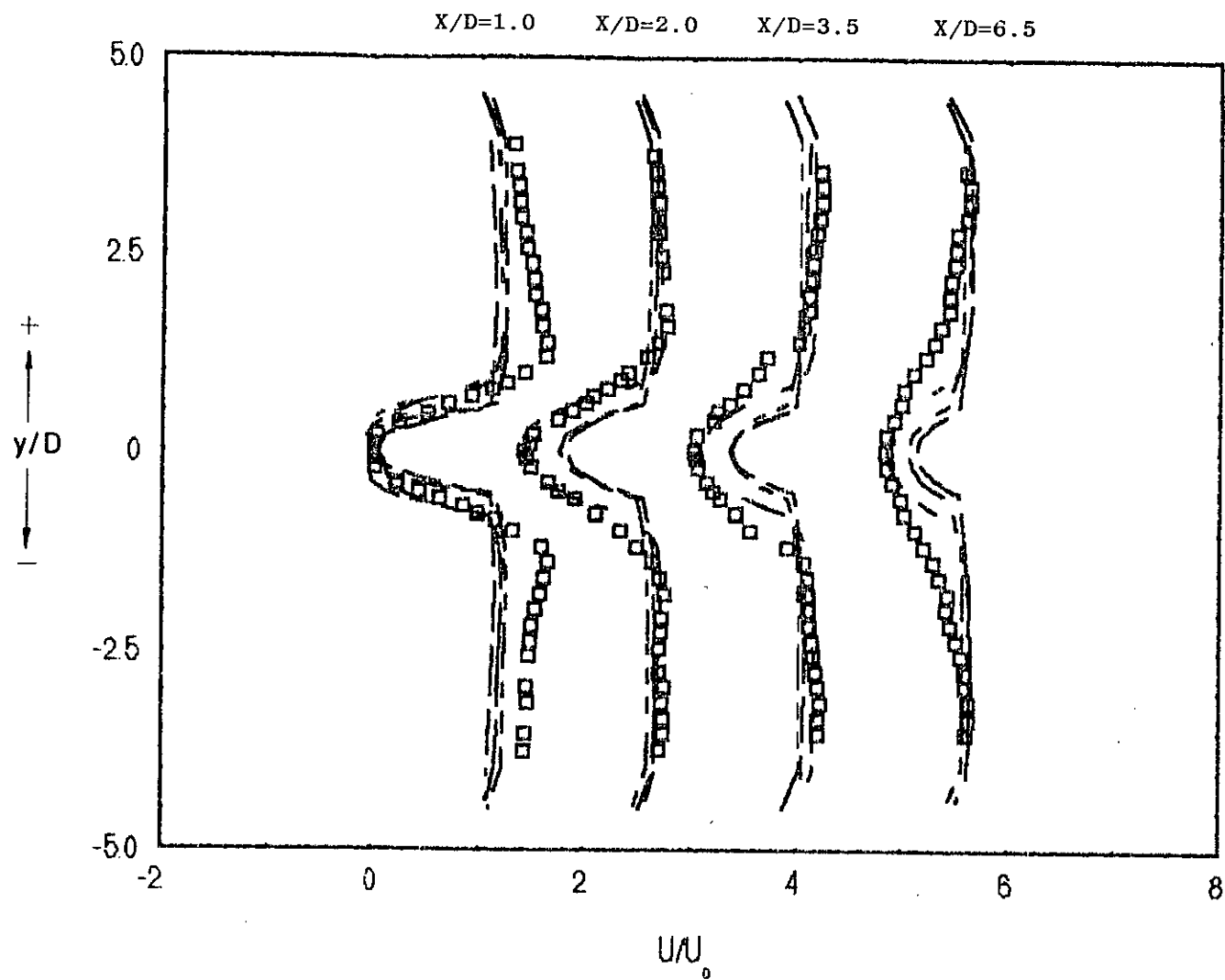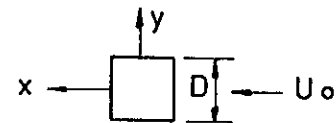
Fig. 4.4 : Grid dependency test for Reynolds number of 2.87×10^4
(49x79) grid ———— ————
(25x40) grid ———— —— ———
(15x22) grid ———— — ———
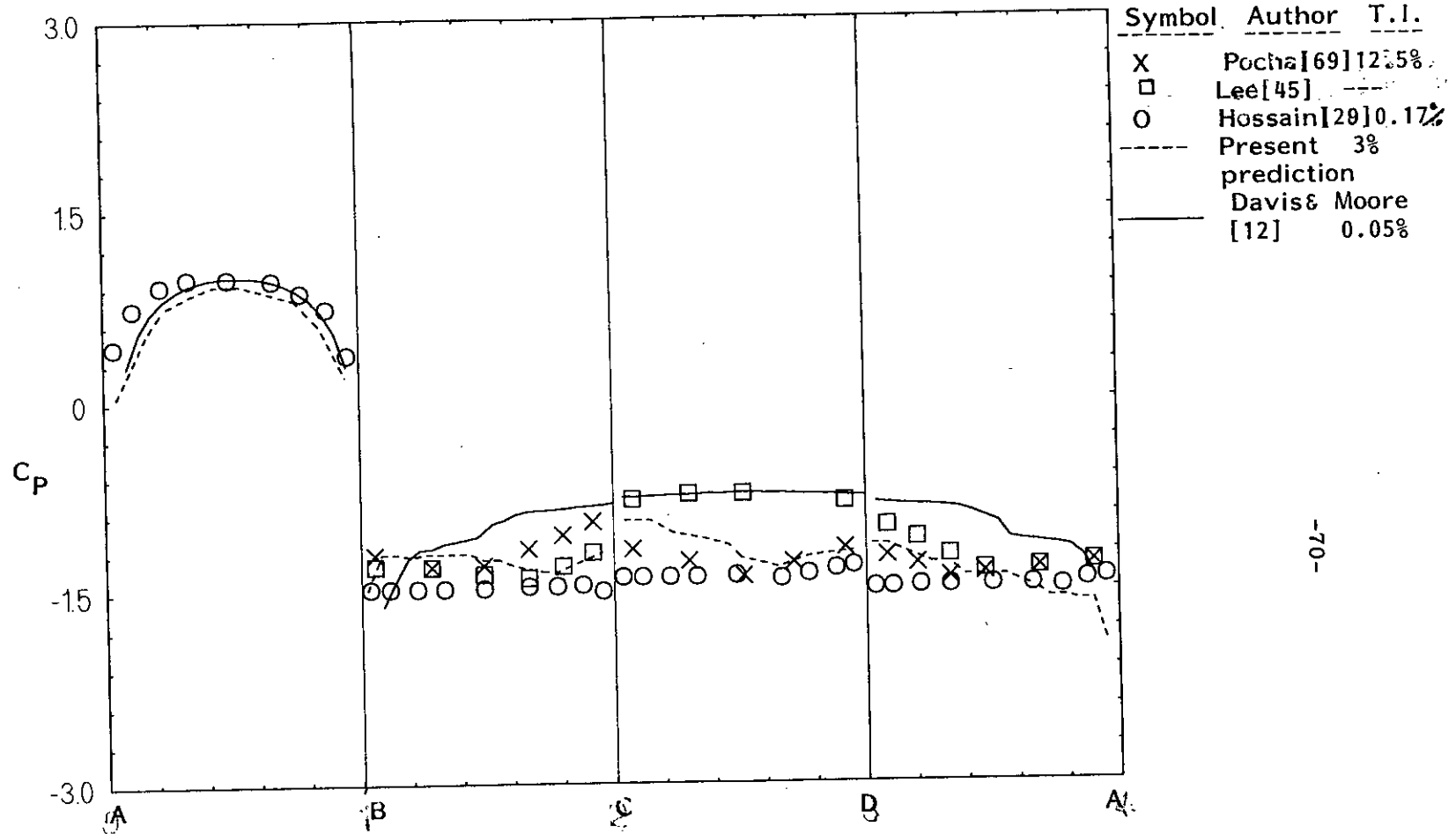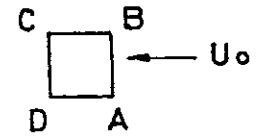
Fig. 5.1: Comparison of C_P-distribution on a square cylinder

$$\Delta U / \Delta U_{max} = [1-(y/b)^{3/2}]^2$$
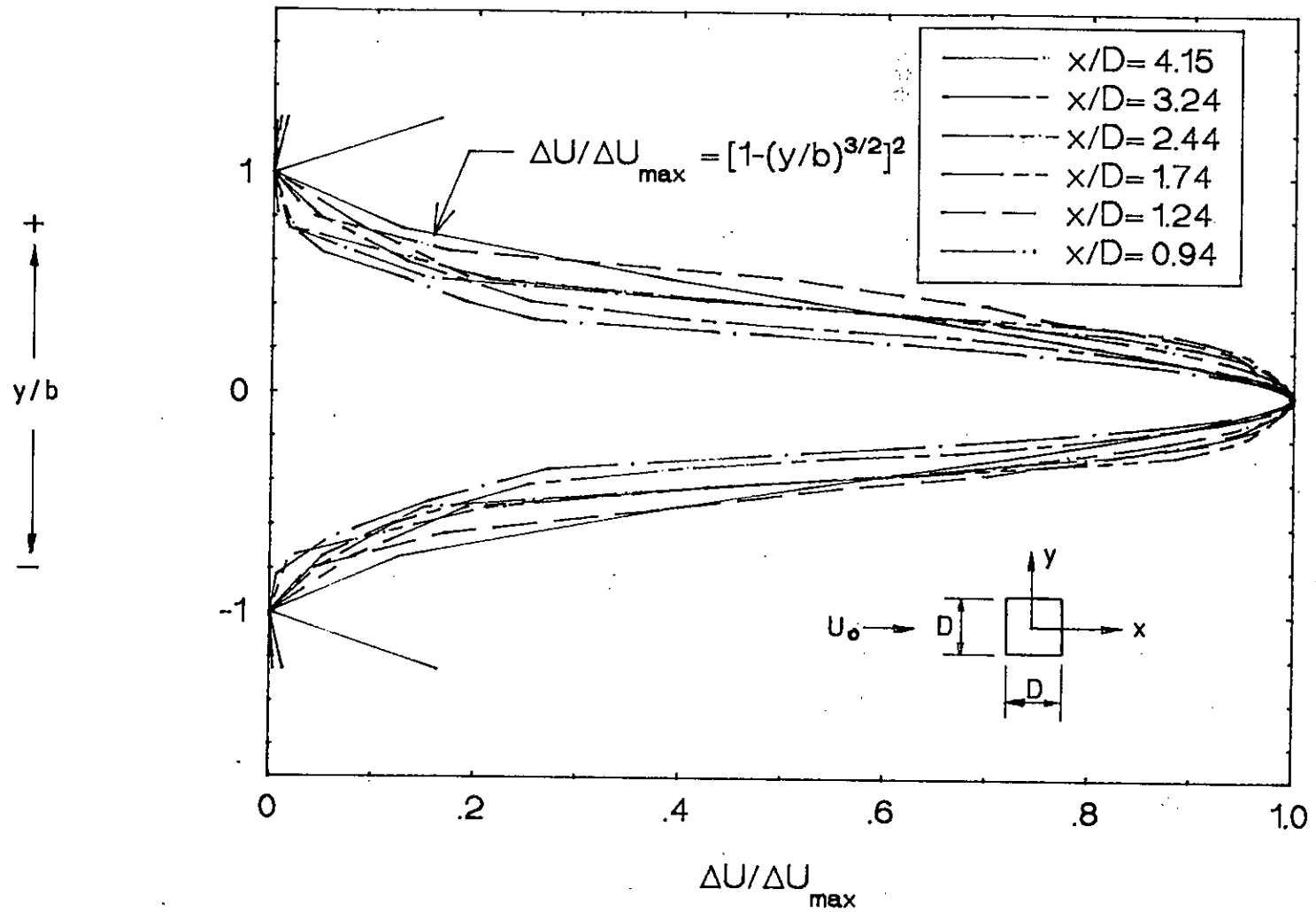
Fig. 5.2 : Velocity defect distribution in a two-dimensional wake behind
a square cylinder.
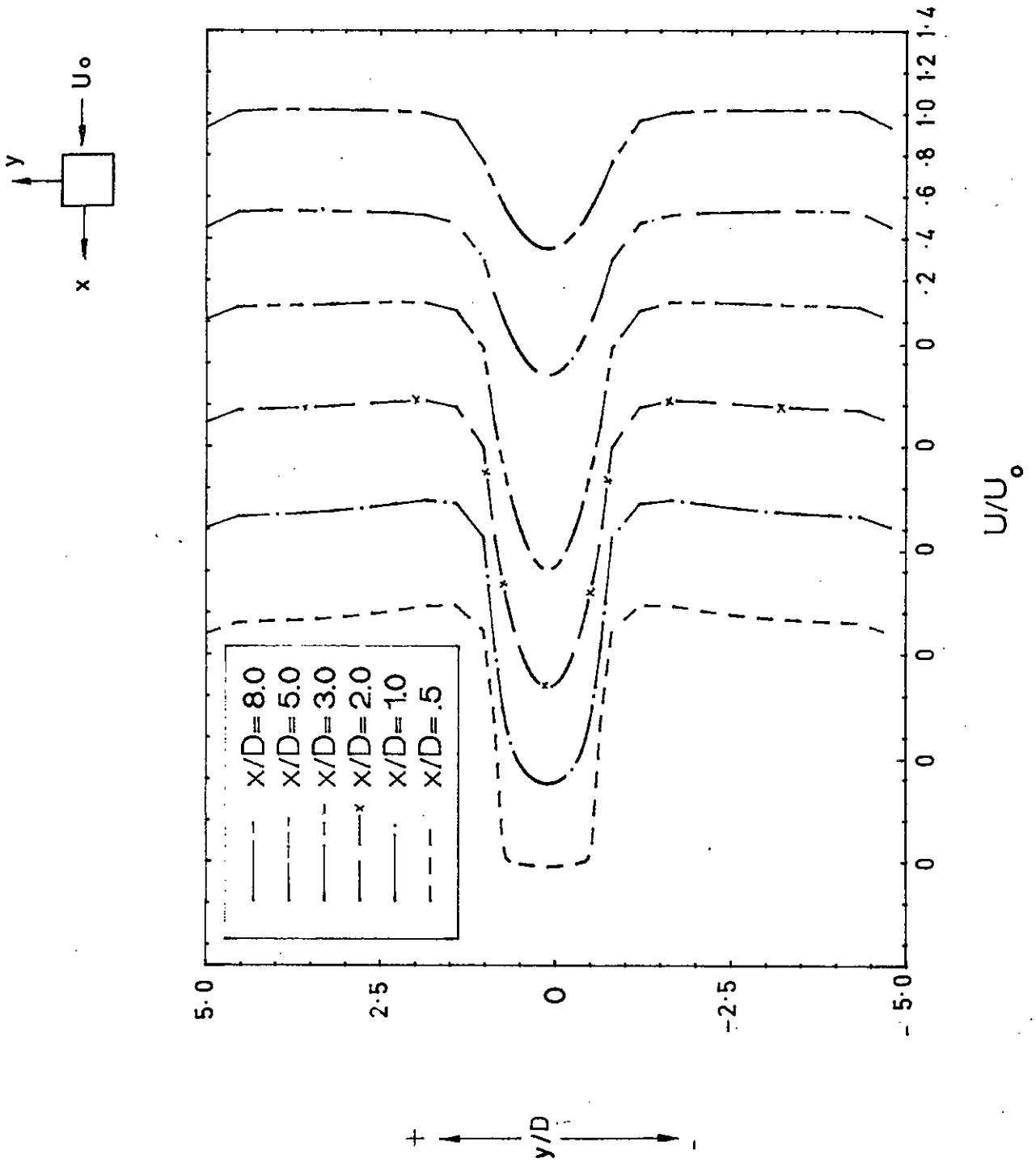
Fig. 5.3 : Mean velocity distribution in a wake behind square cylinder.
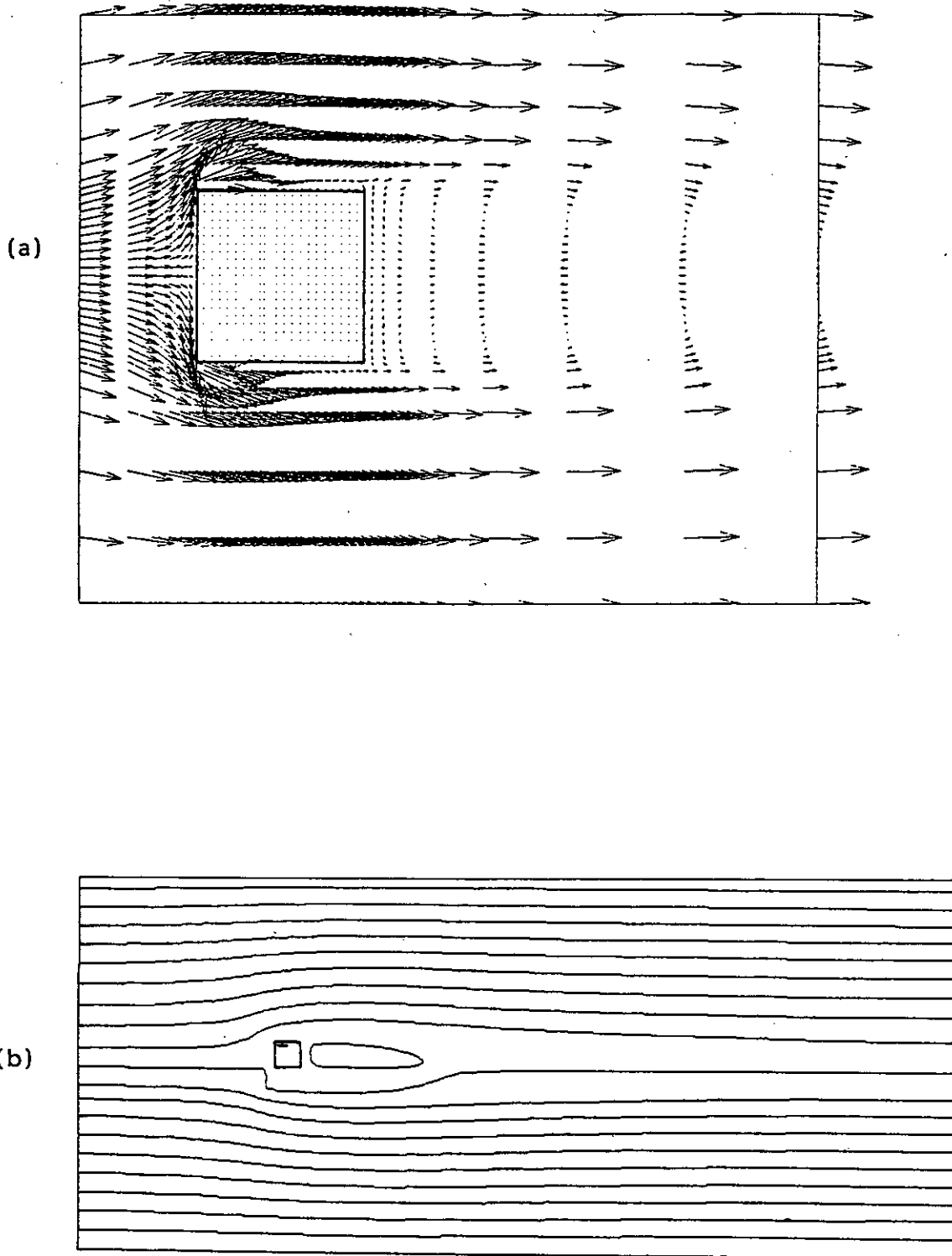
Fig. 5.4 : (a) Velocity field (b) Stream function contour for single cylinder
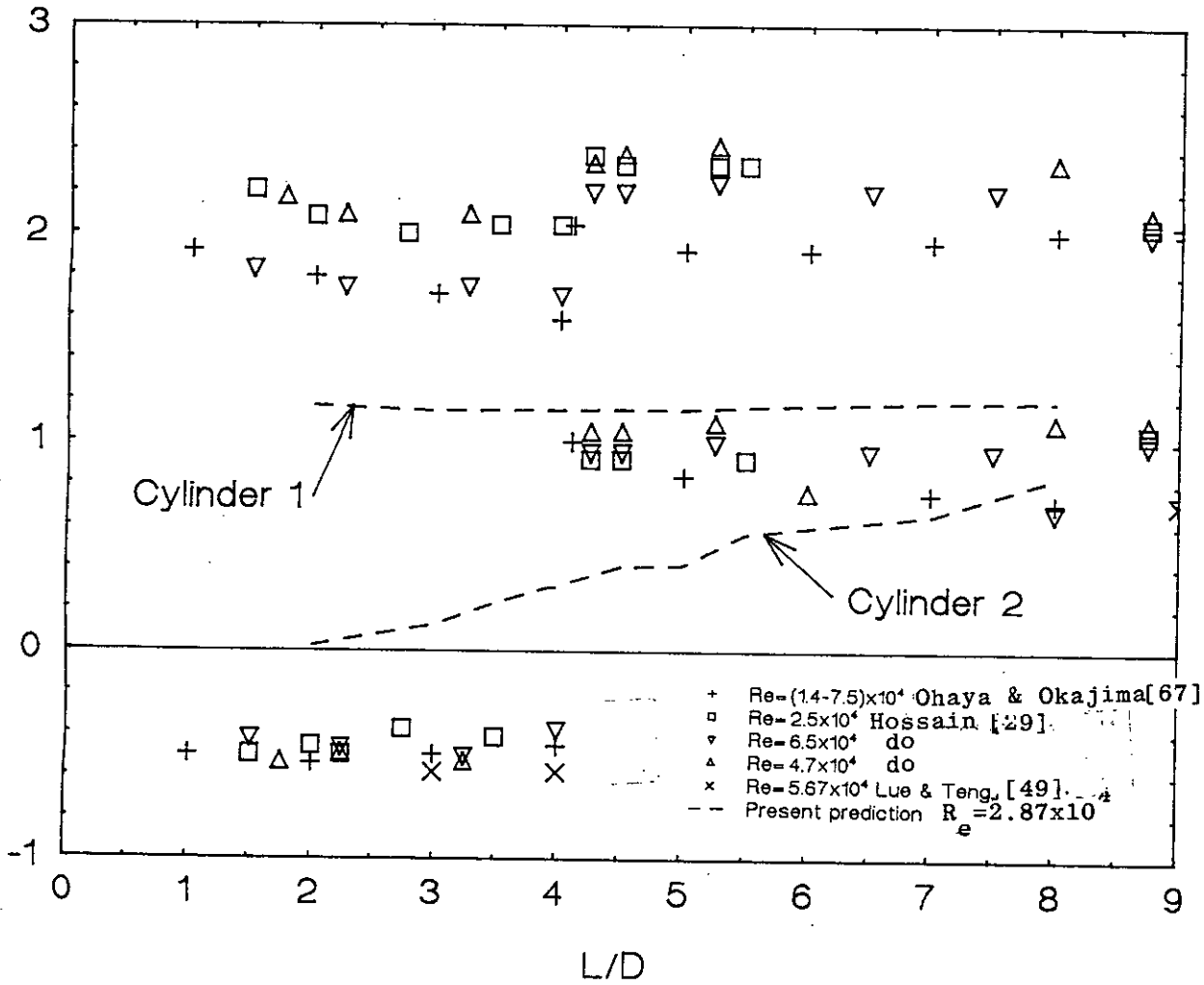
Fig. 5.5 : Comparison of drag co-efficient of the two tandem square
cylinders for d/D = 1.0

(a)

(b)
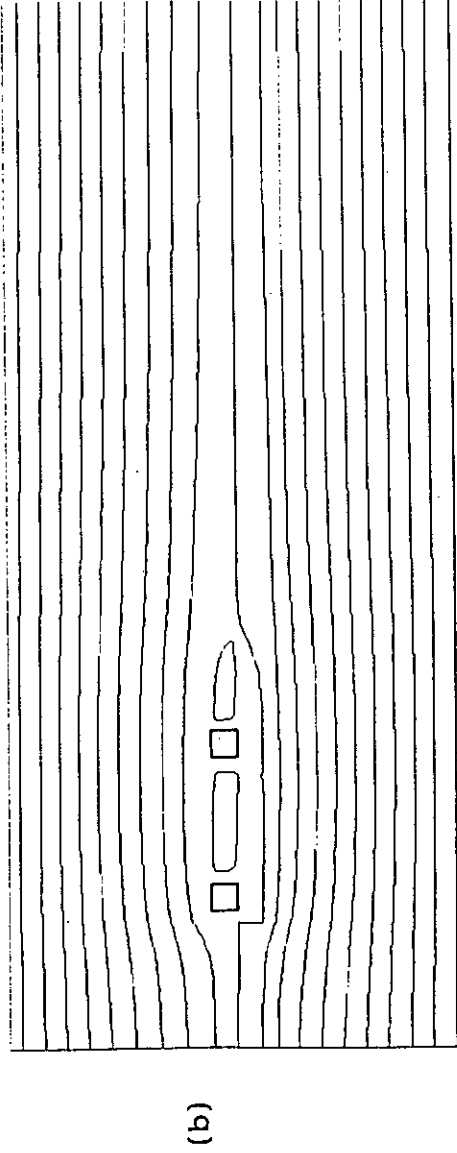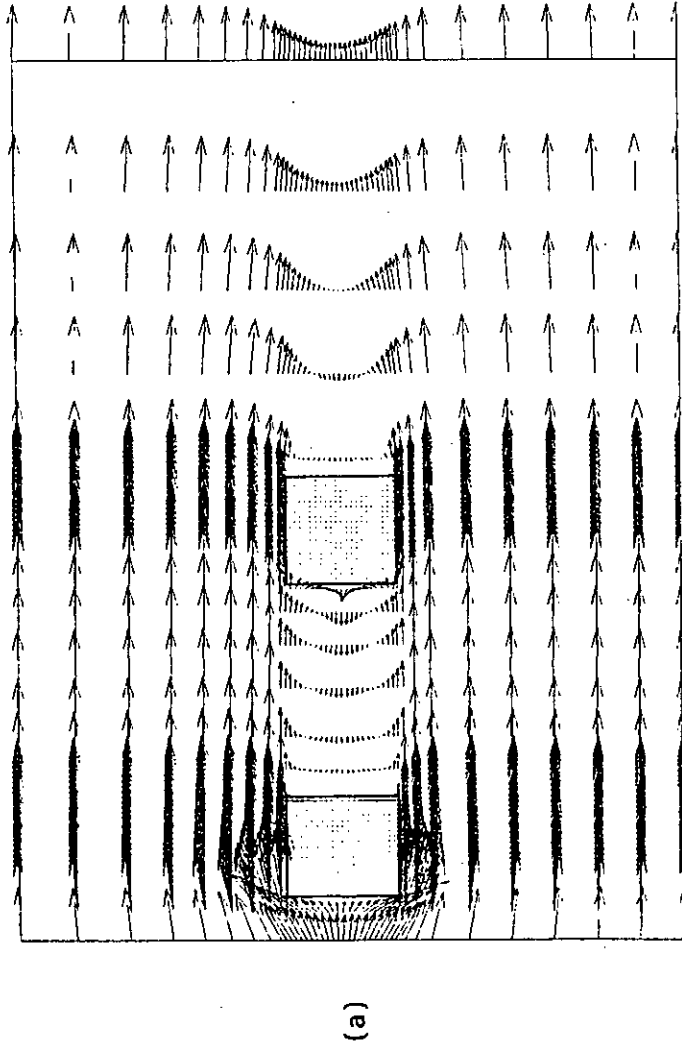
Fig. 5.6 : (a) Velocity field (b) Stream function contour for tandem cylinder of d/D=1.0 and L/D=3.0
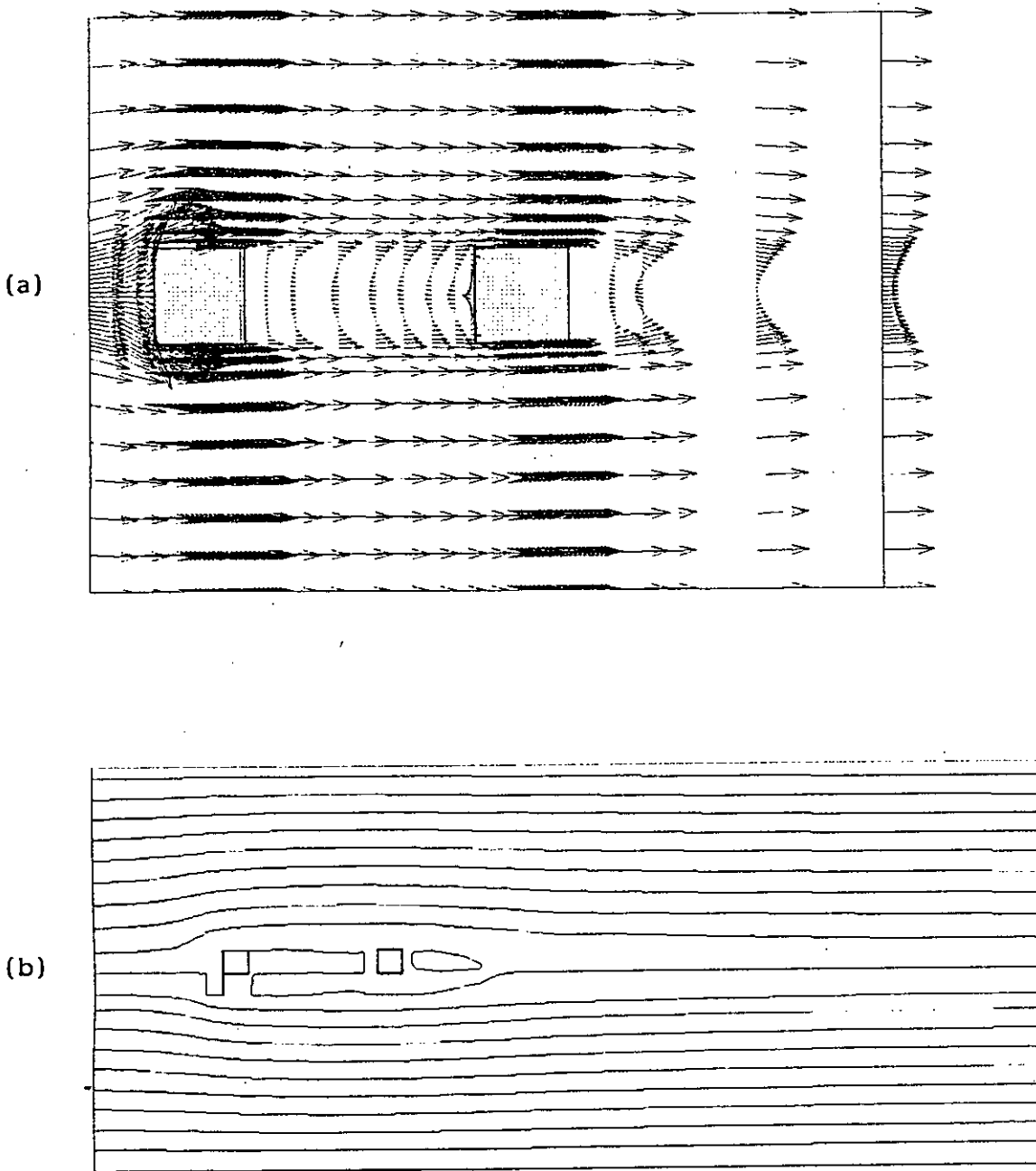
Fig.5.7:(a) Velocity field (b) Stream function contour for tandem cylinder of d/D=1·0 and L/D=3·5
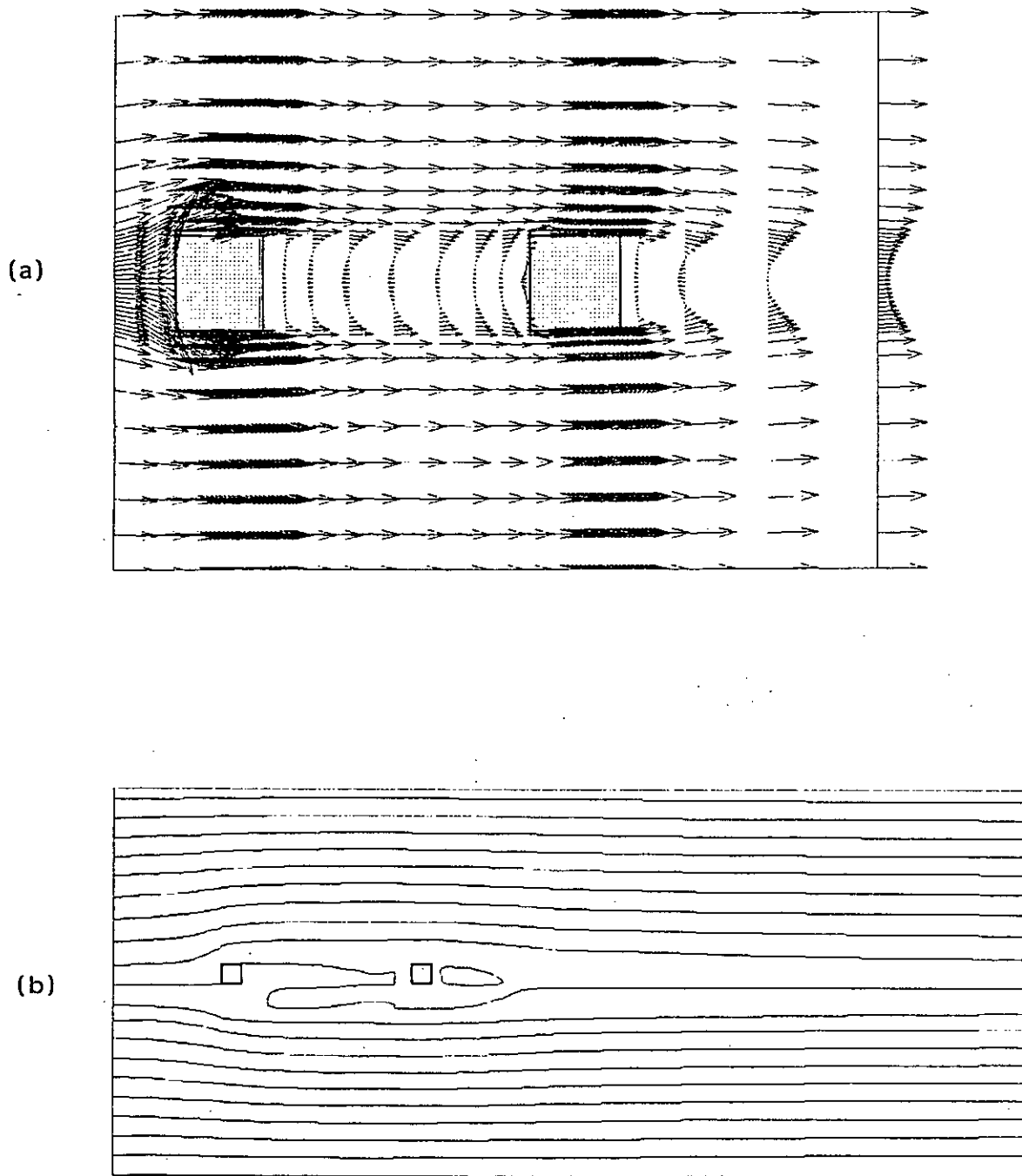
Fig. 5.8 : (a) Velocity field (b) Stream function contour for tandem cylinder of d/D=1·0 and L/D = 4·0
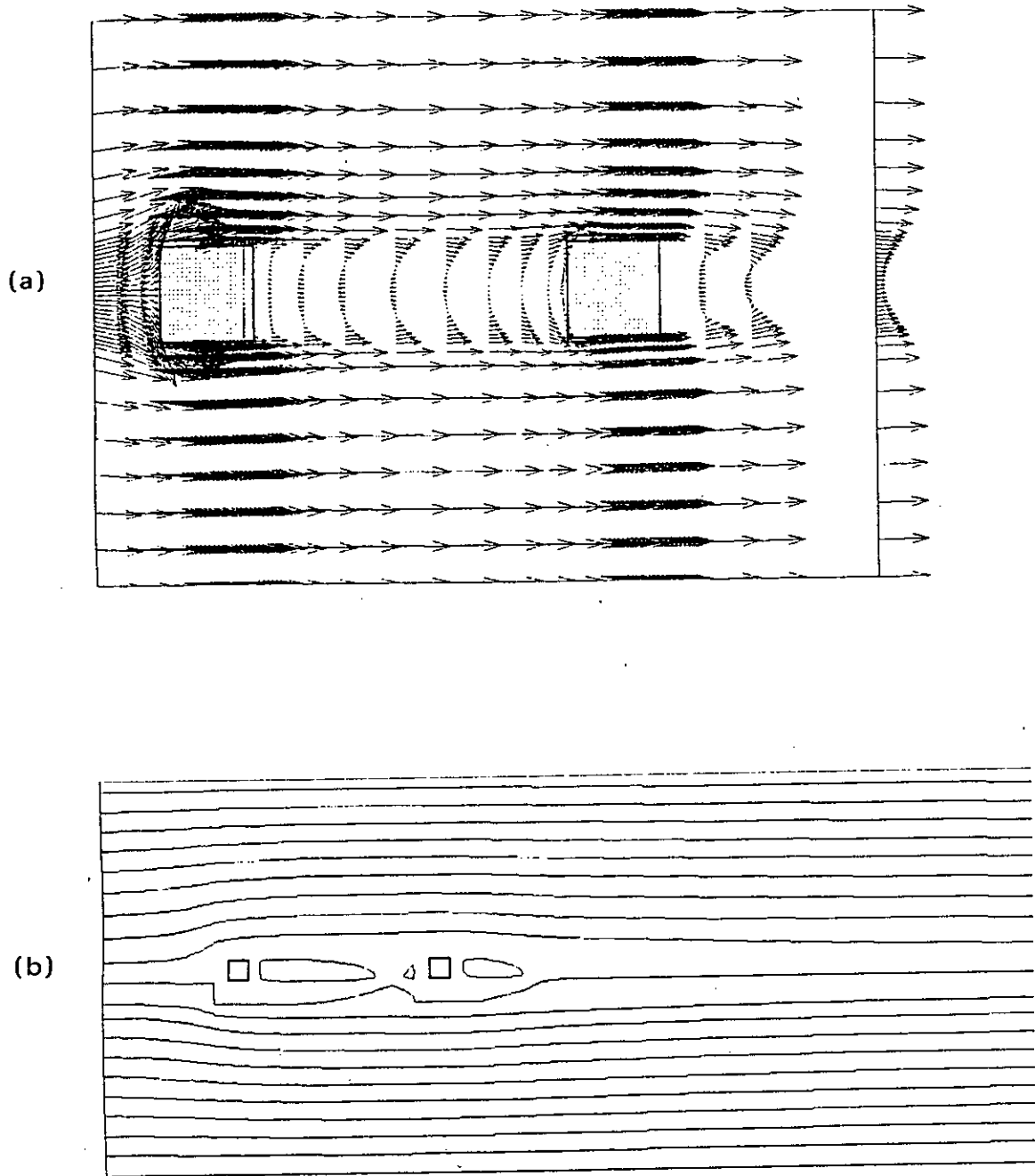
Fig. 5.9: (a) Velocity field (b) Stream function contour for tandem cylinder of $d/D = 1.0$ and $L/D = 4.5$

(a)

(b)
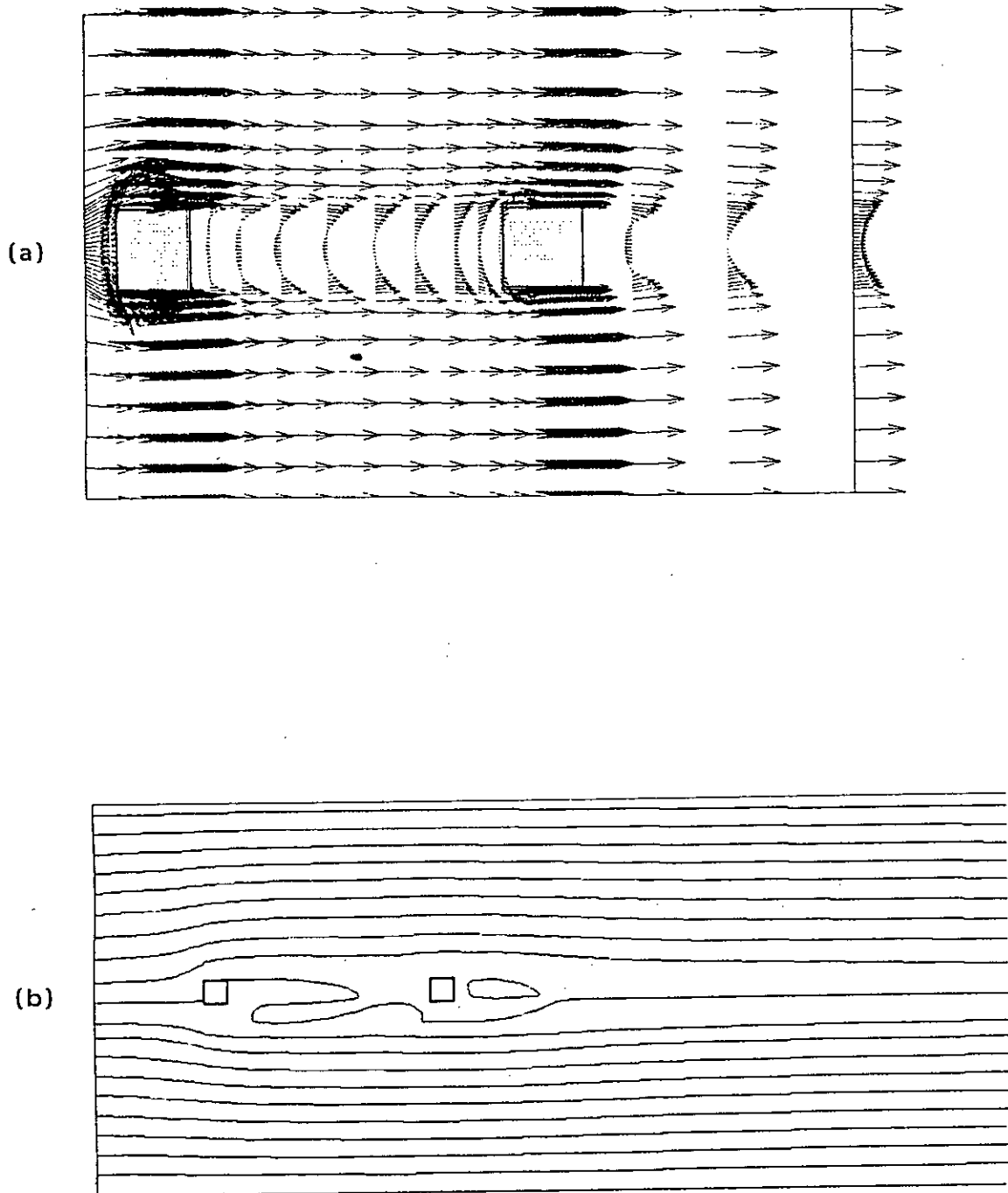
Fig.5.10:(a) Velocity field (b) Stream function contour for
tandem cylinder of d/D = 1·0 and L/D = 5·0
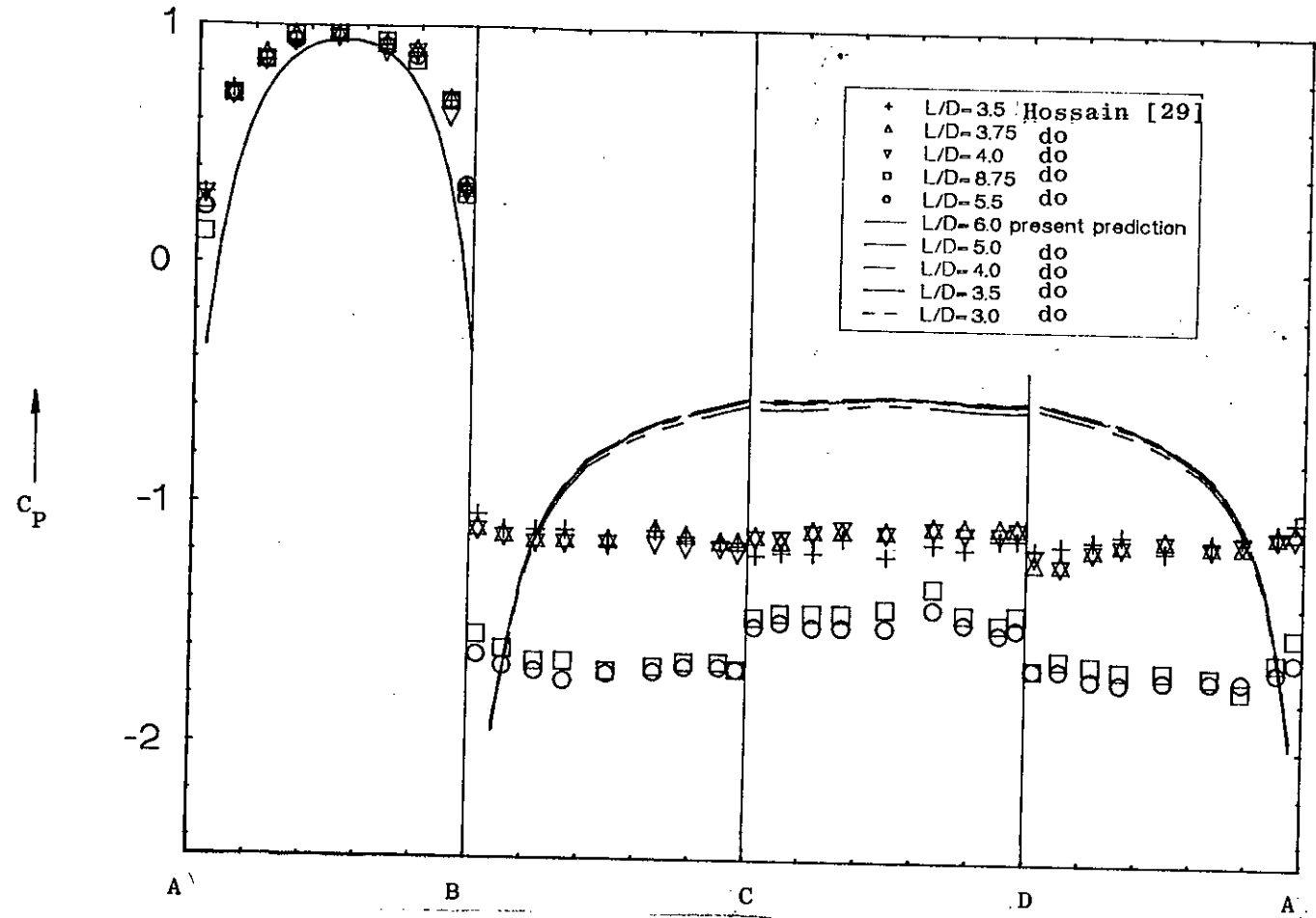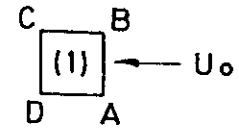
Fig. 5.11 : Effect of L/D on C_p- distribution around front cylinder for d/D = 1.0
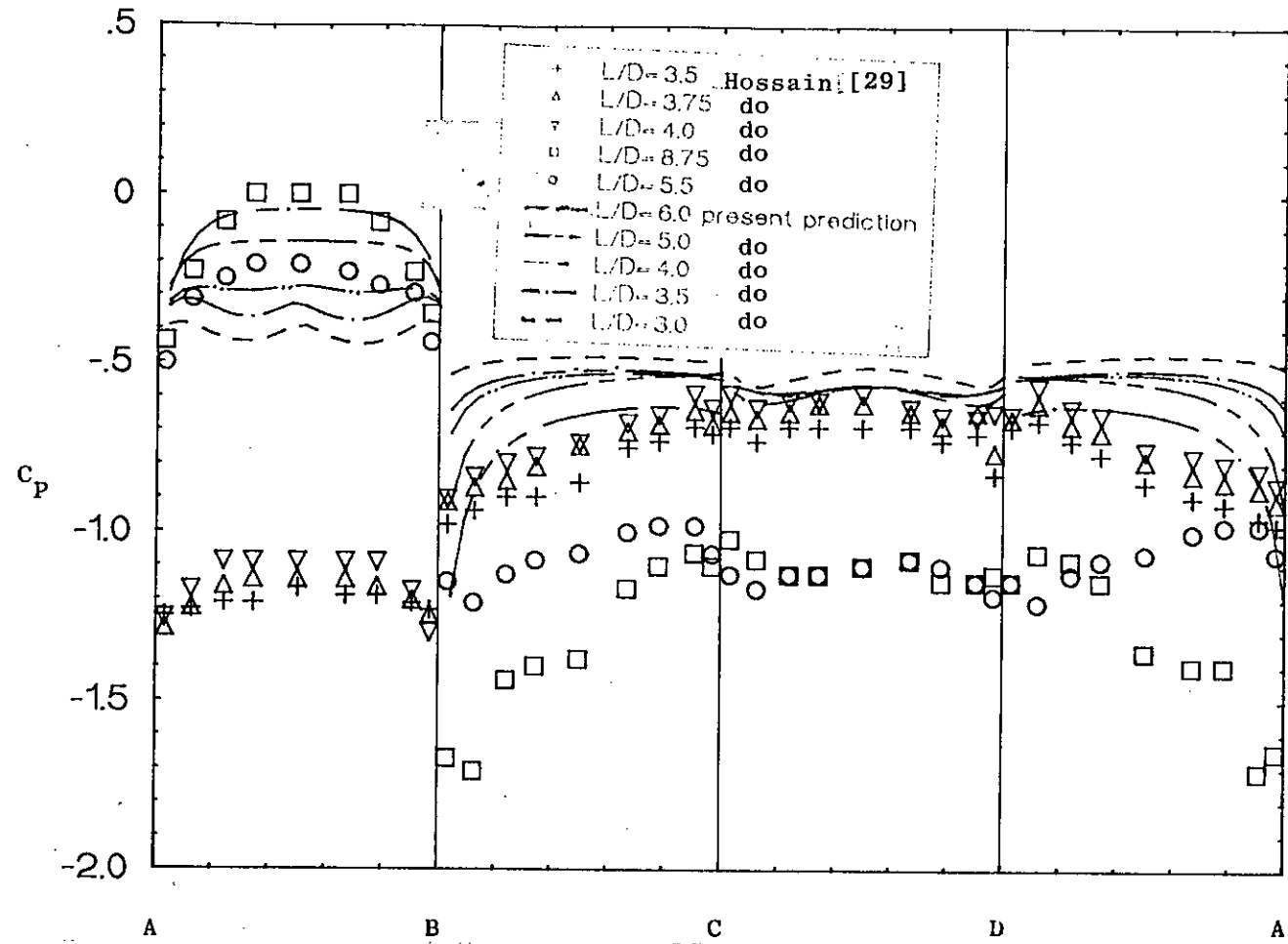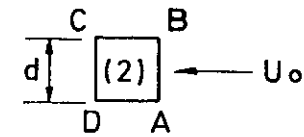
Fig. 5. 12 : Effect of L/D on C_p- distribution around rear cylinder for d/D = 1.0
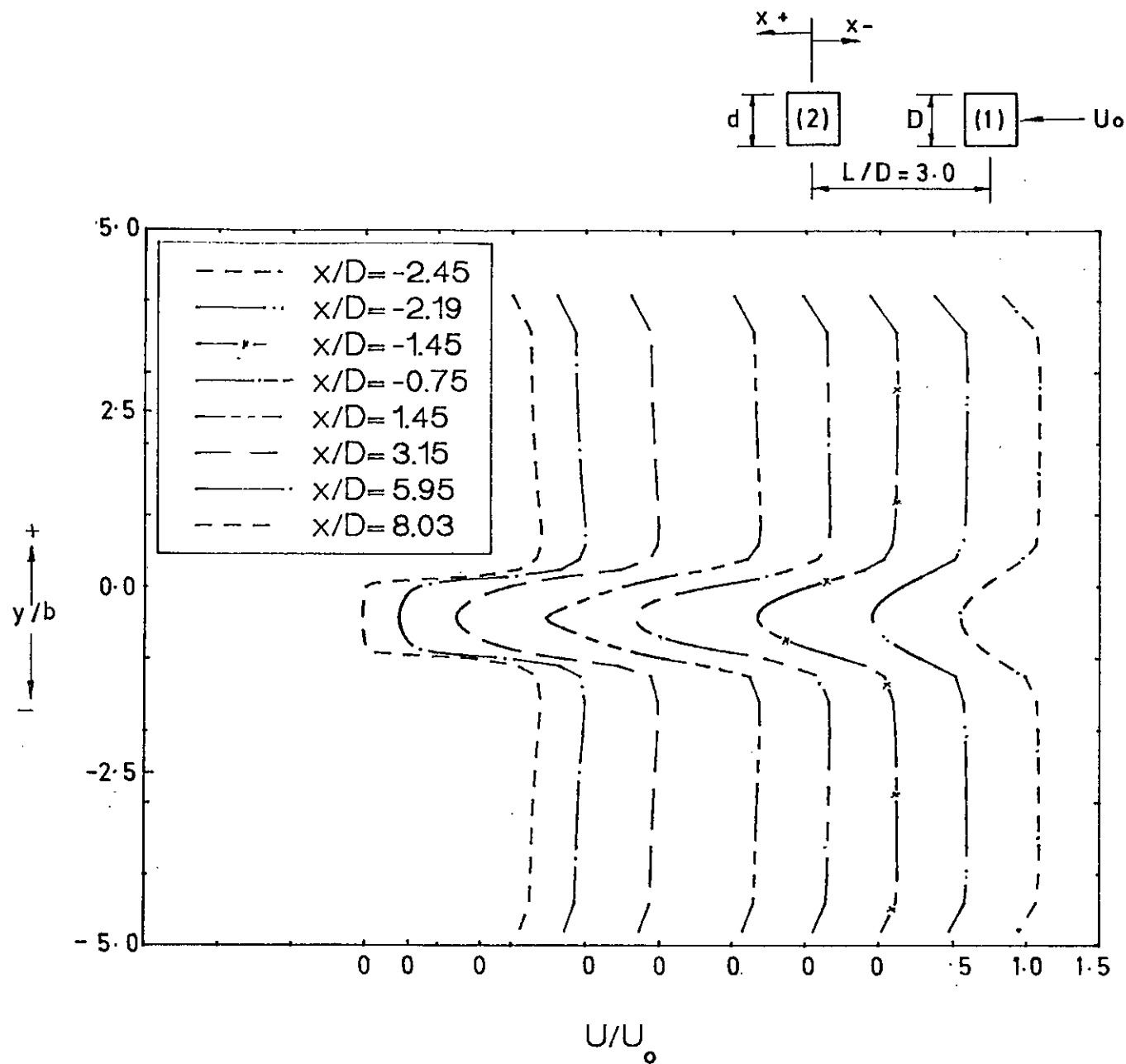
Fig. 5.13 : Mean velocity distribution in wakes behind the cylinders of
d/D = 1.0 for L/D = 3.0
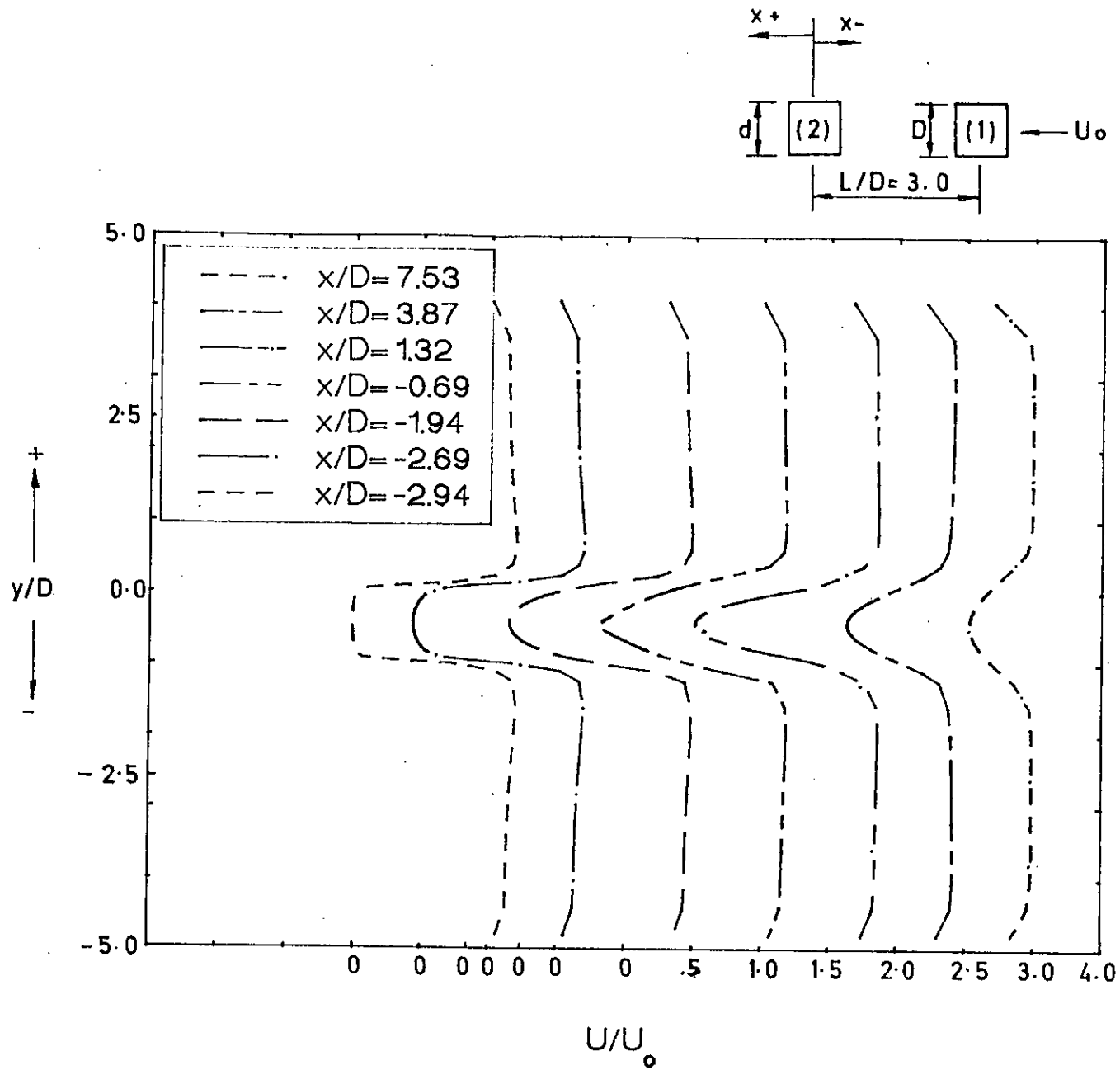
Fig. 5.14 : Mean velocity distribution in wakes behind the cylinders of
d/D = 1.0 for L/D = 3.5
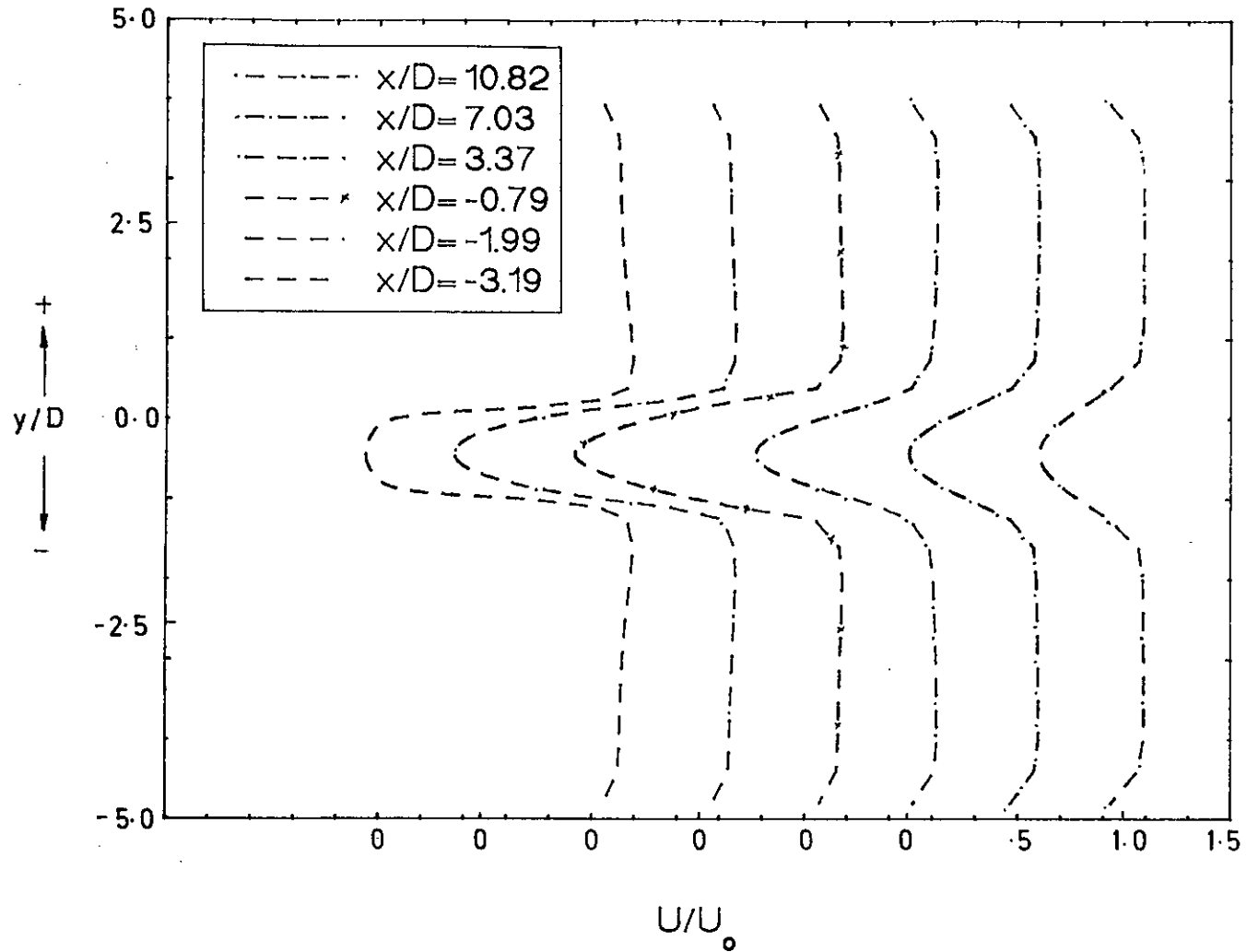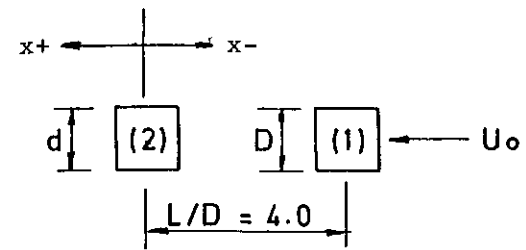
Fig. 5.15 : Mean velocity distribution in wakes behind the cylinders of
d/D = 1.0 for L/D = 4.0
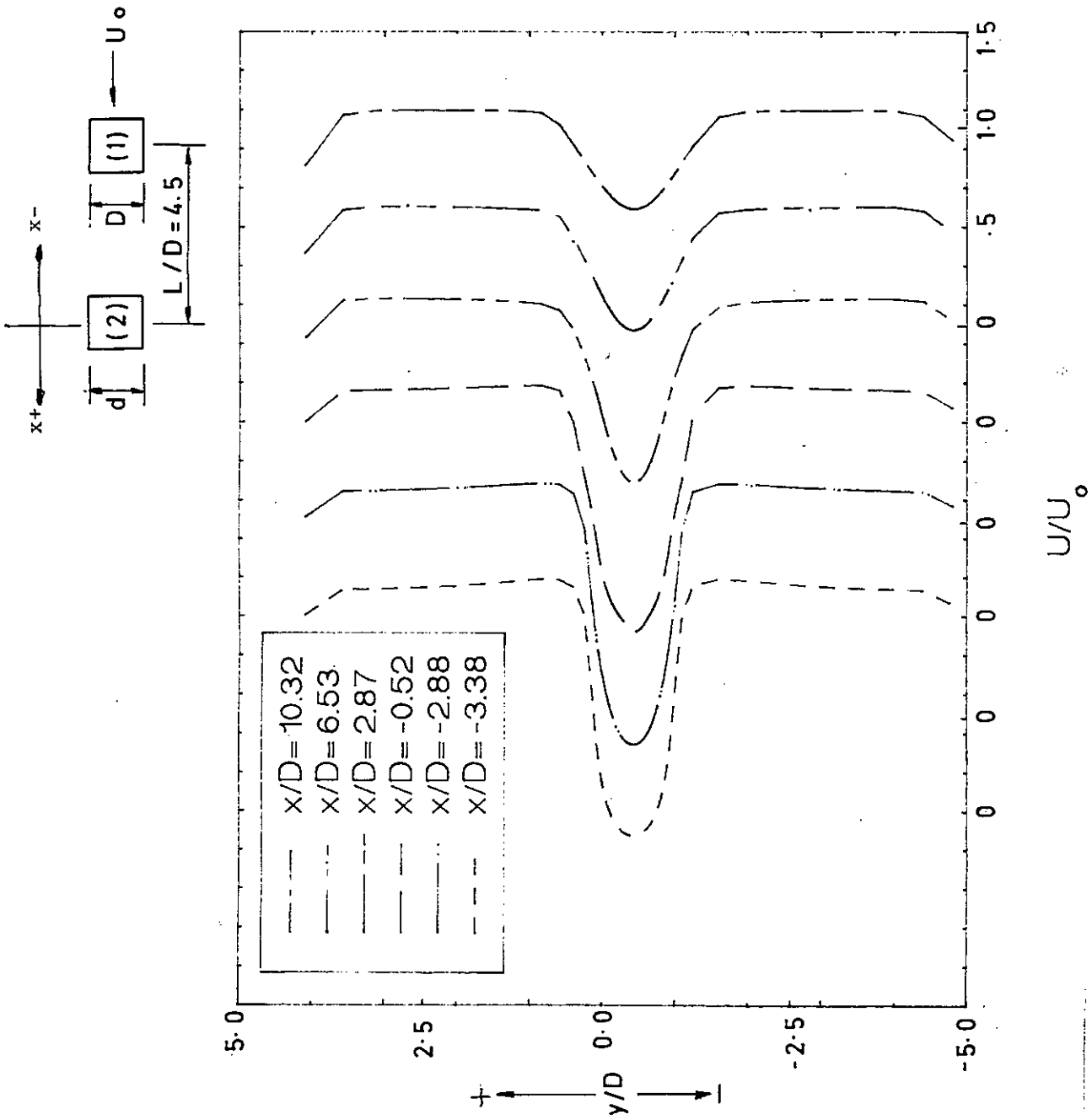
Fig. 5.16 : Mean velocity distribution in wakes behind the cylinders of d/D = 1.0 for L/D = 4.5
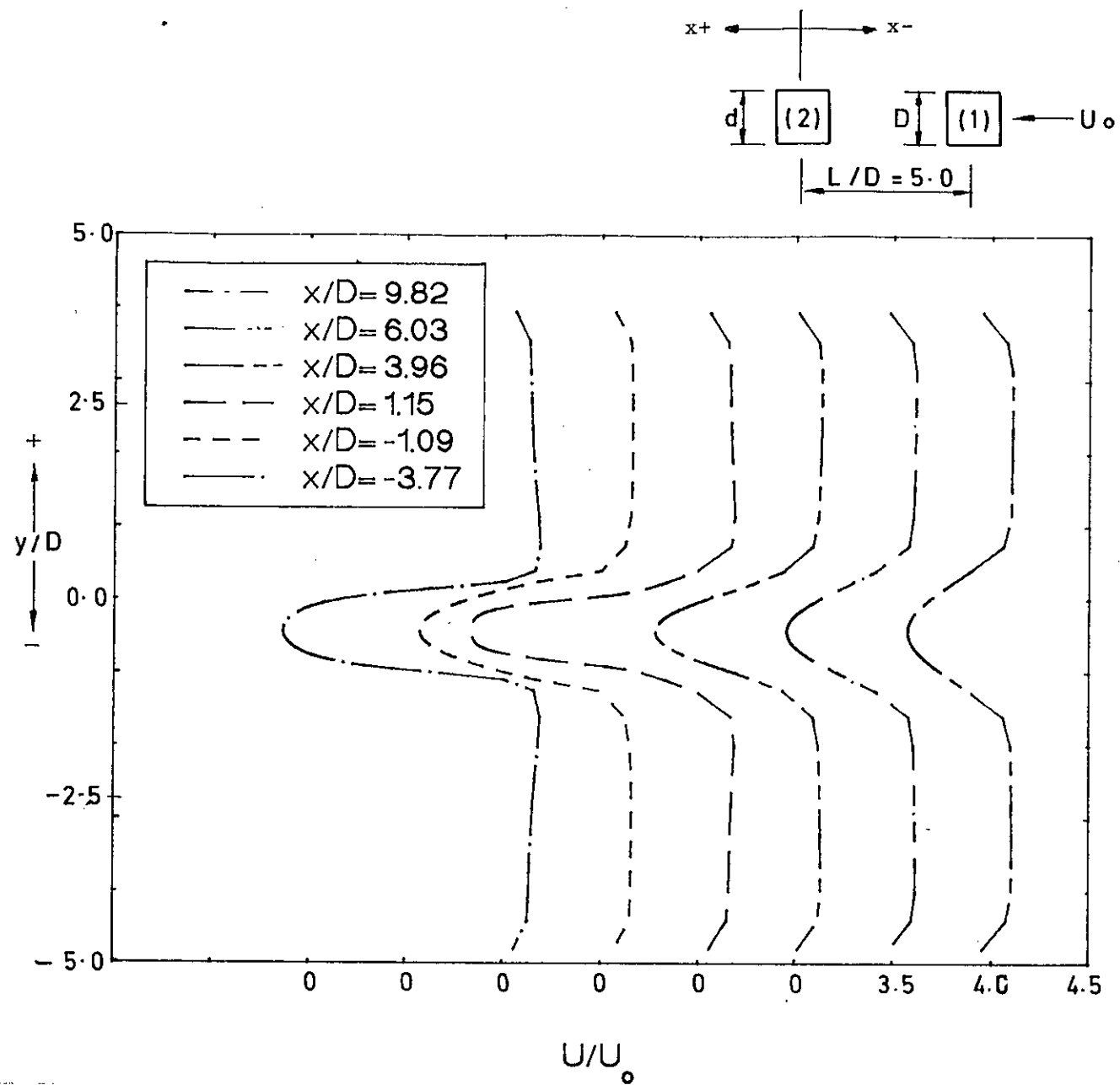
Fig. 5.17 : Mean velocity distribution in wakes behind the cylinders of
d/D = 1.0 for L/D = 5.0

X/D	Symbol	L/D
0.75	□	3.5
1.0	+	3.5
1.5	▽	4.0
0.56	— — —	4.0
0.81	··· ···	4.0
0.56	—·—·—	3.5
0.81	—··—··—	3.5
0.56	··········	3.0
0.81	—·—·—	3.0
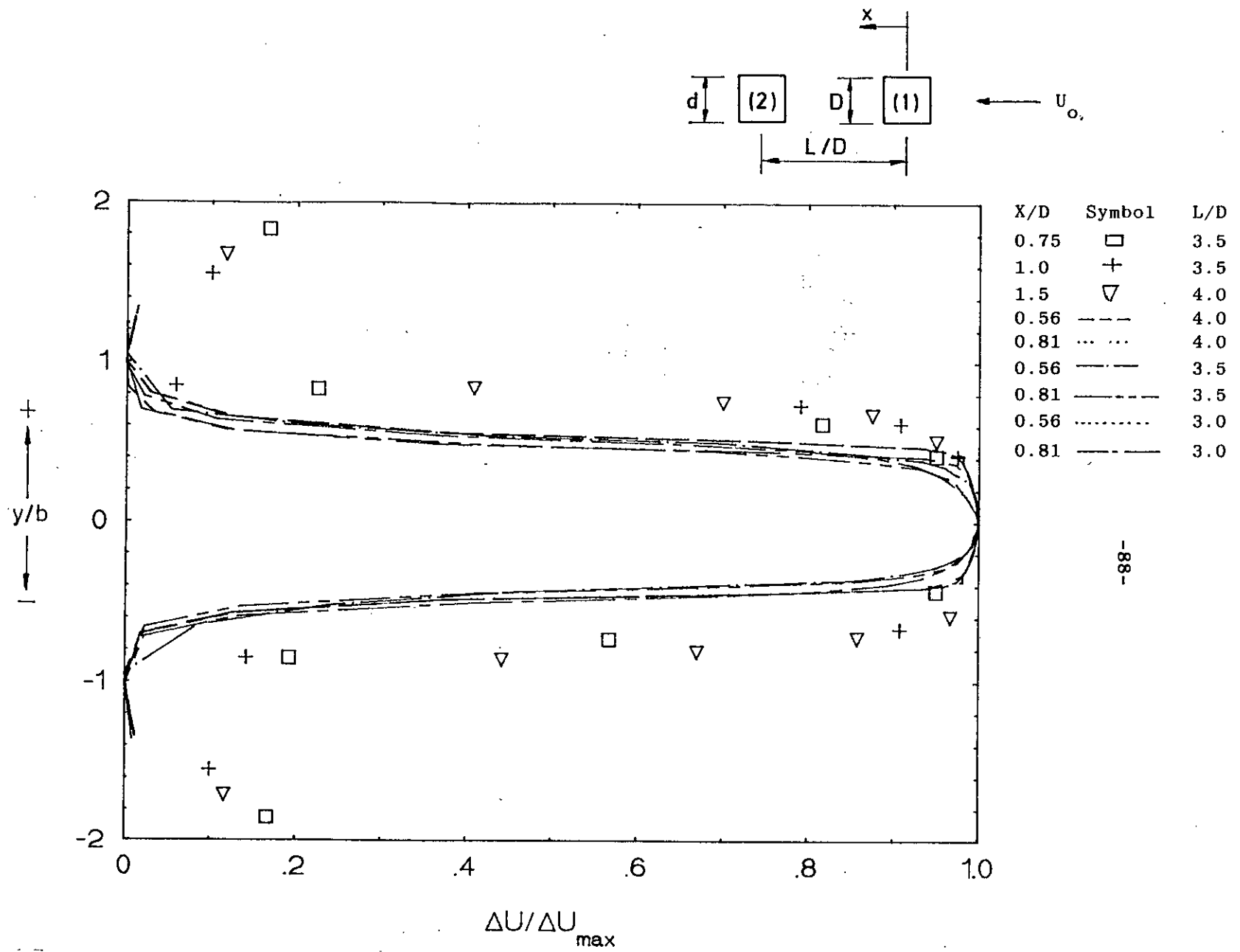
Fig. 5.18 : Velocity defect distribution behind front cylinder of d/D = 1.0
for L/D = 3.0 to 4.0
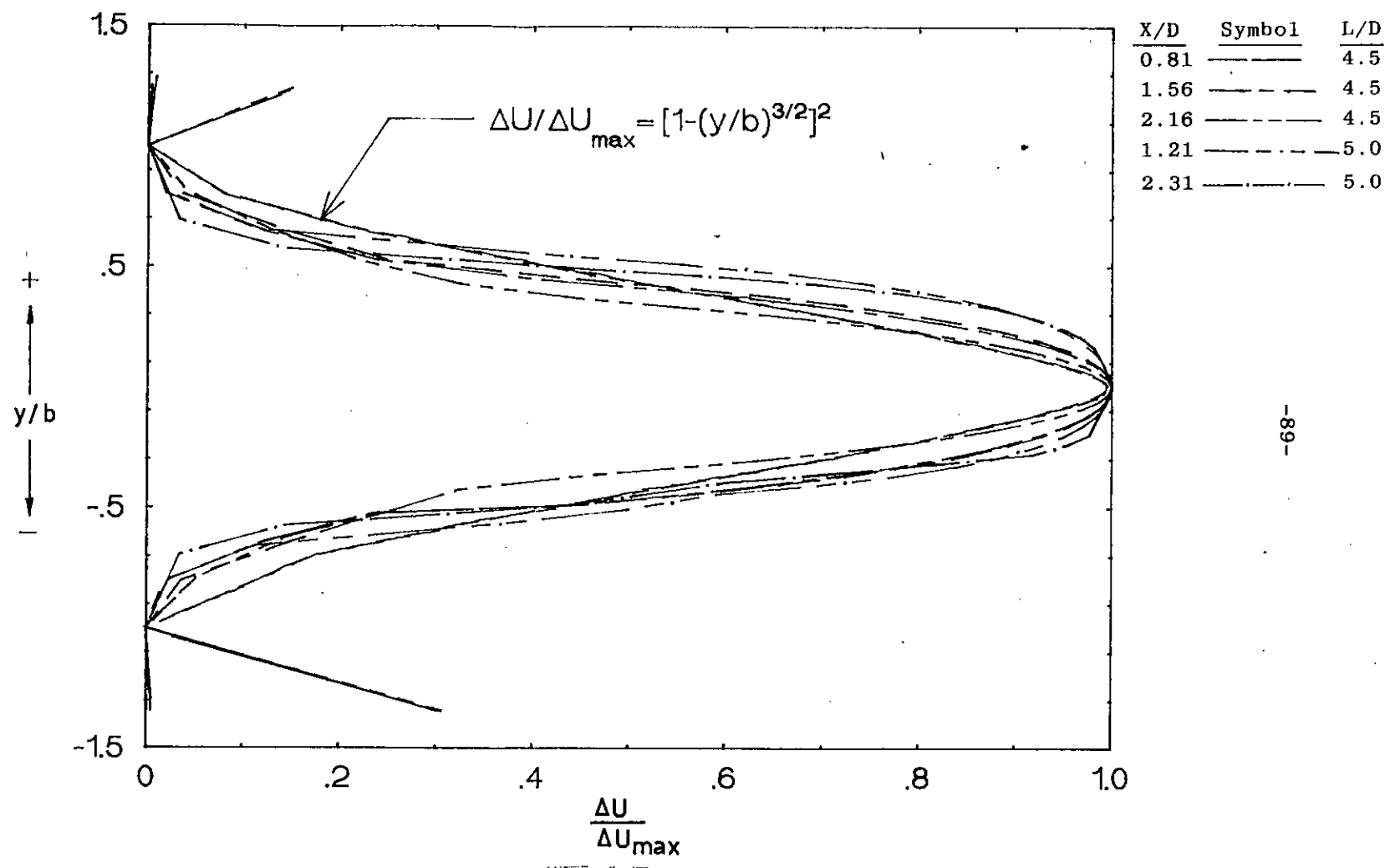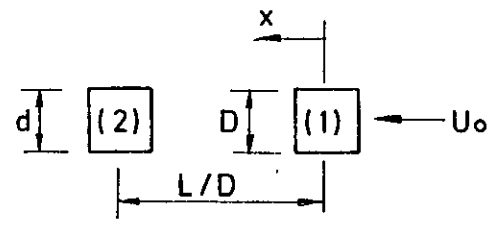
Fig. 5.19 : Velocity defect distribution behind front cylinder of d/D = 1.0
for L/D > 4.0
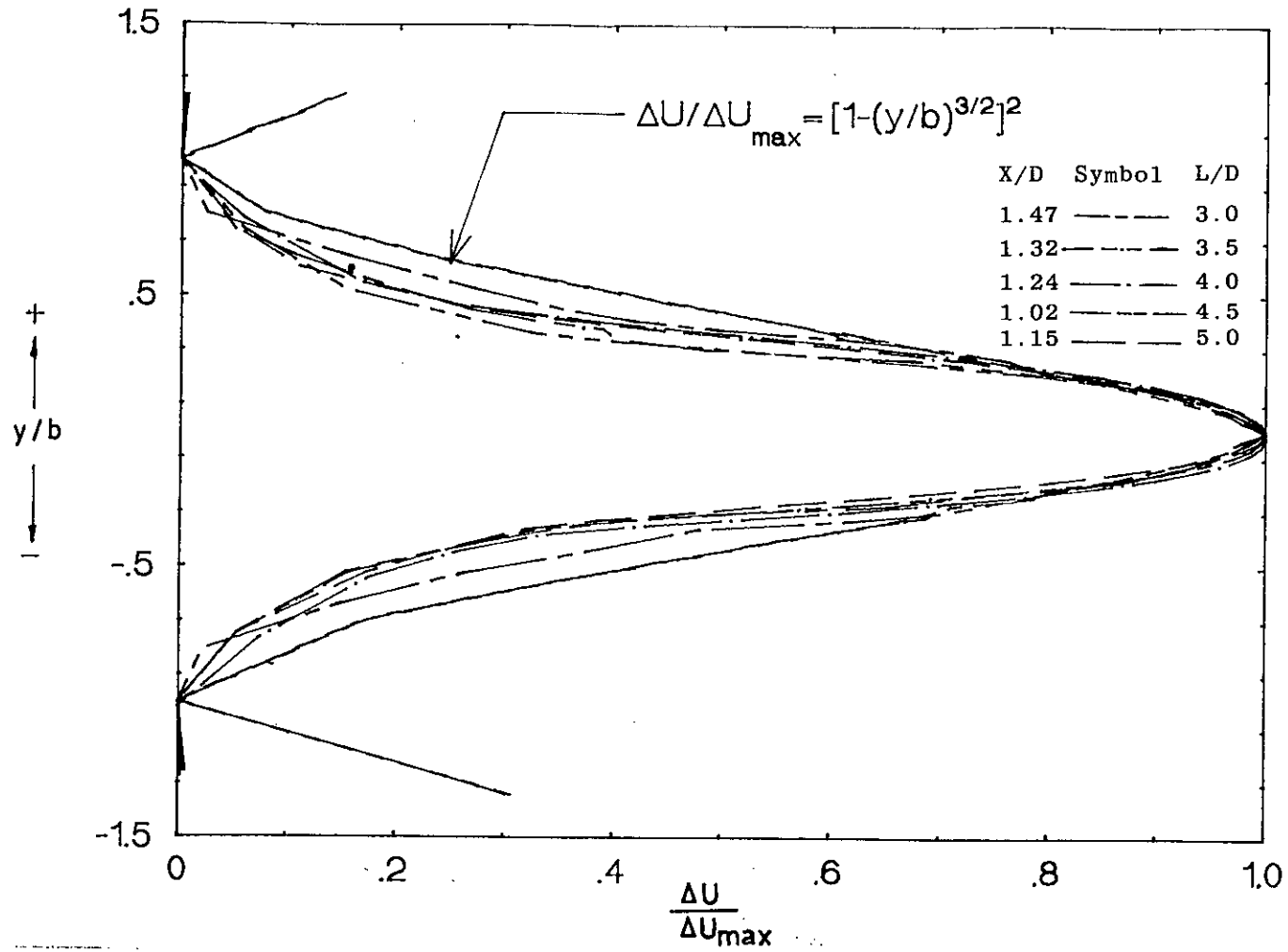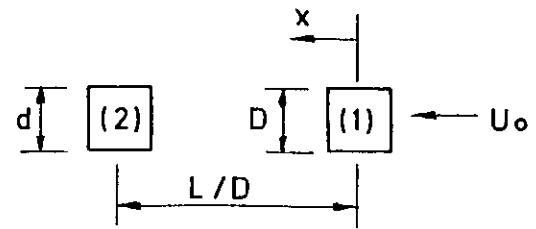
Fig. 5.20 : Velocity defect distribution behind rear cylinder of d/D = 1.0
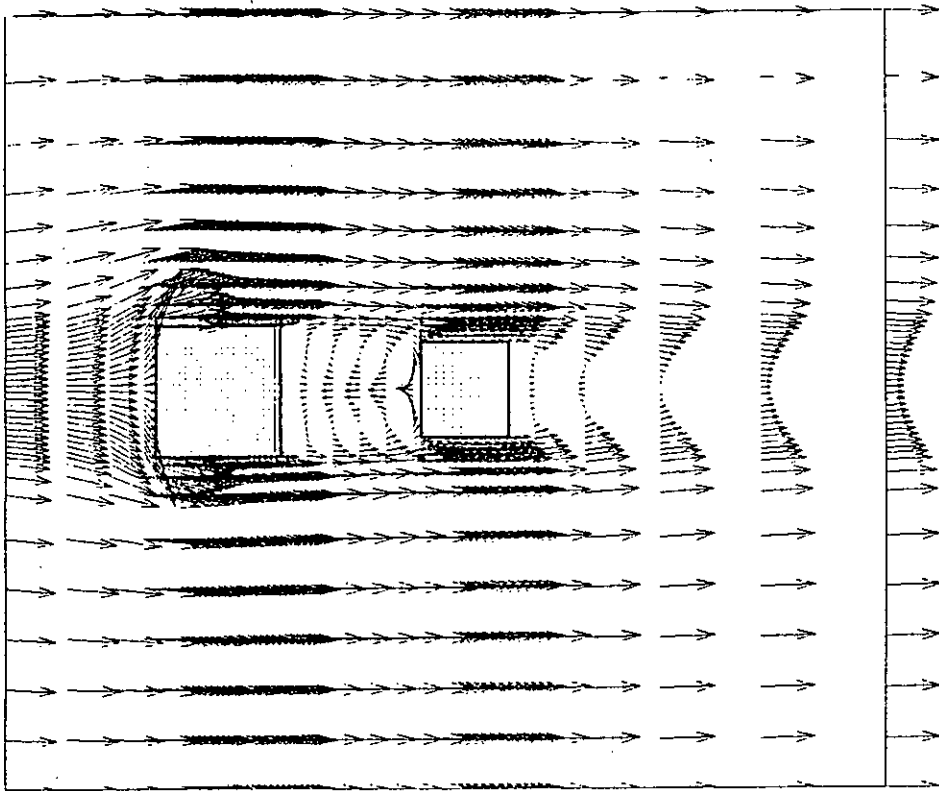for L/D = 3.0 to 5.0
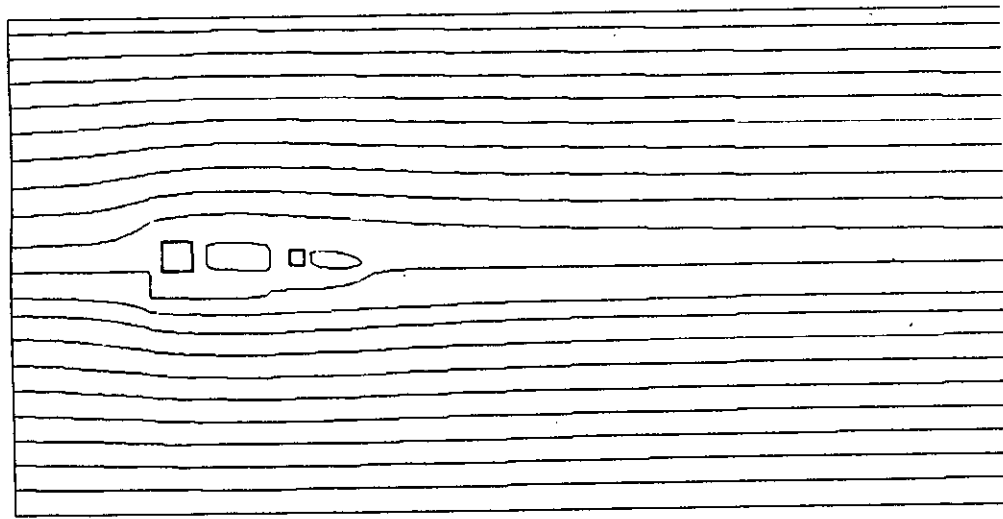
Fig. 5.22 : (a) Velocity field (b) Stream function contour for tandem cylinder of d/D = 0·7 and L/D = 2·0

(a)

(b)
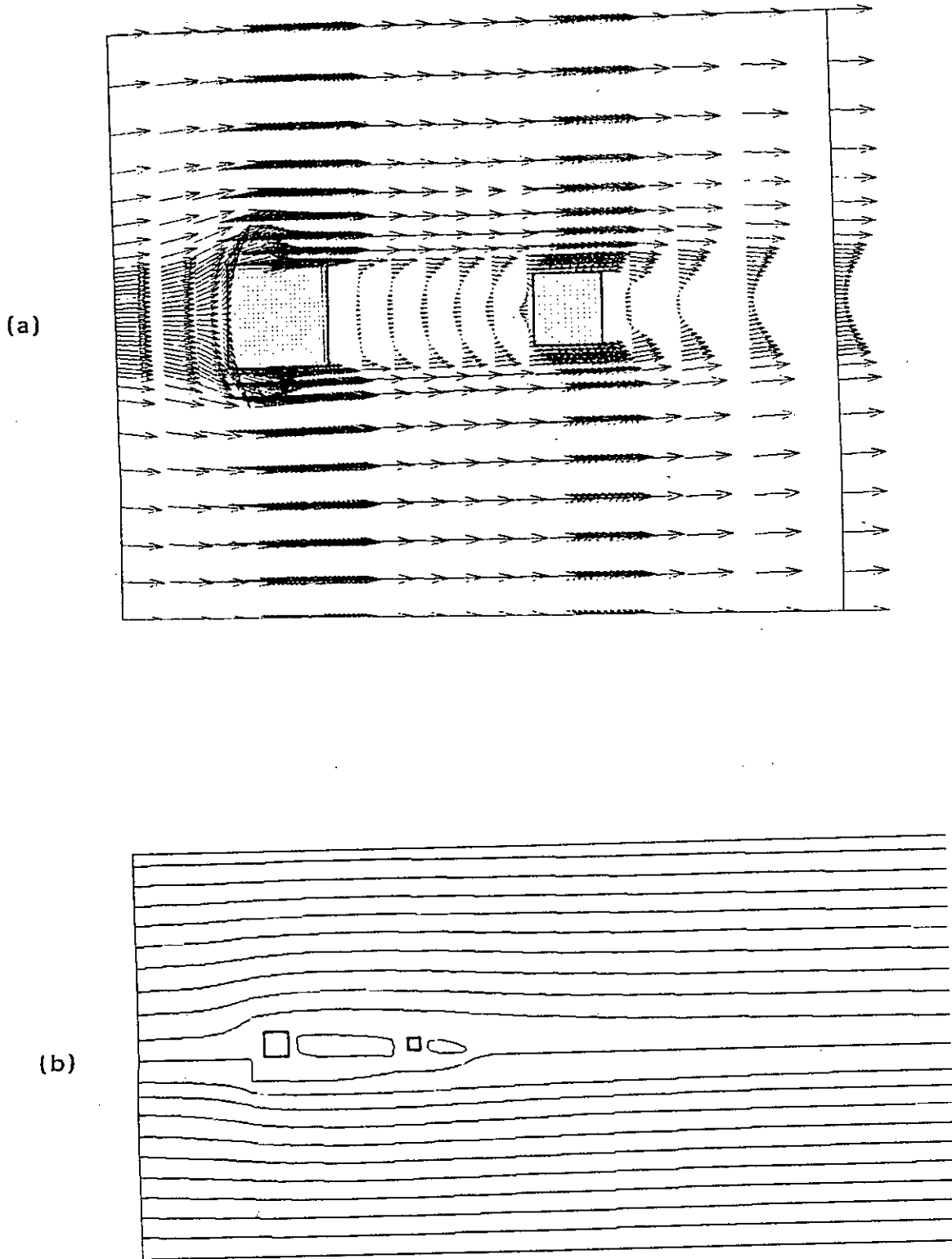
Fig. 5.23 : (a) Velocity field (b) Stream function contour for
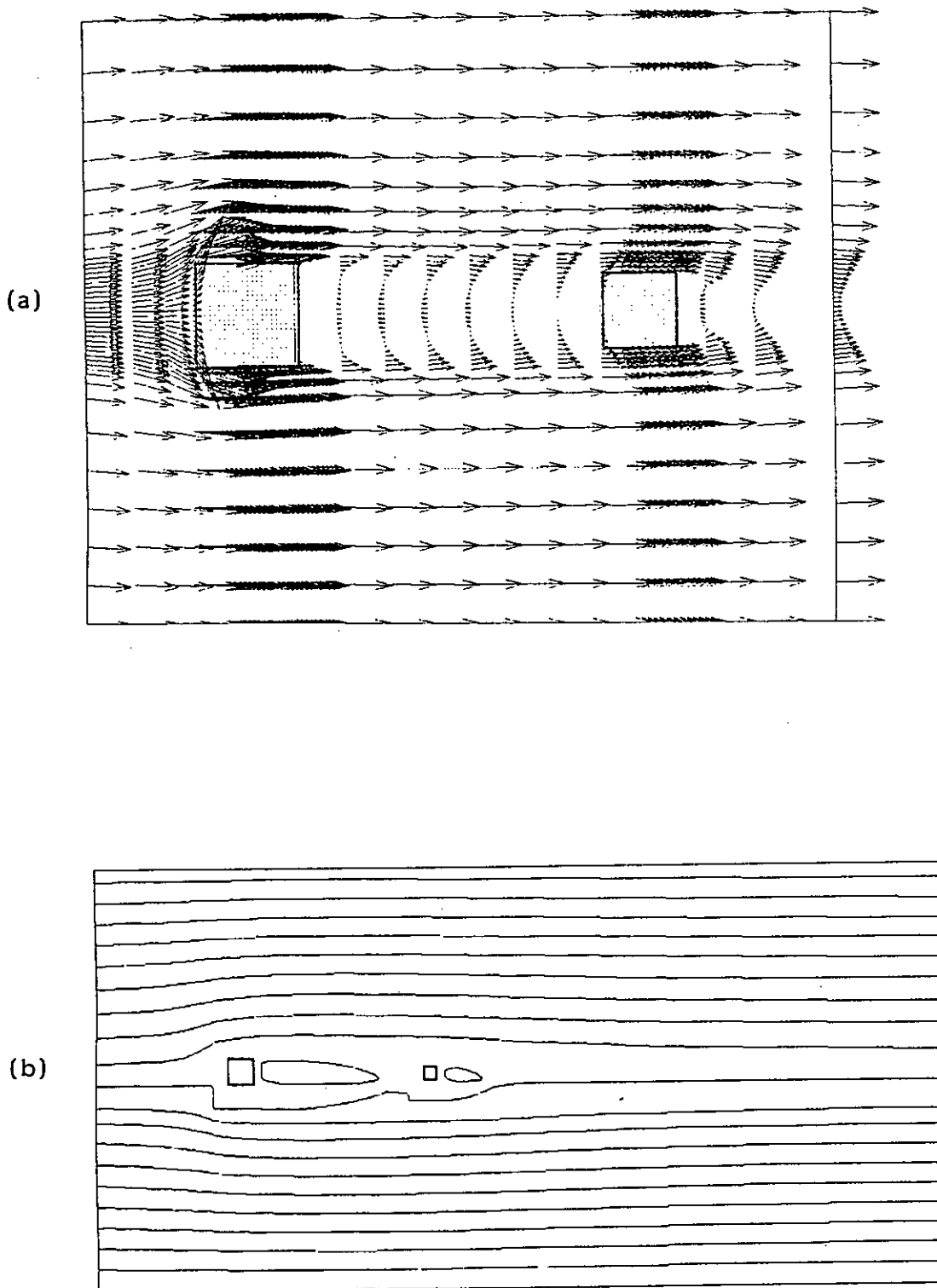tandem cylinder of d/D = 0.7 and L/D = 3.0 .

(a)

(b)

Fig. 5.24 : (a) Velocity field (b) Stream function contour for
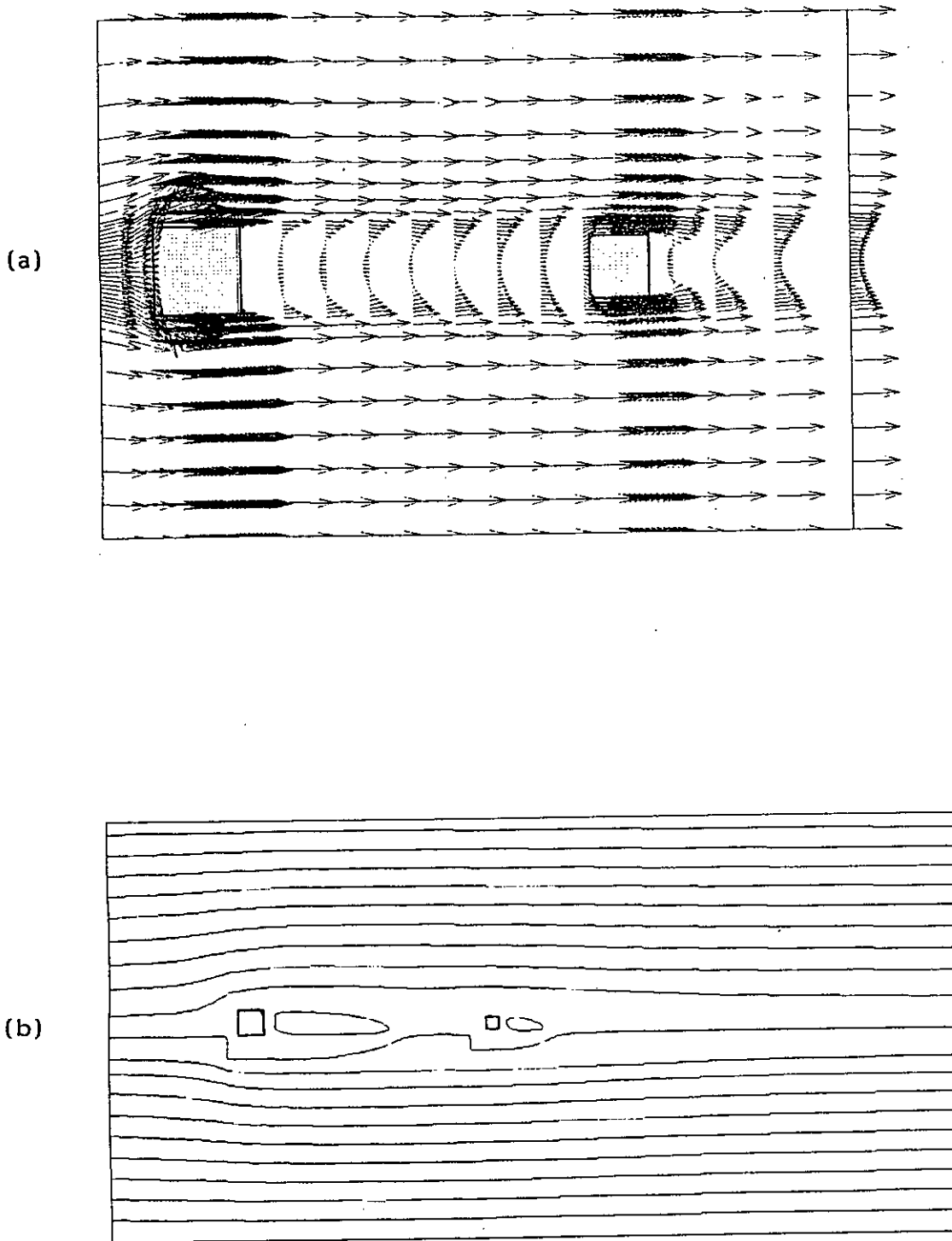tandem cylinder of d/D = 0.7 and L/D =4.0

Fig. 5.25 : (a) Velocity field (b) Stream function contour for
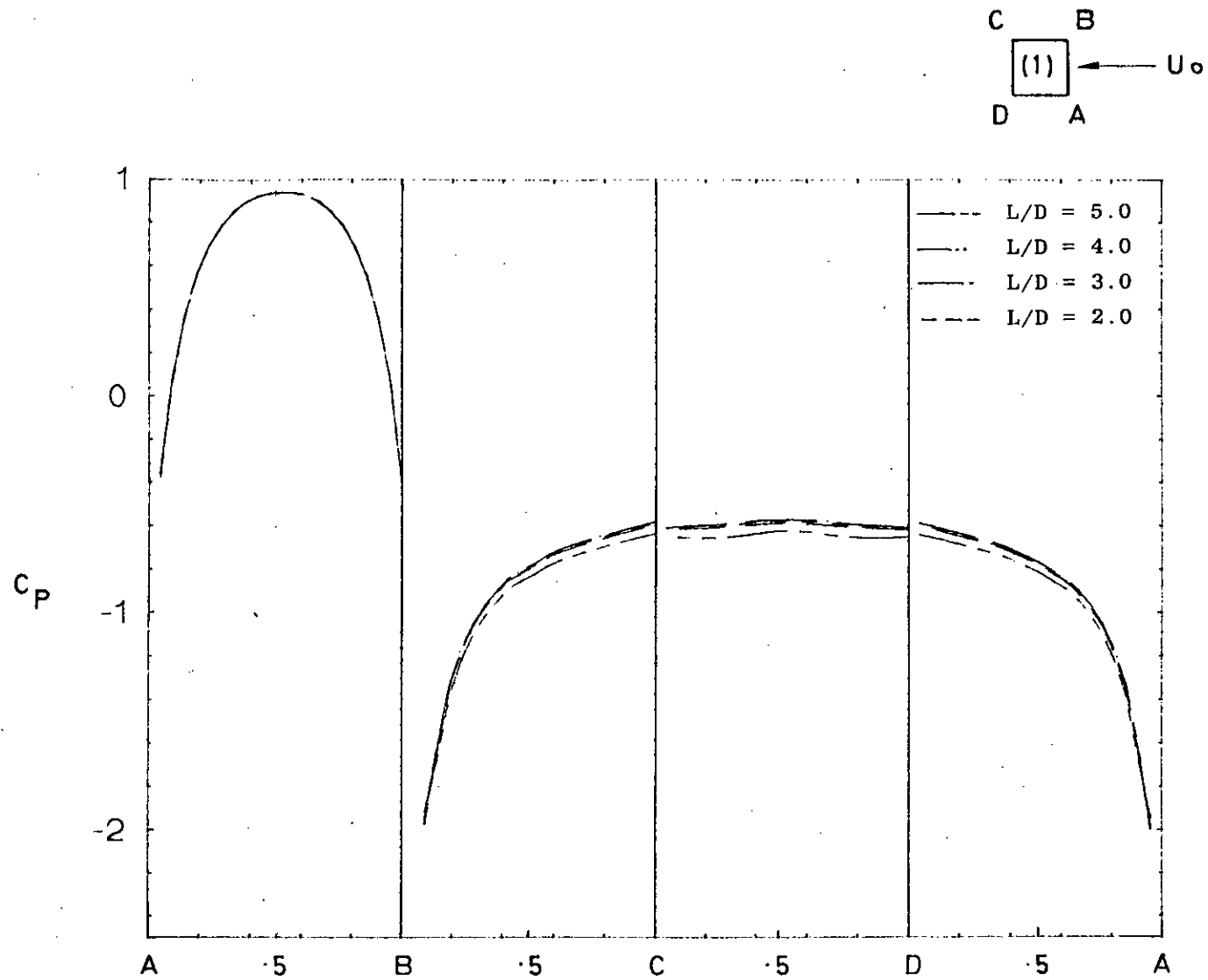tandem cylinder of d/D = 0.7 and L/D =5.0

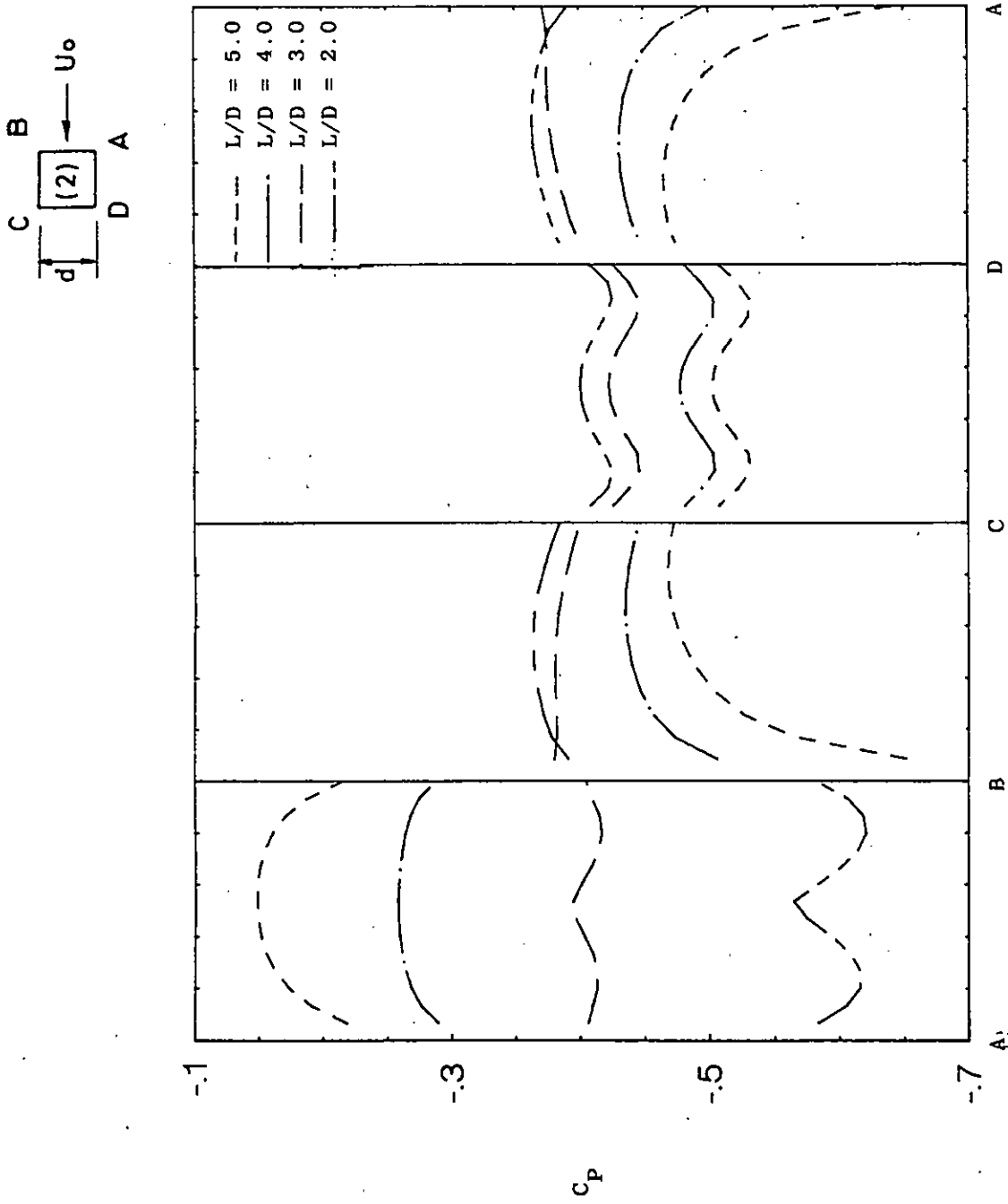Fig. 5.26 : Effect of L/D on C_p- distribution around front cylinder for d/D = 0.7

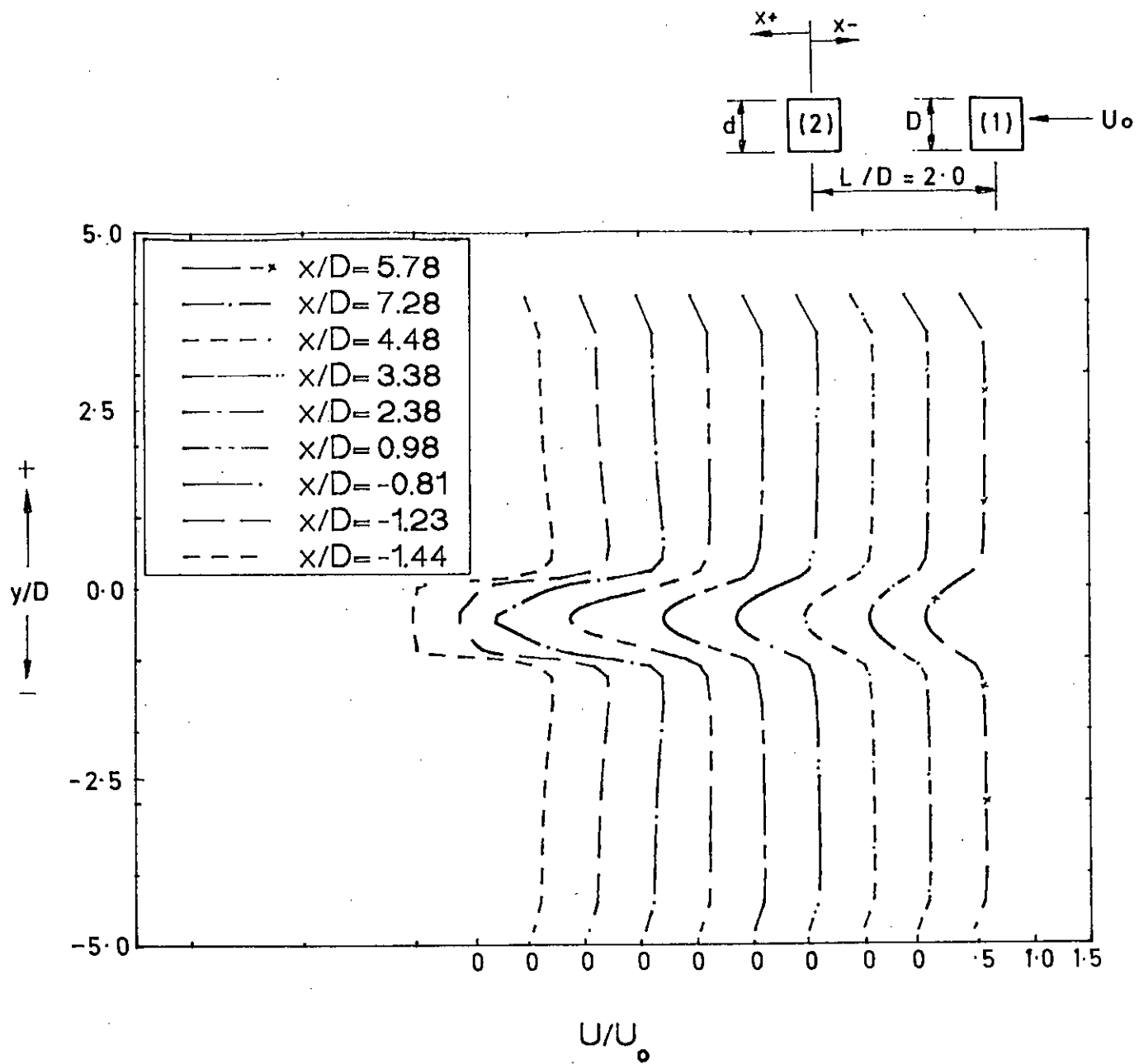Fig. 5.27 : Effect of L/D on C_p - distribution around rear cylinder for d/D = 0.7

x+ | x-

d | (2) | D | (1) ← Uo

L /D = 2·0

5·0

x/D= 5.78
x/D= 7.28
x/D= 4.48
x/D= 3.38
x/D= 2.38
x/D= 0.98
x/D= -0.81
x/D= -1.23
x/D= -1.44

2·5

+

y/D   0·0

-2·5

-5·0

0 0 0 0 0 0 0 0 0 ·5 1·0 1·5

U/U_o

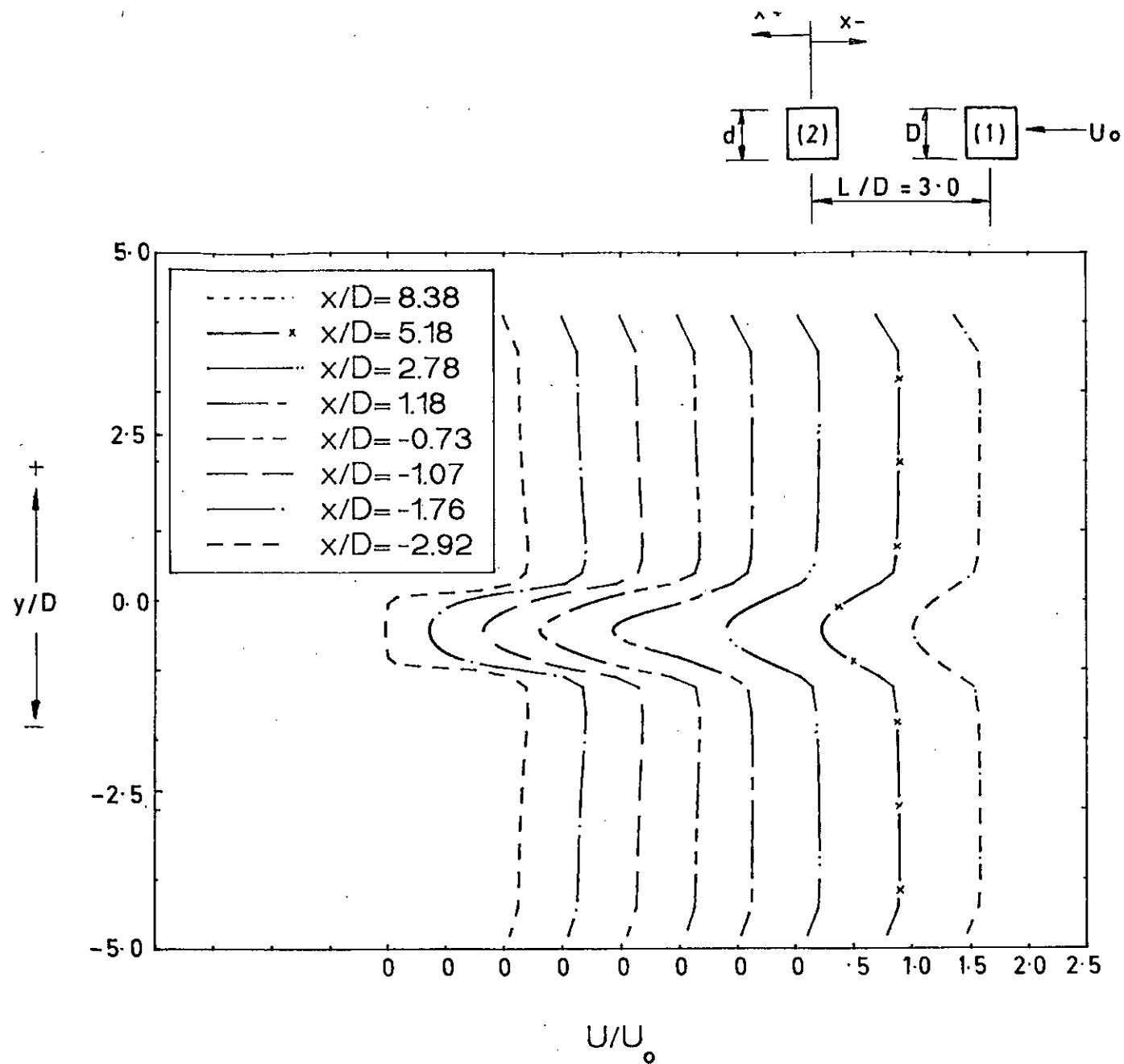Fig. 5.28 : Mean velocity distribution in wakes behind the cylinders of d/D = 0.7
for L/D = 2.0

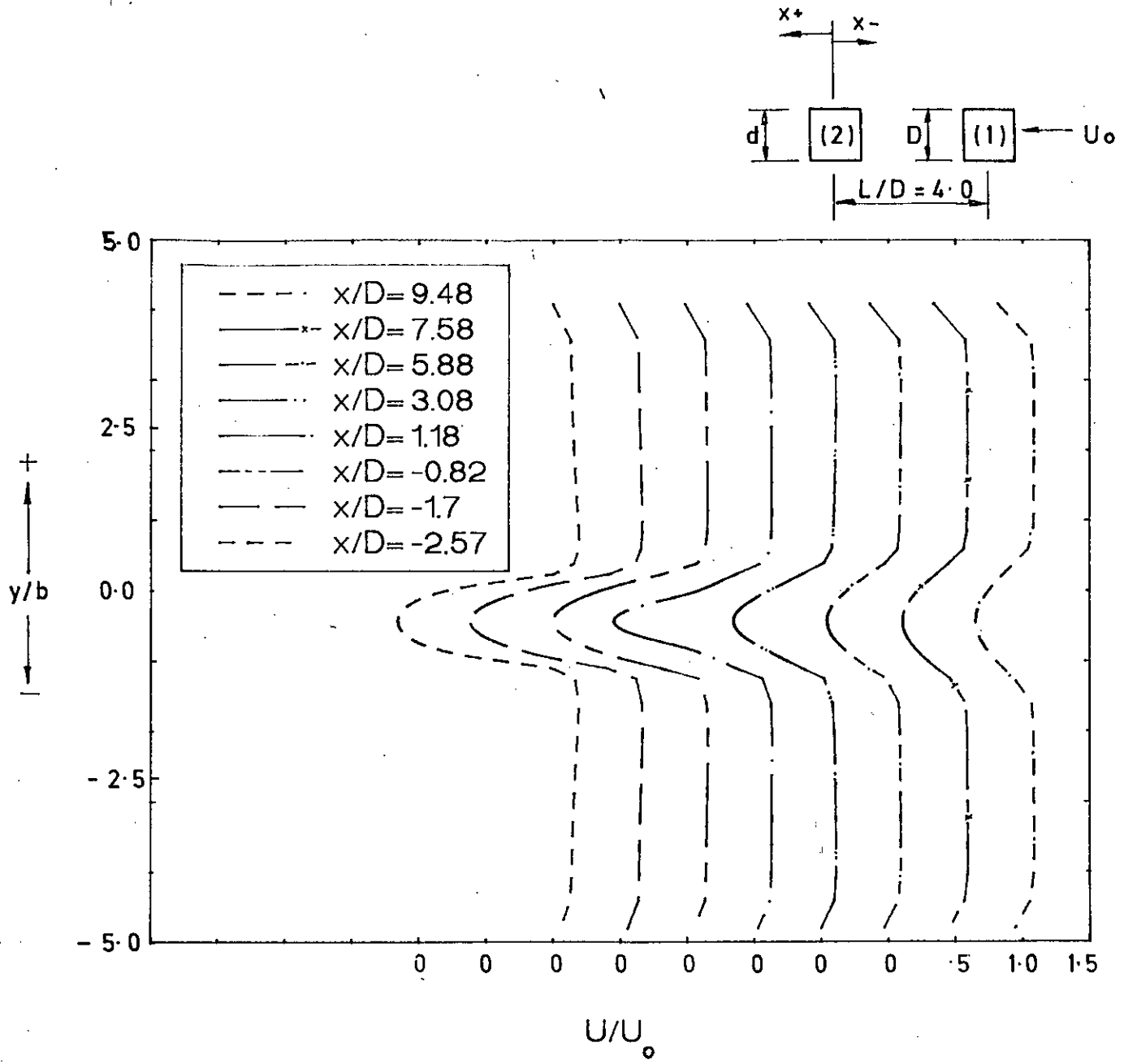Fig. 5.29 : Mean velocity distribution in wakes behind the cylinders of d/D = 0.7 for L/D = 3.0

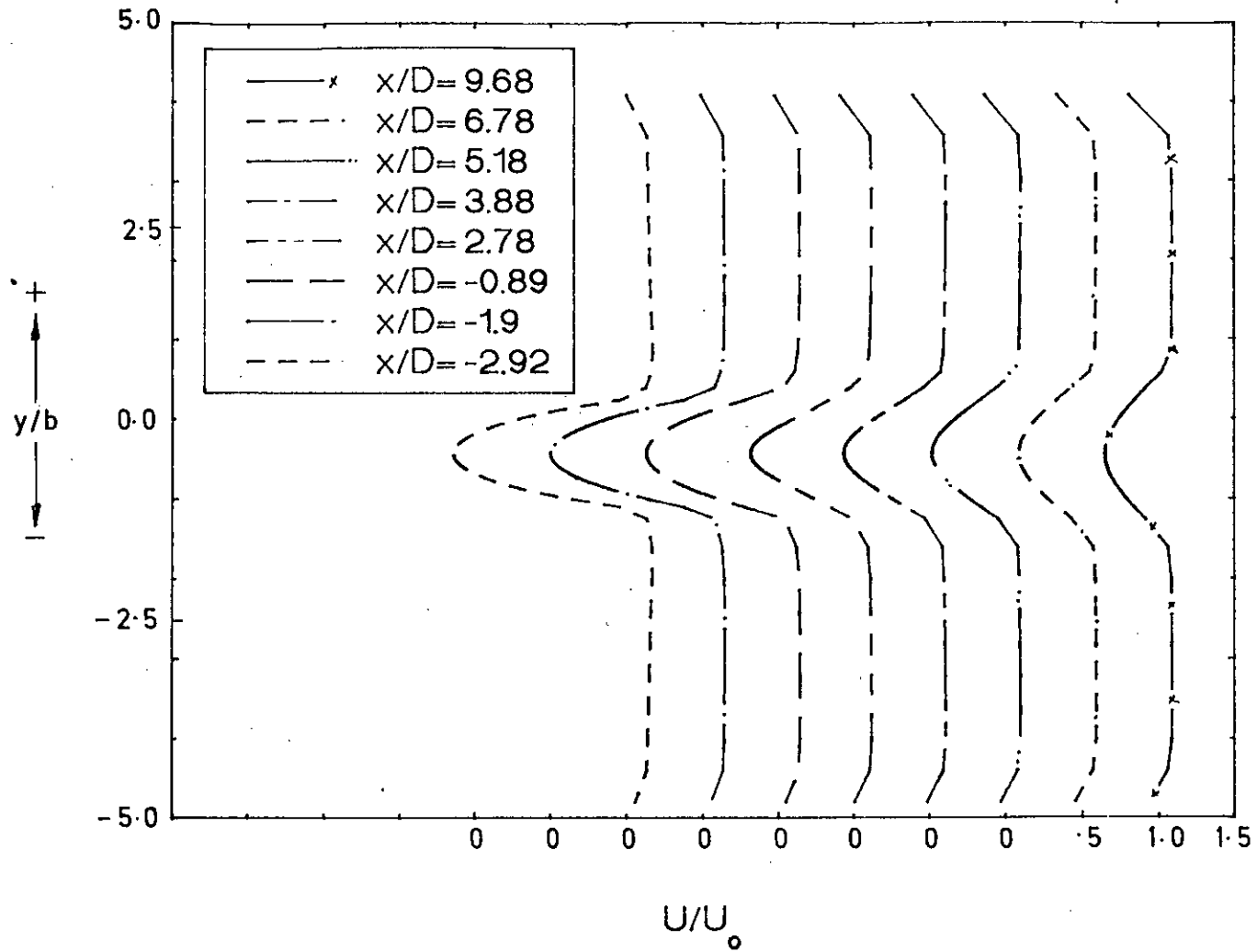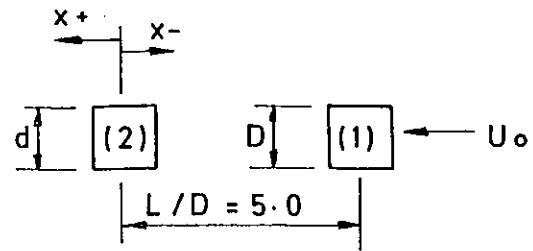Fig. 5.30 : Mean velocity distribution in wakes behind the cylinders of d/D = 0.7 for L/D = 4.0

Fig. 5.31 : Mean velocity distribution in wakes behind the cylinders of
d/D = 0.7 for L/D = 5.0
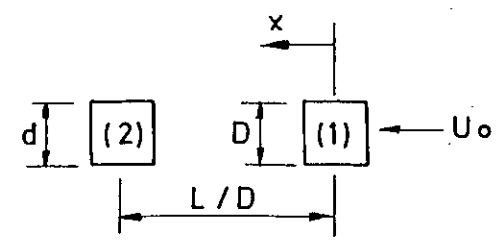
Fig. 5.32 : Velocity defect distribution behind front cylinder of d/D = 0.7
for L/D = 2.0 to 3.0
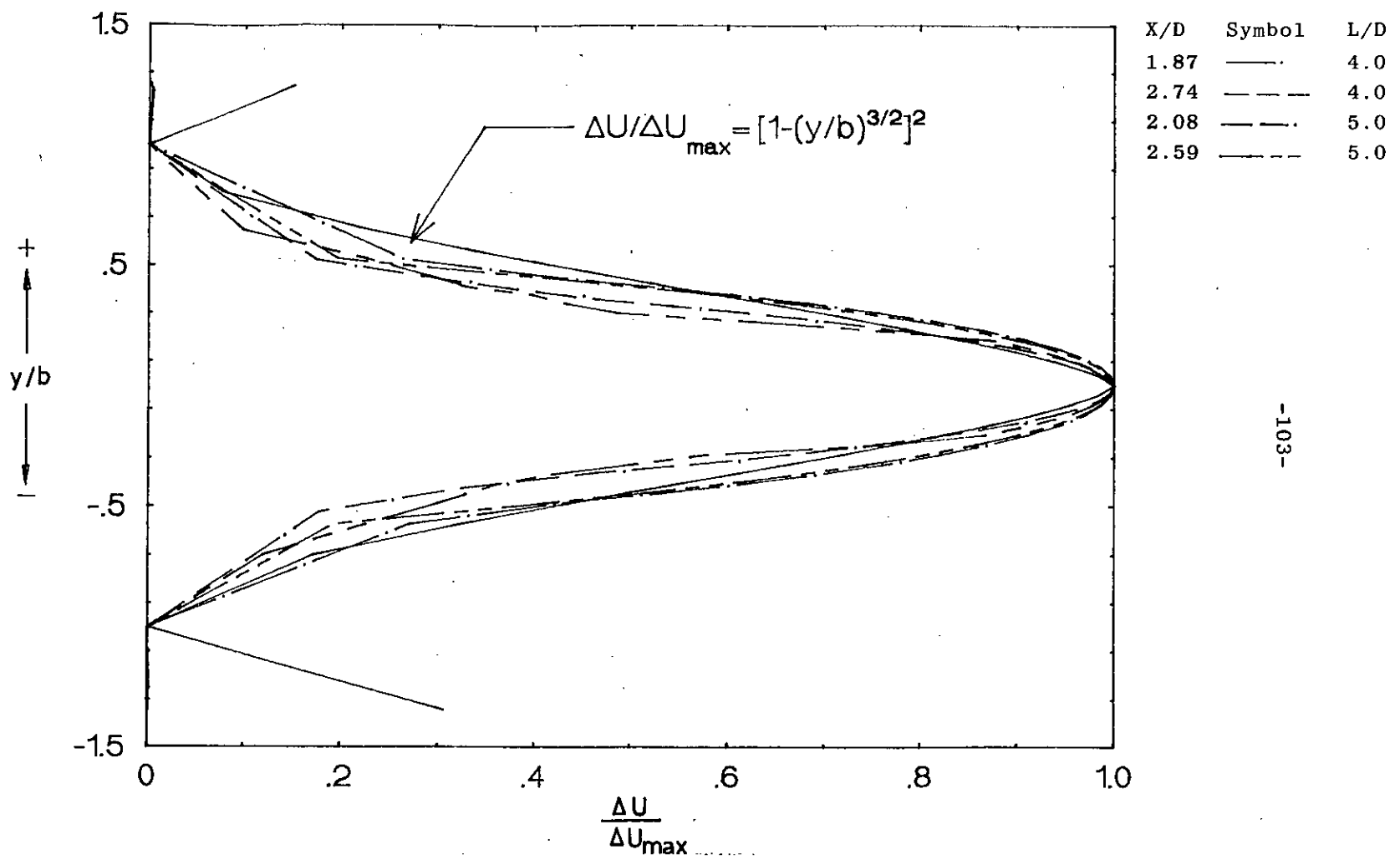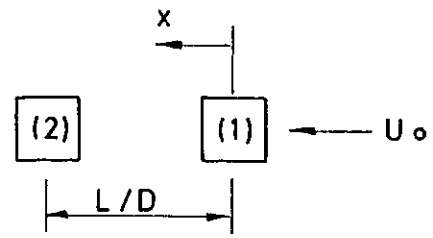
Fig. 5.33 : Velocity defect distribution behind front cylinder of d/D = 0.7
for L/D = 4.0 to 5.0

x

(2)   (1) ← Uo

L / D

1.5

$\dfrac{\Delta U}{\Delta U_{max}} = \left[1-(y/b)^{3/2}\right]^2$

+

.5

y/b

-.5

-1.5

0   .2   .4   .6   .8   1.0

$\dfrac{\Delta U}{\Delta U_{max}}$

X/D	Symbol	L/D
0.68	—·—·—	2.0
0.68	—··—	3.0
1.18	— — —	3.0
0.68	————	4.0
1.18	—··—	4.0
0.68	— —	5.0
1.18	—————	5.0

-104-
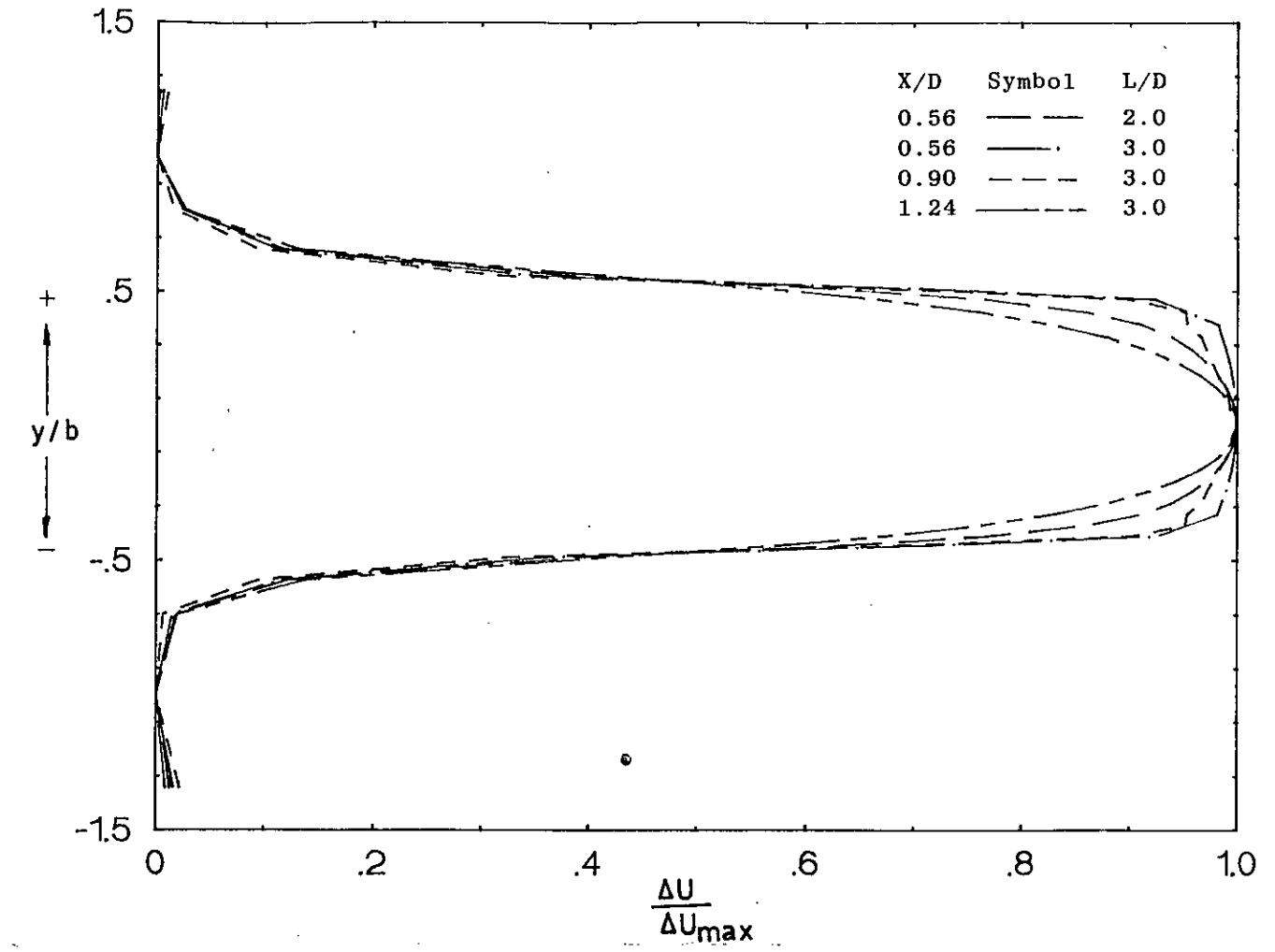
Fig. 5.34 : Velocity defect distribution behind rear cylinder of d/D = 0.7
for L/D = 2.0 to 5.0
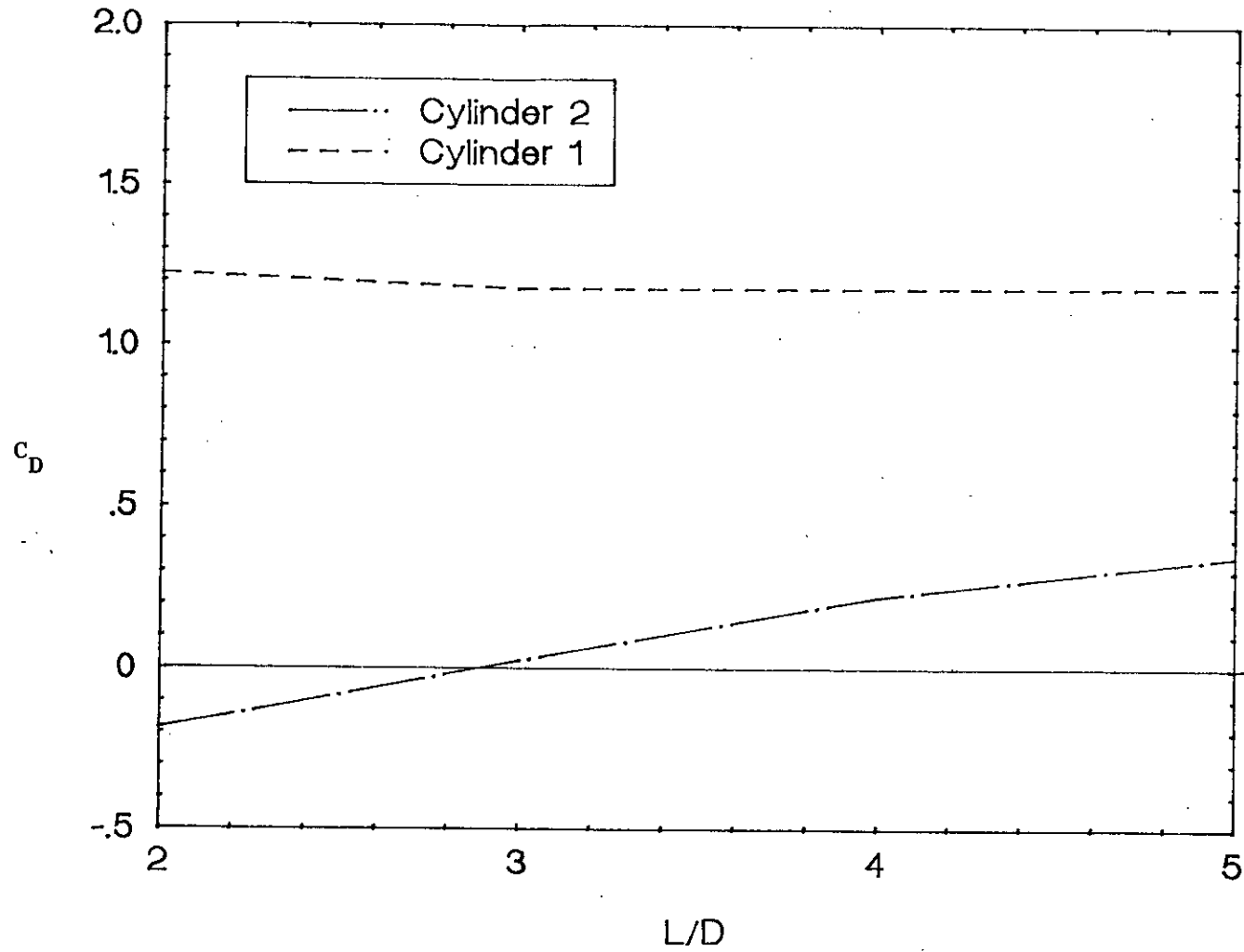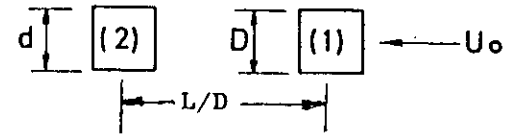
Fig. 5.35 : Comparison of drag co-efficient of the two tandem square cylinders
for d/D = 0.5

(a)

(b)
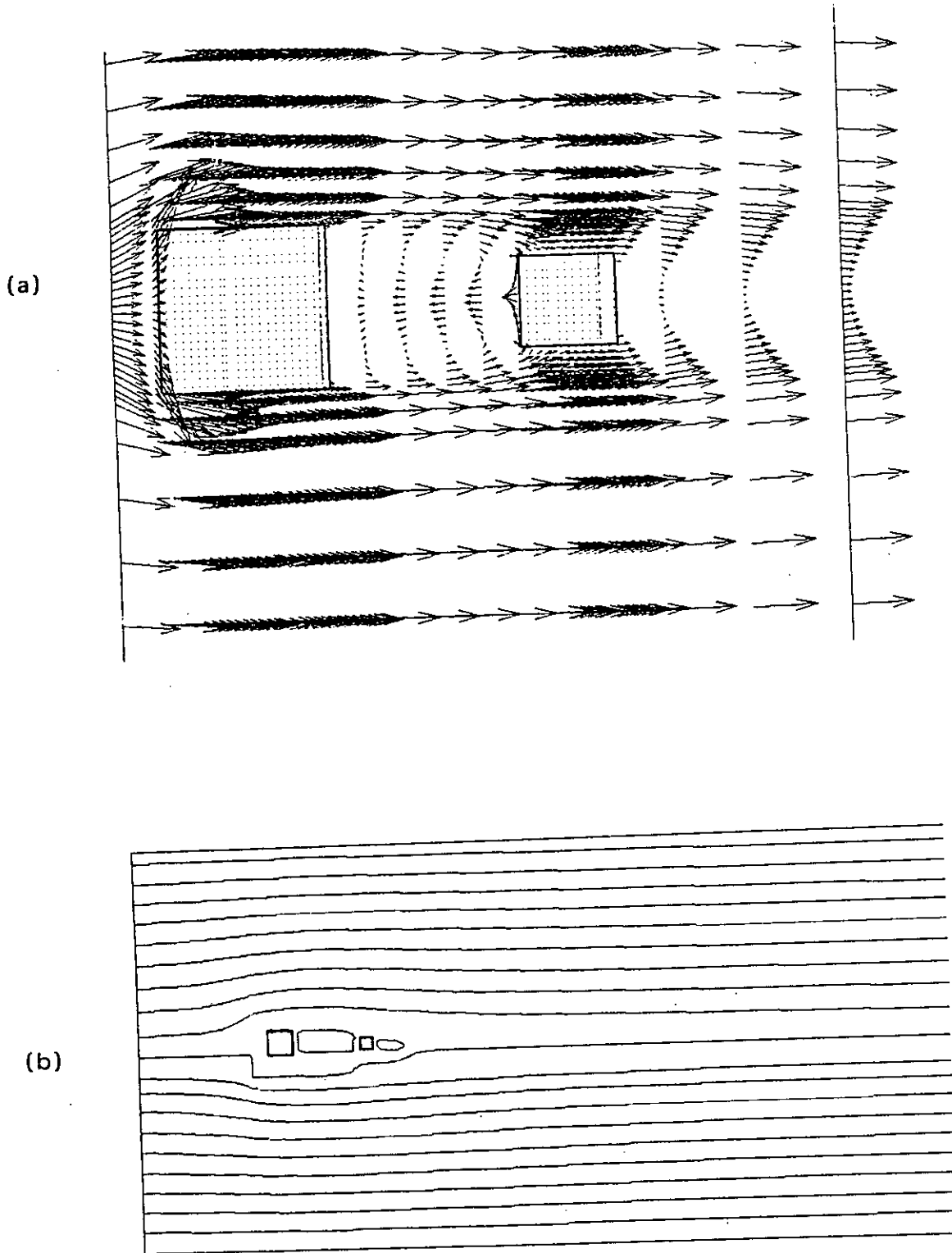
Fig. 5.36 :   (a) Velocity field   (b) Stream function contour for
tandem cylinder of d/D = 0.5 and L/D = 2.0 .

(a)

(b)
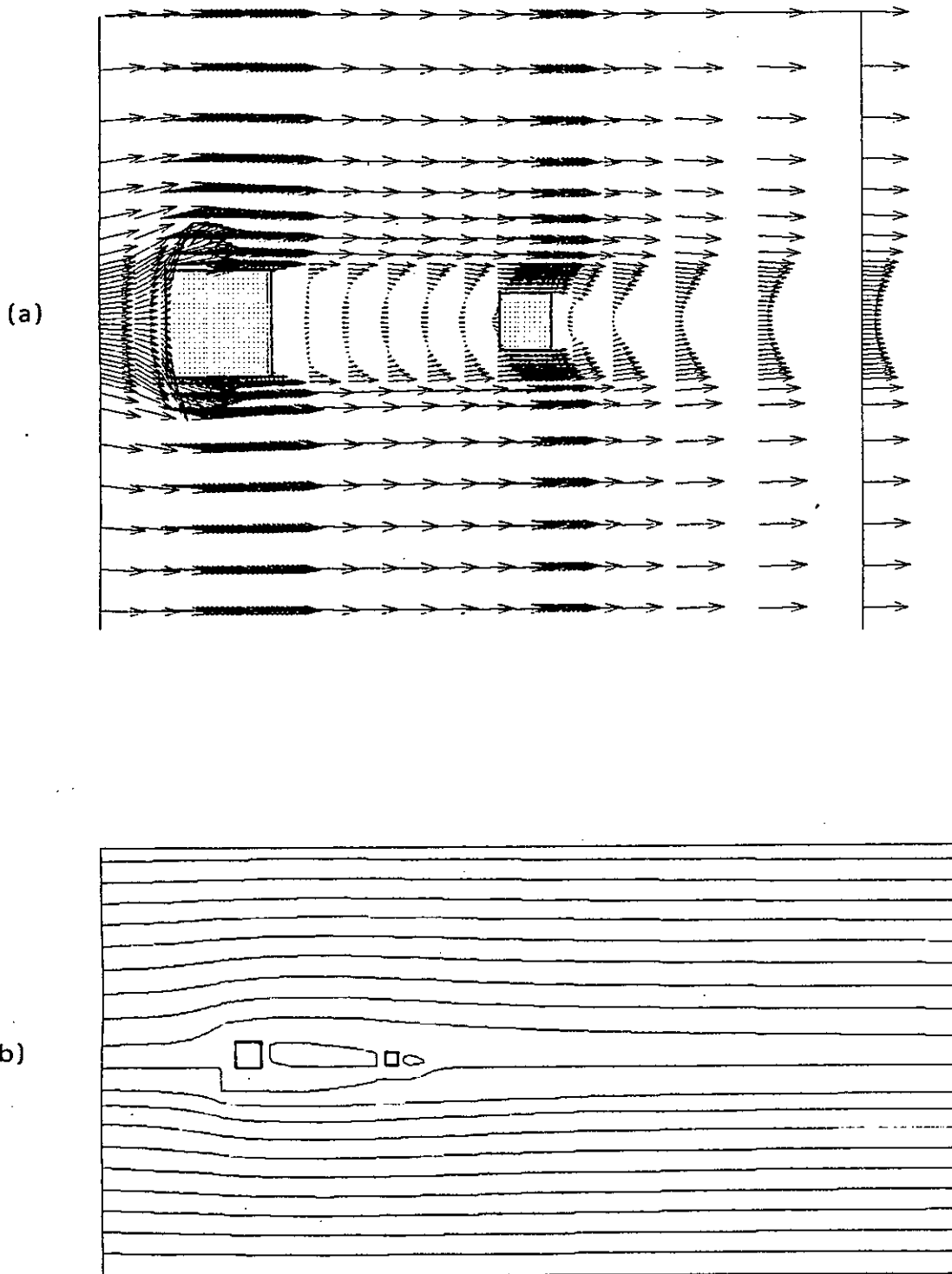
Fig. 5.37 : (a) Velocity field (b) Stream function contour for
tandem cylinder of d/D = 0.5 and L/D = 3.0 .
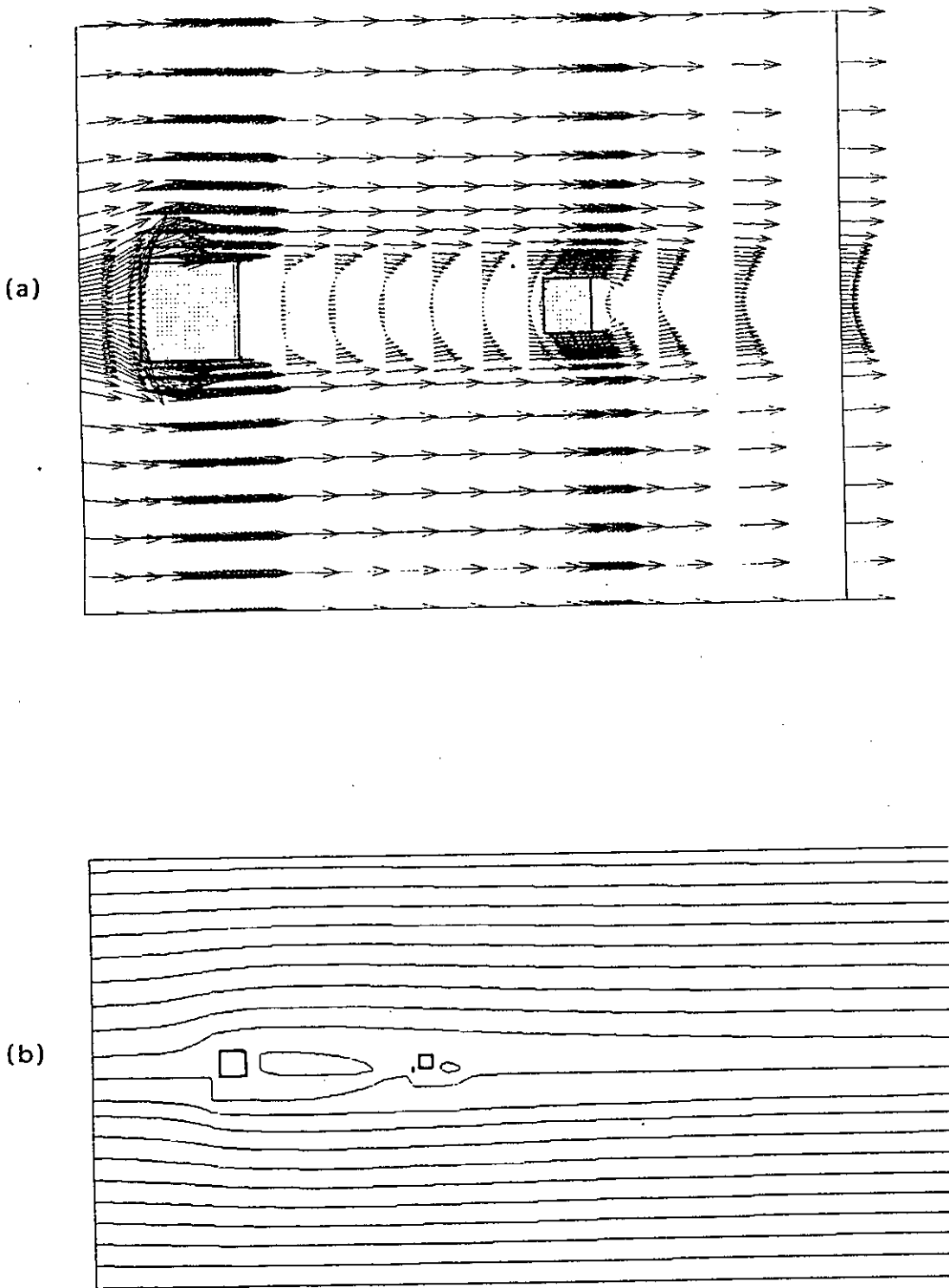
Fig. 5.38 : (a) Velocity field (b) Stream function contour for tandem cylinder of d/D = 0.5 and L/D = 4.0 .
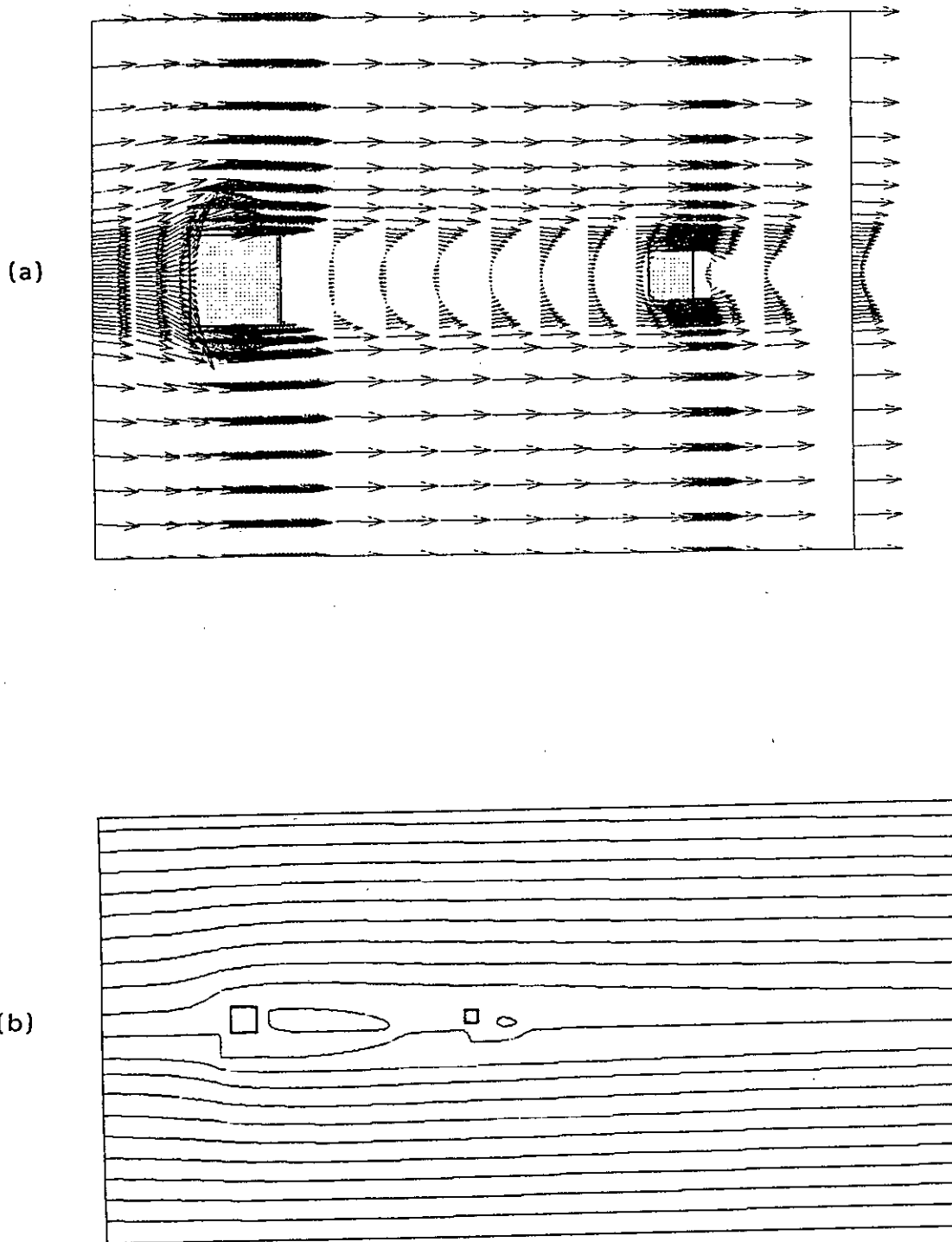
Fig. 5.39 :   (a)   Velocity field   (b)   Stream function contour for
tandem cylinder of d/D = 0.5 and L/D = 5.0 .
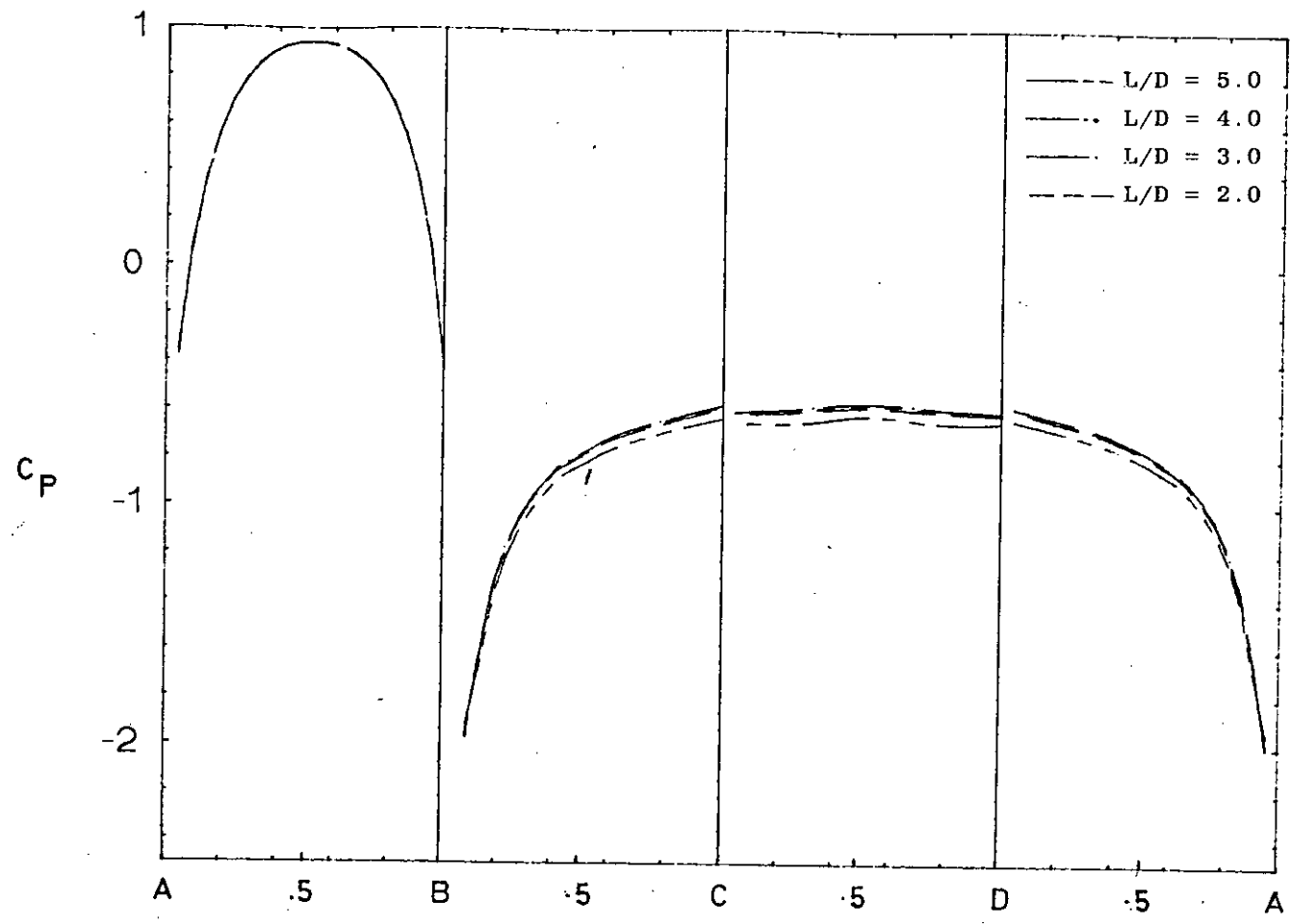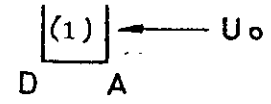
Fig. 5.40 : Effect of L/D on C_p - distribution around front cylinder for d/D = 0.5
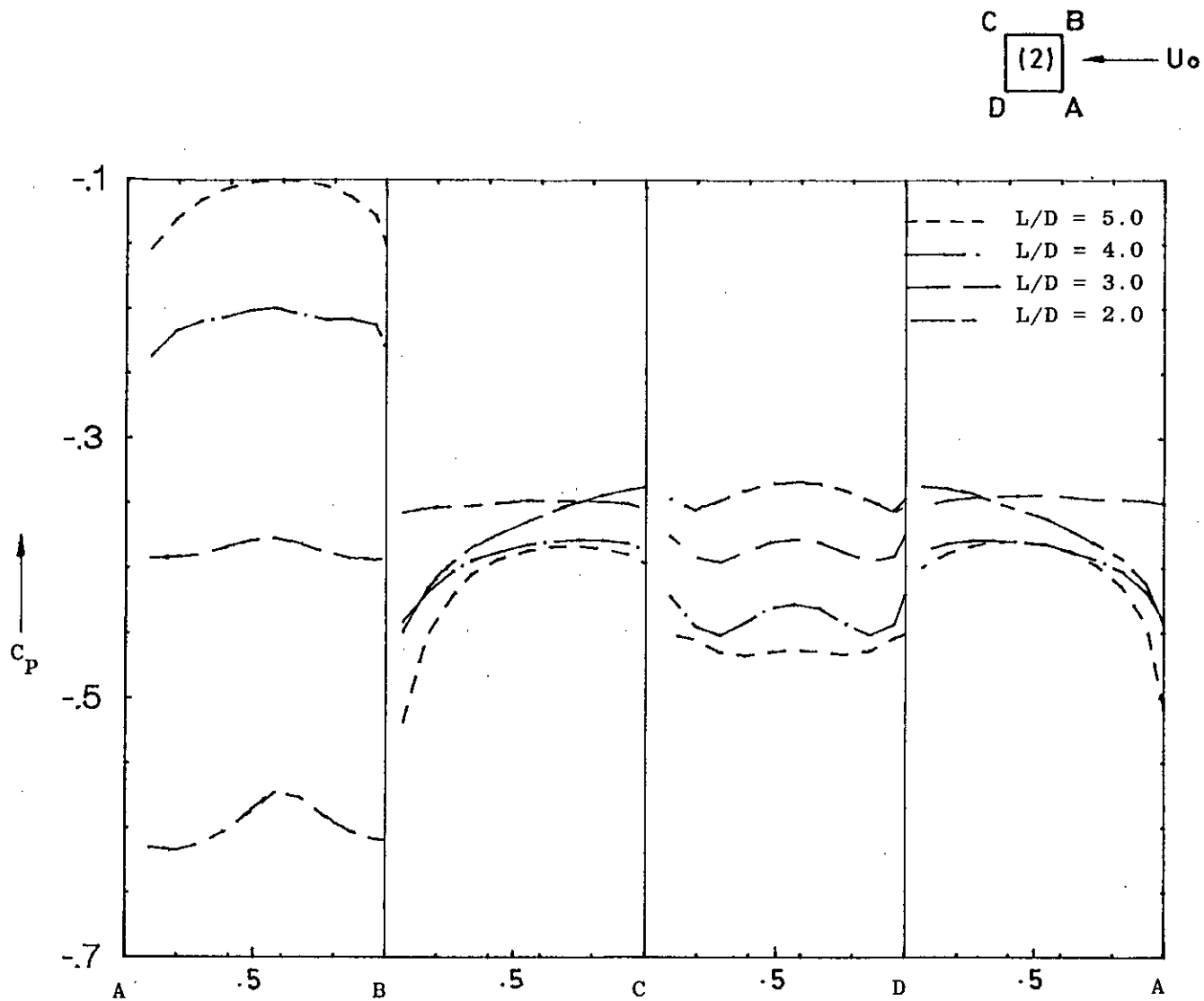
Fig. 5.41 : Effect of L/D on C_p-distribution around rear cylinder for d/D = 0.5
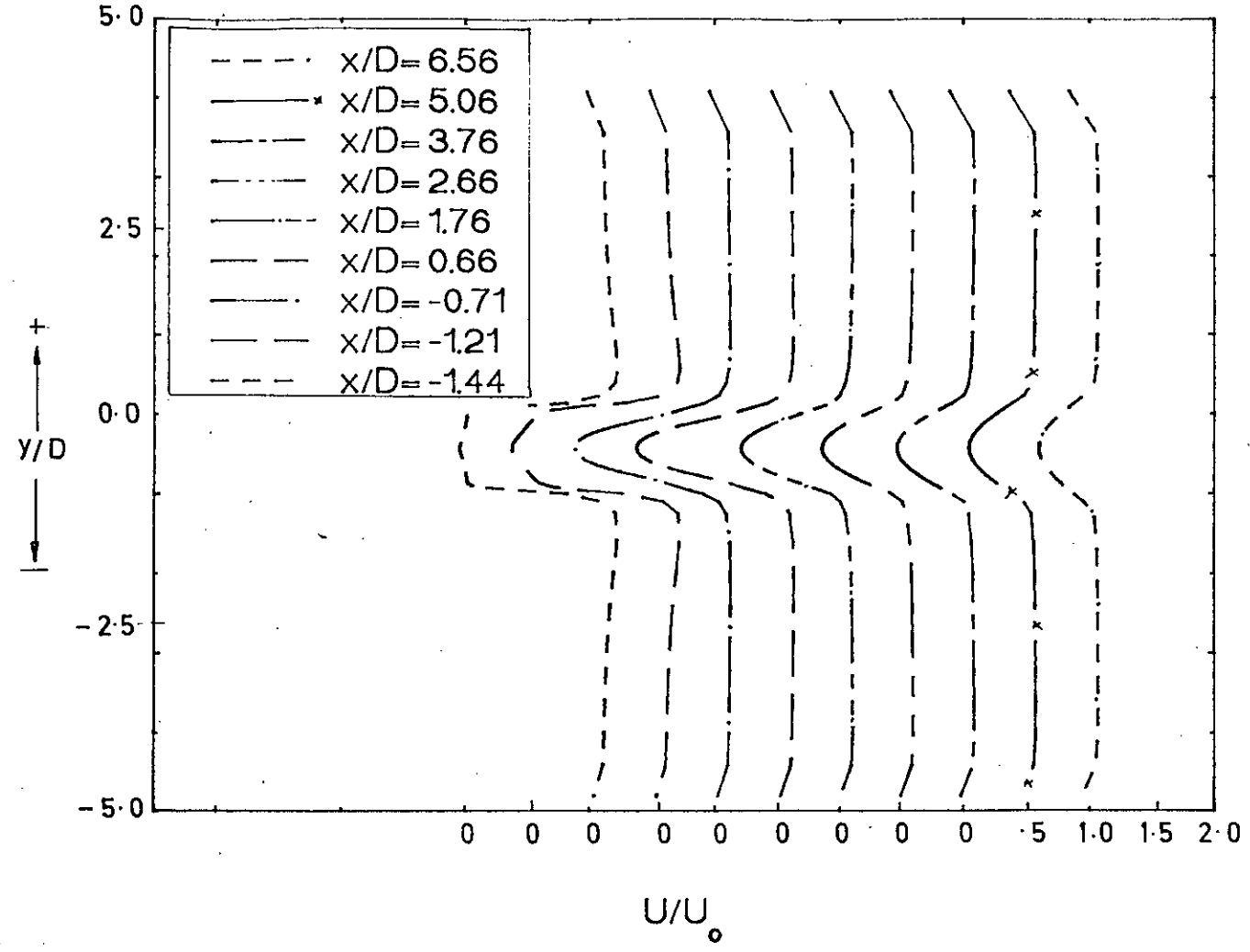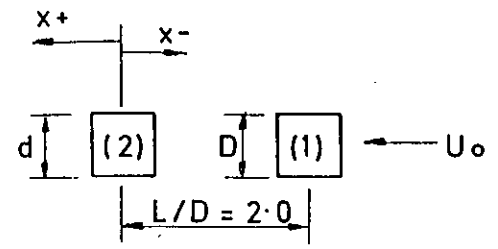
Fig. 5.42 : Mean velocity distribution in wakes behind the cylinders of
d/D = 0.5 for L/D = 2.0
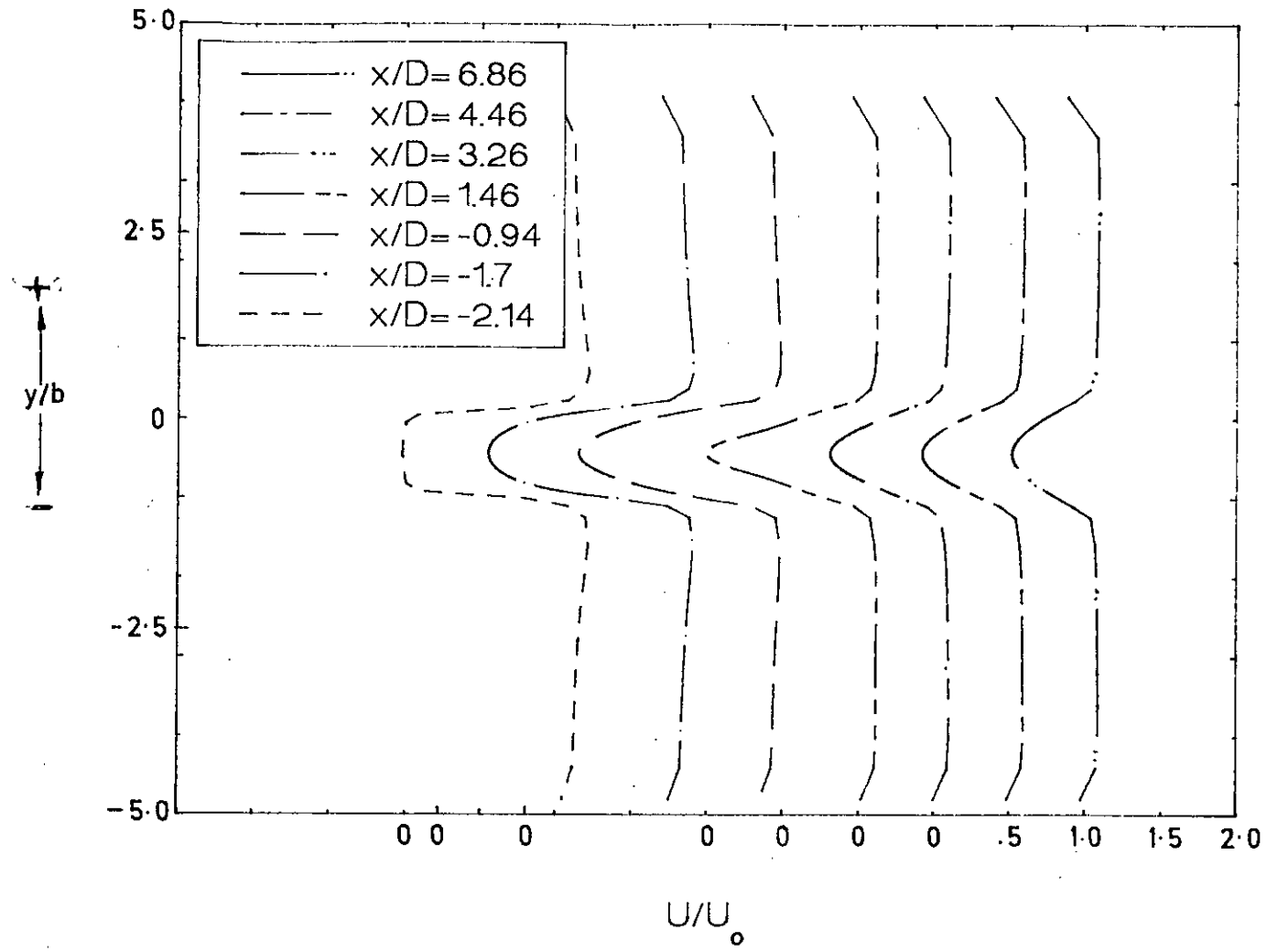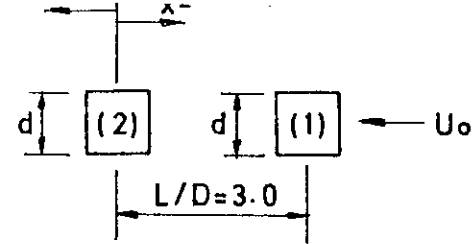
Fig. 5.43 : Mean velocity distribution in wakes behind the cylinders of d/D = 0.5 for L/D = 3.0
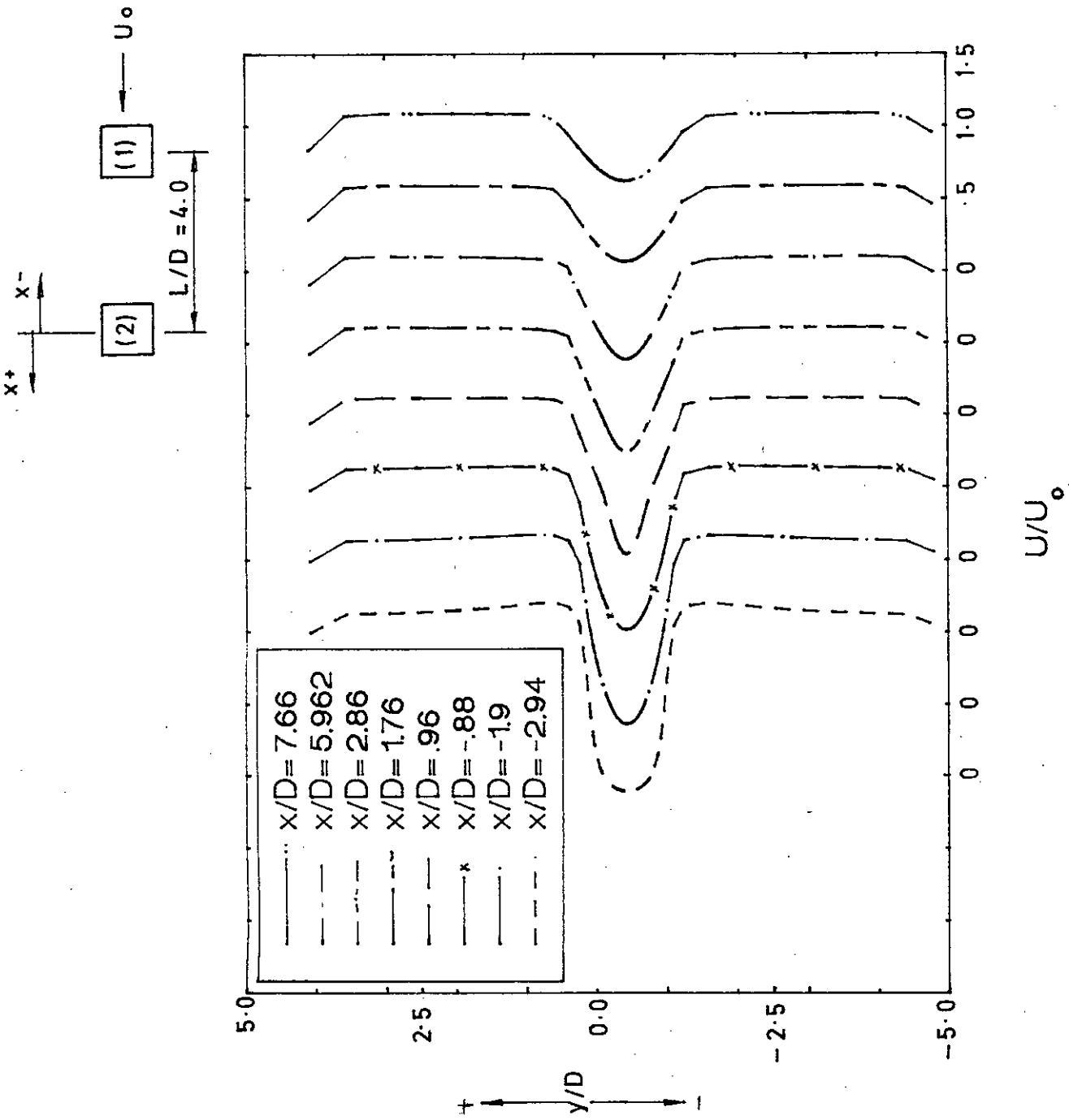
Fig. 5.44 : Mean velocity distribution in wakes behind the cylinders of d/D = 0.5 for L/D = 4.0
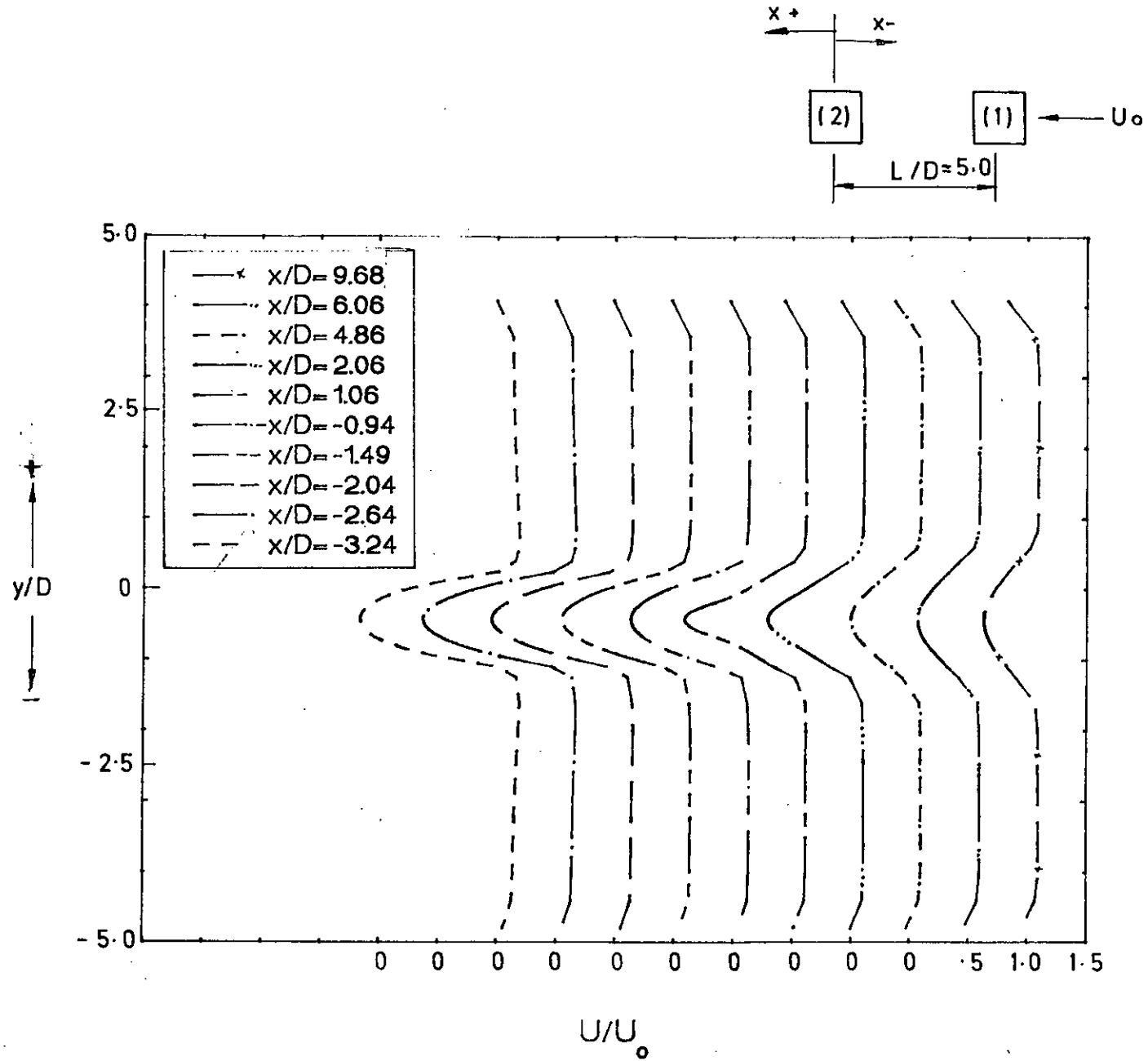
Fig. 5. 45 : Mean velocity distribution in wakes behind the cylinders of
d/D = 0.5 for L/D = 5.0
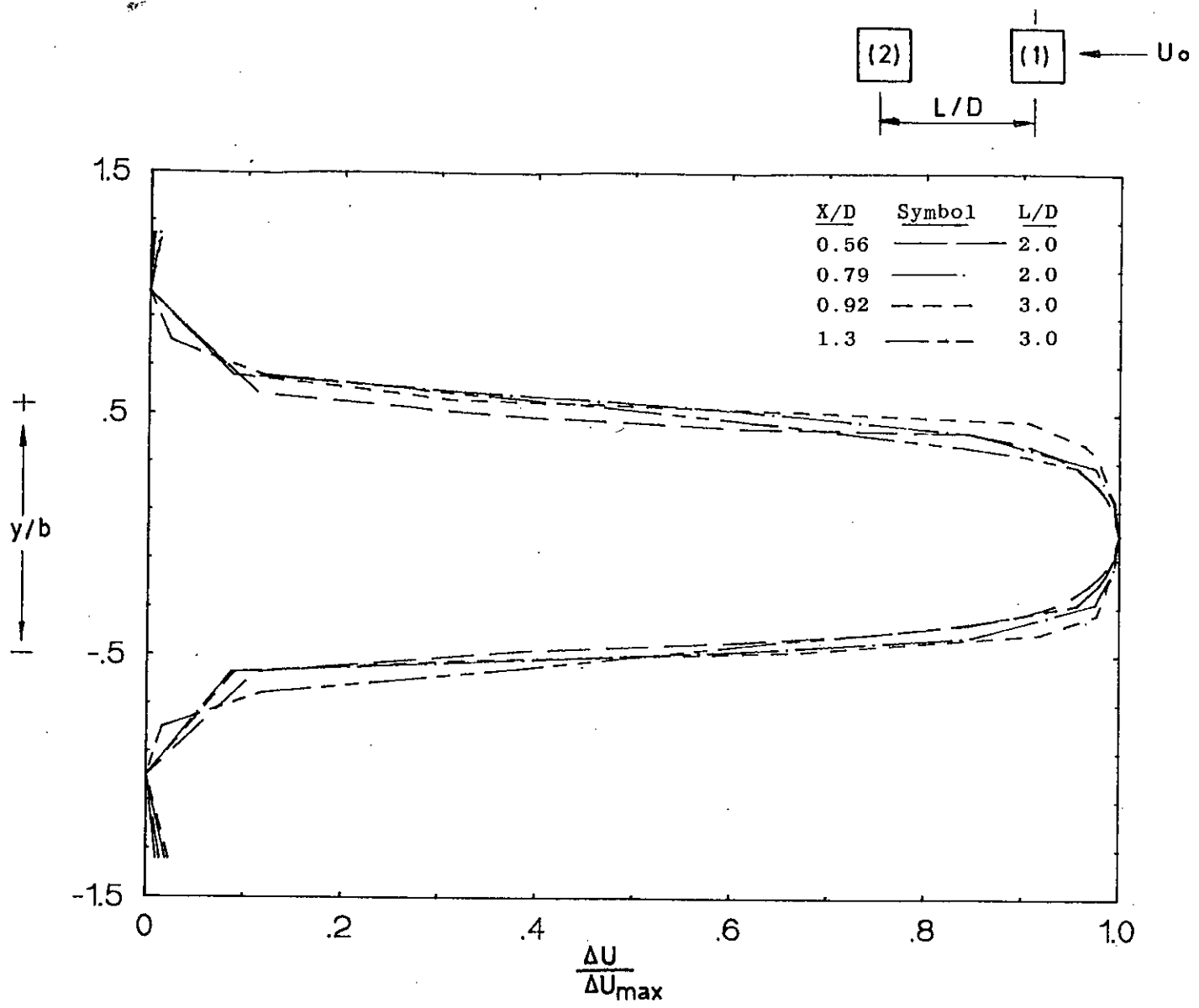
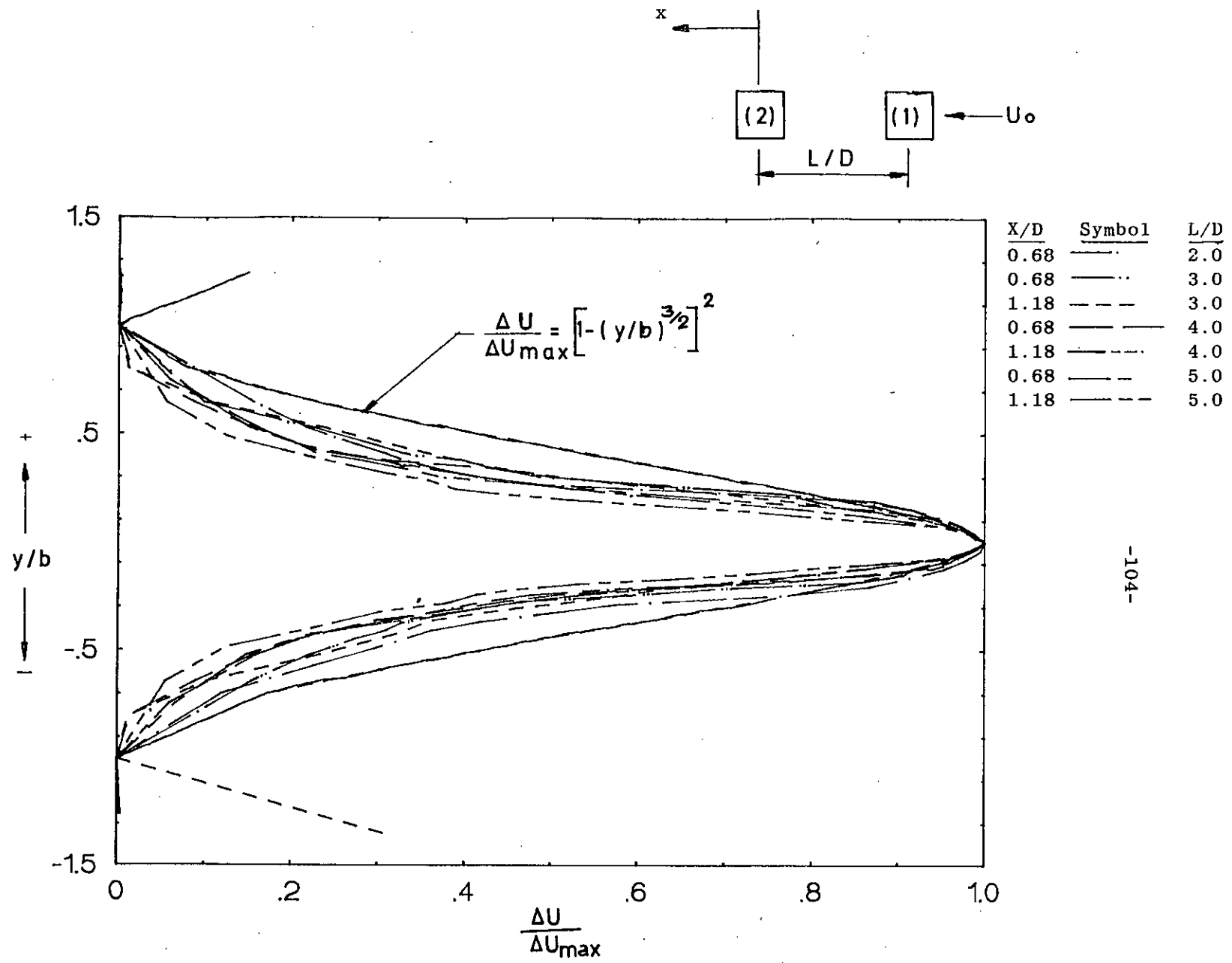Fig. 5.46 : Velocity defect distribution behind front cylinder of d/D = 0.5
for L/D = 2.0 to 3.0

The legend within the figure:

X/D	Symbol	L/D
0.56	—— ——	2.0
0.79	———— ·	2.0
0.92	—— — —	3.0
1.3	—— —·—	3.0

Axis labels: y/b (vertical), $\dfrac{\Delta U}{\Delta U_{max}}$ (horizontal)

x

(2)   (1) ← Uo

L/D

1.5

X/D	Symbol	L/D
1.58	——·—	4.0
2.1	—— ——	4.0
1.76	——— —	5.0
2.36	———	5.0

$\Delta U / \Delta U_{max} = [1-(y/b)^{3/2}]^2$

+

y/b

.5

-.5

-1.5

0   .2   .4   .6   .8   1.0

$\dfrac{\Delta U}{\Delta U_{max}}$
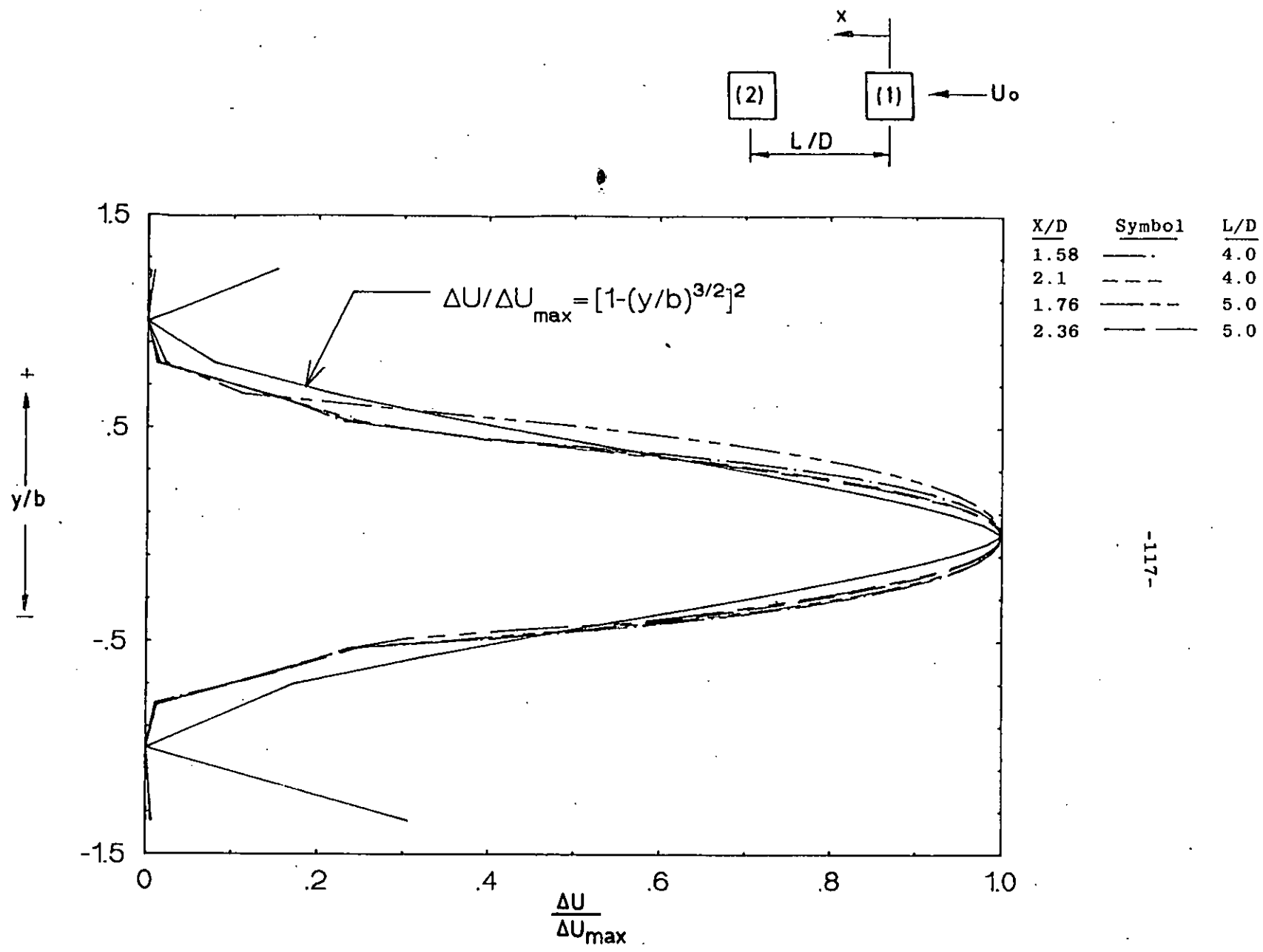
Fig. 5. 47 : Velocity defect distribution behind front cylinder of d/D = 0.5
for L/D = 4.0 to 5.0
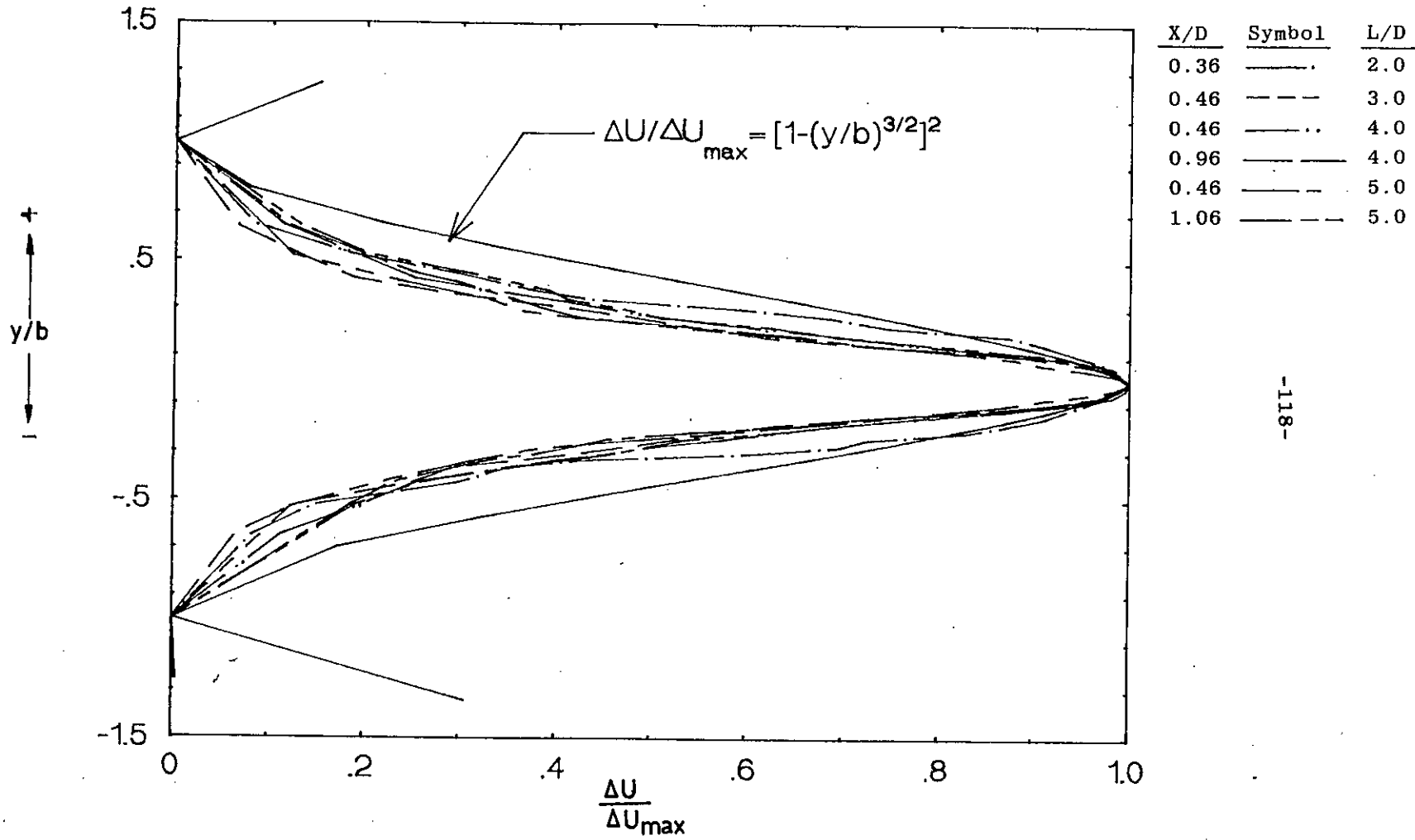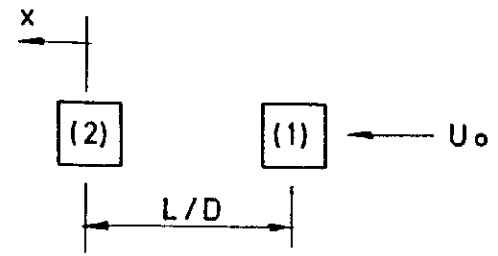
Fig. 5.48 : Velocity defect distribution behind rear cylinder of d/D = 0.5
for L/D = 2.0 to 5.0
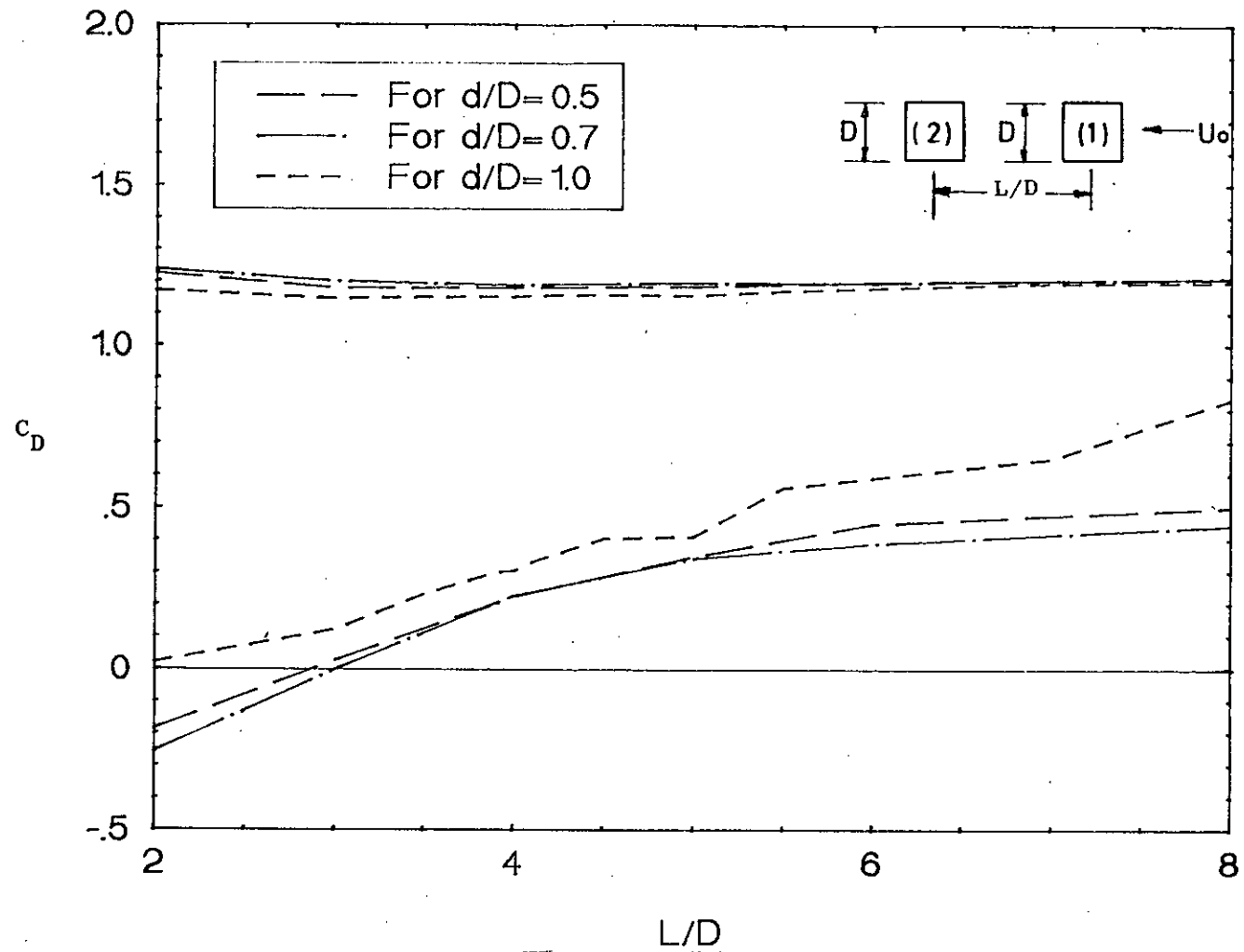
Fig. 5.49 : Comparison of drag co-efficient of two tandem square cylinders
for different size-ratios.

REFERENCES

[1]   Achenback, E. (1968) "Distribution of local pressure and skin friction around a circular cylinder in cross-flow upto Re= 5 X 10^6", Journal of Fluid Mechanics, vol. 34, P. 625-639.

[2]   Ahmed, B. and Betrui. (1985) "Analysis of flow evolution in the cylinders of motored receprocating engine" Ph.D thesis, University of London, P. 97-245.

[3]   Baines, W.D. (1963) "Effects of velocity distribution on wind loads and flow patterns on Buildings", Proceedings of a Symposium on Wind Effects on Buildings and Structures, U.K., P. 197-225.

[4]   Bearman, P.W. and Trueman, D.M. (1972) " An Investigation of the flow around rectangular cylinders," The Aeronautical Quarterly, vol. 23, P. 229-237.

[5]   Bostock, B.R. and Mair, W.A. (1972) " Pressure distributions and forces on Rectangular and D-shaped cylinders", The Aeronautical Quarterly, vol. 23, P. 1-5.

[6]   Bearman, P.W. and Wadcock, A.J. (1973) " The Interaction between a pair of circular cylinders normal to a stream", Journal of Fluid Mechanics, vol. 61, P. 499-511.

[7]   Bariga, A.R., Crowe, C.T. and Roberson, J.A. (1975) "Pressure distribution on a square cylinder at small angle of attack in a turbulent cross flow", Proceedings of the 4th International Conference on Wind Effects on Buildings and Structures, London, U.K., P. 89-93.

[8]   Bearman, P. W. (1980) "Bluff body flows applicable to vehicle aerodynamics", Trans. A.S.M.E.I. J. Fluids Engineering, vol. 102, P.265- 274.

[9]   Bearman, P.W. and Graham, J.M.R. (1980) "Vortax shedding from bluff bodies in oscillatory flow: a report on Euromech 119", J. Fluid Mech. vol. 99, P. 225-245.

[10]   Bradshaw, P., Cebeci, T. and Whitelaw, J.H. (1981) "Engineering calculation methods for turbulant flow"

[11]   Carl, E.P. (1965) "A computational method for viscous flow problems", Journal of Fluid Mechanics, vol.25, P. 611-622.

[12]   Davis, R.W. and Moore, E.F. (1982) "A Numerical study of vortex shedding from rectangulars", Journal of Fluid Mechanics, vol. 116, P. 475-506.

[13]   Frederick, H.A., and Richard, E.K. (1962) "The formation of vortex streets", Journal of Fluid Mechanics, vol.13, P. 1-20.

[14]   Fromm, J.E. and Harlow, F.H. (1963) "Numerical solution of the problem of vortex street development", Phys. Fluids, vol. 6, P. 975-982.

[15]   Faruque, O. (1983) "Experimental investigation of two-dimensional wakes behind flat plates", M.Sc. Thesis (ME Deptt.), BUET.

[16]   Frank, N., "Model law and Experimental Technique for determination of wind loads on Buildings", Proceedings of the 1st International Conference on Wind Effects on Buildings and Structures, Teddington, London, P. 181-189.

[17]   Gerrard, J.H. (1966) "The mechanics of the formation region of vortices behind bluff bodies", Journal of Fluid Mechanics, vol. 25, P. 401-413.

[18]   Gosman, A.D., Pun, W.M., Runchal, A.K., Spalding, D.B. and Wolfshtein, M. (1969) "Heat and Mass Transfer in Recirculating Flows", Academic Press, London and New York.

[19]   Gandemer, J. (1975) "Wind environment around buildings; Aerodynamic Concepts", Proceedings of the 4th International Conference on Wind Effects on Buildings and Structures. London, U.K., P. 423-432.

[20]   Gosman, A.D. and Ideriah, F.J.K. (1976) "TEACH-T : A general computer program for two-dimensional,Turbulent,Recirculating flows".

[21]   Gibson, M.M. and Launder, B.E. (1976) "On the calculation of horizontal turbulent shear flows under gravitational influence", J. Heat Transfer, vol. 98, P. 81.

[22]   Gosman, A.D., Khalil, E.E. and Whitelaw, J.H. (1979) " The calculation of two-dimentional turbulent recirculating flows. In 'TURBULENT SHEAR FLOWS', Springer-Verlag, Berlin, vol. 1, P. 287.

[23]   Hinze, J.O. (1959) "Turbulence : An introduction to its mechanism and theory", McGraw-Hill Book Company Inc., New York.

[24]   Hua, C.K. (1971) "The Behaviour of lift fluctuations on the square cylinders in the wind tunnel test", Proceedings of the 3rd International Conference on Wind Effects on Buildings and Structures, Tokyo, Japan, P. 911-920.

[25]   Hanjalic, K. and Launder, B.E. (1972) "A Reynolds stress model of turbulece and its application to thin shear flows", J. Fluid Mech., vol. 52, P. 609.

[26]   Honji, H. (1973) "Formation of reversed flow bubble in the time mean wake of a row of circular cylinders", Journal of the Physical Society of Japan, vol. 35, no. 5, P. 1533-1536.

[27] Hayashi, M., Akirasakurai and Yuji, O. (1986) "Wake interference of a row of normal flat plates arranged side by side in a uniform flow". Journal of Fluid Mechanics, vol. 164, P.1-25.

[28] Huot, J.P., Rey, C. and Arby, H. (1986) "Experimental analysis of the pressure field induced on a square cylinder by a turbulent flow", Journal of Fluid Mechanics, vol. 162, P. 283-298.

[29] Hossain, M.M. (1991) "Flow characteristics around square cylinders in tandem", M.Sc. Thesis (ME department, BUET).

[30] Ideriah, F.J.K. (1975) "Review of equations solved in TEACH-T", Taken from reference [20].

[31] Islam, O. (1976) " Part-1 : Possibilities of studies of wind effects in Bangaldesh", University of salford, U.K.

[32] Igarashi, T. (1982) "Characteristics of a flow around two circular cylinders of different diameters arranged in tandem", Bulletin of JSME, vol. 25, no.201, P. 349-357.

[33] Igarashi, T. and Suzuki, K. (1984) "Characteristics of the flow around three circular cylinders arranged in line", Bulletin of JSME, vol. 27, no. 233, P. 2397-2404.

[34] Igarashi, T. (1986) "Characteristics of flow around four circular cylinders arranged in line", Bulletin of JSME, vol. 29, no.249, P. 751-757.

[35] Islam, A.M.T. (1988) "An experimental investigation of wind effects on rectangular cylinders", M.Sc. Thesis (ME Department, BUET).

[36] Jones, W.P. and Launder, B.E. (1972) "The prediction of laminarization with a two-equation model of turbulence", Int. J. Heat Mass Transf., vol. 15, P. 301.

[37] Jonji, H. (1973) "Viscous flow past a group of circular cylinders", Journal of the Physical Society of Japan, vol. 34, no. 3, P. 821-828.

[38] Kelnhoffer, J. (1971) "Influence of a neighbouring buildings on flat roof wind loading", Proceedings of the 3rd International Conference on Wind Effects on Buildings and Structures", Tokyo, Japan, P. 221-230.

[39] Koening, K. and Roshko, A. (1985) "An experimental study of geometrical effects on the drag and flow field of two bluff bodies seperated by a gap", Journal of Fluid Mechanics, vol.156, P.167-204.

[40] Lanveville, A. and Parknison, G.V. (1971) "Effects of turbulence on galloping of bluff cylinders", Proceedings of the 3rd International Conferecne on Wind Effects on Buildings and Structures, Tokyo, Japan, P. 787-797.

[41] Leutheusser, J. (1971) "Static wind loadings of grouped buildings", Proceedings of the 3rd International Conference on Wind Effects on Buildings and Structures, Tokyo, Japan, P.211-220.

[42] Launder, B.E. and Spalding, D.B. (1972) "Mathematical model of turbulence", Academic press, London.

[43] Launder, B.E. and Spalding, D.B. (1974) " The numerical computation of turbulent flows", Comp. Methods in App. Mech. and Engr., vol. 3, P. 269-289.

[44] Laneville, A., Gartshore, I. S. and Parkinson, G.V. (1975) "An explanation of some effects of turbulence on bluff bodies", Proceedings of the 4th International Conference on Wind Effects on Buildings and Structures, London, U.K., P. 333-341.

[45] Lee, B.E. (1975) "The effect of turbulence on the surface pressure field of a square prism", Journal of Fluid Mechanics, vol. 69, P. 263-282.

[46] Leonard, B.P., Leschziner, M.A. and Mcguirk, J. (1978) "Third-order finite difference method for steady two-dimensional convection", In Numerical Methods in Laminar and Turbulent Flow (ed. C. Taylor, K. Morgan asnd C.A. Brebbia), P. 807-819, Wiley.

[47] Leonard, B.P. (1979) "A stable and accurate convective modeling procedure based on quadratic upstream interpolation", Comp. Meth. Appl. Mech. and Engng, vol. 19, P. 59-98.

[48] Lawson, T.V. (1980) "Wind effects on buildings", vol. 1, Applied Science Publisher Ltd., London.

[49] Luo, S.C. and Teng, T.C. (1990) "Aerodynamic forces on a square section cylinder that is down-stream to an identical cylinder", Aeronautical Journal, P. 203-212.

[50] Mclaren, F.G., Sherratt, A.F.C. and Morton, A.S. (1969) "Effect of the free stream turbulence on drag coefficient of bluff sharp edged cylinders", Nature, vol. 224, no.5222, P. 908-909.

[52] Mair, W. A. and Maull, D. J. (1971) "Bluff bodies and vortex shedding-a report on Euromech 17", J. Fluid Mech., vol. 45, P. 209-224.

[53] Modi, V.J. and El-Sherbiny, S. (1975) "Wall confinement effect on bluff bodies in turbulent flows", Proceedings of the 4th International Conference on Wind Effects on Buildings and Structures, London, U.K., P. 121-132.

[54]   Mandal, A.C. (1979) "A study of wind effects on square cylinders", M.Sc. Thesis (ME Deptt.), BUET.

[55]   Mandal, A.C. and Islam, O. (1980) "A study of wind effect on a group of square cylinders with variable longtudinal spacings", Mechanical Engineering Research Bulletin, vol. 3 no. 1.

[56]   Mandal, A.C. and Islam, O. (1981) "Study of wind effect on a group of square cylinders with variable transverse and longitudinal spacings", Journal of the Institution of Engineers, Bangladesh, vol. 9, no. 1.

[57]   Matsumoto, M. "The dynamical forces acting on the vibrating square prism in a steady Flow", Proceedings of the 3rd International Conference on Wind Effects on Buildings and Structures, Tokyo, Japan, p. 921-930.

[58]   Masanori, H. and Sakurai, A. (1986) "Wake interfarence of a row of normal flat plates arranged side by side in a uniform flow", Journal of Fluid Mechanics, vol. 164, P. 1-25.

[59]   Naudascher, E.(ed.) (1974) "Flow-induced structural vibrations" Springer.

[60]   Nakamura, Y. and Ohya, Y. (1983) "The effects of turbulence on the mean flow past square rods", Journal of Fluid Mechanics, vol. 137, P. 331-345.

[61]   Nakamura, Y. and Ohya, Y. (1986) "Vortex shedding from square prism in smooth and turbulent flows", Journal of Fluid Mechanics, vol. 164, P.77-89.

[62]   Nakamura, Y. and Matsukawa, T. (1987) "Vortex excitation of rectangular cylinders with a long side normal to the flow", Journal of Fluid Mechanics, vol. 180, P. 171-191.

[63]   Newberry, C.W. " The measurements of wind pressures on tall buildings and structures", Proceedings of the 1st International Conference on Wind Effects of Buildings and Structures, Teddington, U.K., p. 113-149.

[64]   Okajima, A. (1979) "Flow around two tandem circular cylinders at very high Reynolds numbers", Bulletine of the JSME, vol. 22, no. 166, P.504-511.

[65]   Okajima, A. (1982) "Strouhal numbers of rectangular cylinders", Journal of Fluid Mechanics, vol. 123, P. 379-398.

[66]   Okajima, A. (1988) "Numerical simulation of flow around rectangular cylinders", Journal of Wind Engineering, No. 37, P. 281-290.

[67]   Ohaya, Y., Okajima, A.and Hayashi, M.(1990) "Ed.,wake interfarence and vortex shedding",Encyclopedina of Fluid Mechanics, (ed.NP Cheremisinoff), Gulf Publishing Co., vol.8, Ch.10, P.323-388.

[68] Parkinson, G.V. and Modi, V.J. (1967) "Recent research on wind effects on bluff two-dimensional bodies", Proceedings of International Research Seminar, Wind Effects on Buildings and Structures, Ottowa, Canada, P. 485-514.

[69] Pocha, J.J. (1971) " Ph.D. thesis", Department of Aeronautical Engineering, Queen Mery College.

[70] Patanker, S.V. and Spalding, D.B. (1972) "A calculation procedure for heat, mass & momentum transfer in three-dimensional parabolic flows", Int. J. Heat Mass Transfer, vol. 15, P. 787. (Also, Imperial College, BL/TN/A/45-1971)

[71] Pope, S.B. and Whitelaw, J.H. (1976) "The calculation of near-wake flows", J. Fluids Mech. vol. 73, P. 9.

[72] Patanker, S.V. (1980) "Numerical Heat Transfer and Fluid Flow".

[73] Roshko, A. (1961) "Experiments on the flow past a circular cylinder at very high Renolds number", Journal of Fluid Mechanics, vol.10, P. 345-356.

[74] Roberson, J.A., Lin, Chi Yu, Rutherford, G.S. (1972) "Turbulence effects on drag of sharp-edged bodies", Journal of Hydraulics Division, vol. 98, no. HY7, P. 1187-1201.

[75] Roberson, J. A., Crowe, C. T., Tseng, R. (1975) "Pressure distribution on two and three dimensional models at small angle of attack in turbulent flow", Proceedings of the 2nd U.S.National Conference on Wind Engineering Research, P.22-25, Colorado.

[76] Rockwell, D.O. (1977) "Organized fluctuations due to flow past a square cross section cylinder", Trans. ASMEI, J. Fluids Engng., vol. 99, P. 511-516.

[77] Sovran, G., Morel, T. and Mason, W.T.(eds.) (1978) "Aerodynamic drag mechanisms of bluff bodies and road vehicles", Plenum.

[78] Swanson. J.C. and Spaulding, M.L. (1978) "Three-dimensional numerical model of vortex shedding from a circular cylinder", In Nonsteady Fluid Dynamics (ed. D.E. Crow and J.A. Miller), ASME book no. H00118, P. 207-216.

[79] Sakamoto, H. and Arie, M. (1983) "Vortex shedding from a rectangular prism and a circular cylinder placed vertically in turbulent boundery layer", Journal of Fluid Mechanics, vol.126, P. 147-165.

[80] Sakamoto, H., Haniu, H. and Bata, Y. (1987) "Fluctuating forces acting on two square prisms in tandem arrangements", Journal of Wind Engineering and Industrial Aerodynamics, vol. 26, no. 1, P. 85-103.

[81] Sakamoto, H. and Haniu, H. (1988) "Effect of free-stream turbulence on characteristics of fluctuating forces acting on two square prism in tandem arrangement", Trans ASME Journal of Fluids Engineering, vol. 110, P. 110-145.

[82] Thoman, D. and Szewezyk, A.A. (1969) "Time dependent viscous flow over a circular cylinder", Phys. Fluids Suppl.,II-76-II-87.

[83] Vickery, B.J. (1966) "Fluctuating lift and drag on a long cylinder of square cross-section in a smooth and in a turbulent stream", Journal of Fluid Mechanics, vol. 25, part.3, P. 481-491.

[84] Whitbread, R.E. (1963) "Model simulation wind effects on structures", Proceedings of the 1st International Conference on Wind Effects on Buildings and Structures, Teddington, U.K., P. 283-301.

[85] Wyngaard, J.C., Arya, S.P.S and Cote, O.R. (1974) "Some aspects of the structure of convective planetary boundary layers", J. Atmos. Sci., vol. 31, P. 747.

[86] Wilkinson, R.H., Chaplin, J.R. and Shaw, T.L. (1974) "On the correlation of dynamic pressures on the surface of a prismatic bluff body", In Flow-Induced Structural Vibrations (ed. E. Naudascher), P. 471-487, Springer.

[87] Wiren, B.G. (1975) "A wind tunnel study of wind velocities in passages between and through buildings", Proceedings of the 4th International Conference on Wind Effects on Buildings and Structures, London, U.K., P. 465-475.

[88] West, G.S. and Apelt, C.J. (1981) "The effects of wind tunnel blockage and aspect ratio on the mean flow past a circular cylinder with Reynolds number between 10^4 to 10^5 ", Journal of Fluid Mechanics, vol. 13.

[89] Williamson, C.H.K. (1985) "Evolution of a single wake behind a pair of bluff bodies", Journal of Fluid Mechanics, vol.159, P.1-18.

[90] Zdravkovich, M.M. (1968) "Smoke observation of the wake of a group of three cylinders at low Renolds number", Journal of Fluid Mechanics, vol. 322, P. 339-351.

[91] Zdravkovich, M.M. (1977) "Review of flow interference between circular cylinders in various arrangements", ASME Journal of Fluids Engineering, vol. 99. no. 4, P. 618-633.

DISCRETIZED EQUATIONS

General momentum equations:

The standard control volume for the x-momentum discretization equation is shown in figure (A.1).
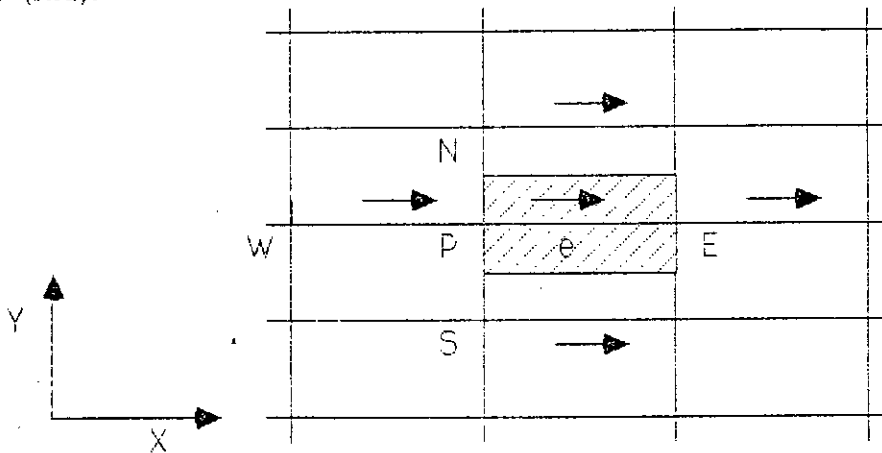

Fig. A.1 : Control volume for U

The resulting discretization equation for U_e can be written as :

$$a_e U_e = \Sigma(a_{nb} U_{nb}) + b + (P_p - P_E)A_e \qquad (A.1)$$

Where the neighbour coefficients a_{nb} account for the combined convection diffusion influence at the control volume faces and the U neighbours U_{nb} are shown outside the control volume. The term $(P_p - P_E)A_e$ is the pressure force acting on the U control volume, A_e being the area on which the pressure difference acts i.e. for two dimension, A_e will be $\Delta y x 1$.

Figure (A.2) shown the control-volume for the V-momentum equation and the discretization equation for V_n can be written as :

$$a_n V_n = \Sigma(a_{nb} V_{nb}) + b + (P_p - P_N)A_n \qquad (A.2)$$

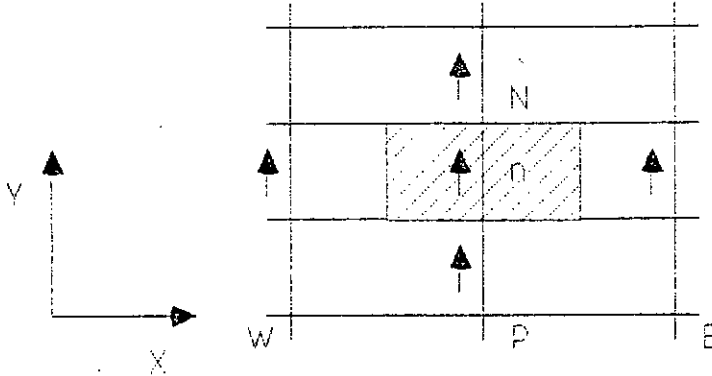Where $(P_p - P_N)A_n$ is the appropiate pressure force.

Fig. A.2 : Control volume for V

The momentum equations can be solved only when the pressure field is known or is somehow estimated. Unless the correct pressure field is employed, the resulting velocity field will not satisfy the continuity equations. Such an imperfect velocity field based on a guessed pressure field P^* will be denoted by U^*, V^*. This "starred" velocity field will results from the solution of the following discretization equations :

$$a_e U_e^* = \Sigma(a_{nb} U_{nb}^*) + b + (P_p^* - P_E^*)A_e \qquad (A.3)$$

$$a_n V_n^* = \Sigma(a_{nb} V_{nb}^*) + b + (P_p^* - P_N^*)A_n \qquad (A.4)$$

The pressure and velocity corrections:

The main objective is to improve the guesses pressure P^* such that the resulting "starred" velocity field will progressively get closser to satisfying the continuity

equation. Let the corrected pressure P is obtained from the follwing relation:

$$P = P^* + P^/ \tag{A.5}$$

where $P^/$ is the pressure correction. The corresponding velocity corrections $U^/$, $V^/$ can be introduced as :

$$U = U^* + U^/ \; ; \quad V = V^* + V^/ \tag{A.6}$$

Substituting (A.3) from (A.1), we have

$$a_e U_e^/ = \Sigma(a_{nb} U_{nb}^/) + (P_P^/ - P_E^/) A_e \tag{A.7}$$

Dropping the term $\Sigma a_{nb} U_{nb}^/$ from the equation (A.7) for computational convenience, then the equation (A.7) becomes

$$a_e U_e^/ = (P_P^/ - P_E^/) A_e \tag{A.8}$$

$$U_e^/ = d_e(P_P^/ - P_E^/) \tag{A.9}$$

where $d_e = A_e/a_e$

Equation (A.9) is the velocity correction formula. Hence the corrected velocity equation becomes :

$$U_e = U_e^* + d_e(P_P^/ - P_E^/) \tag{A.10}$$

Similarly we can write

$$V_n = V_n^* + d_n(P_P^/ - P_N^/) \tag{A.11}$$

Again the pressure correction equations can be obtained from the continuity equation.

The continuity equation is (for steady state)

$$\partial(\rho U)/\partial x + \partial(\rho V)/\partial y = 0 \qquad (A.12)$$

The integrated form of equation (A.12) becomes :

$$[(\rho U)_e - (\rho U)_w]\Delta y \Delta z + [(\rho V)_n - (\rho V)_s]\Delta x \Delta z = 0 \qquad (A.13)$$

Substituting the velocity components from equation (A.10)-(A.11), the descretization equation becomes for P' :

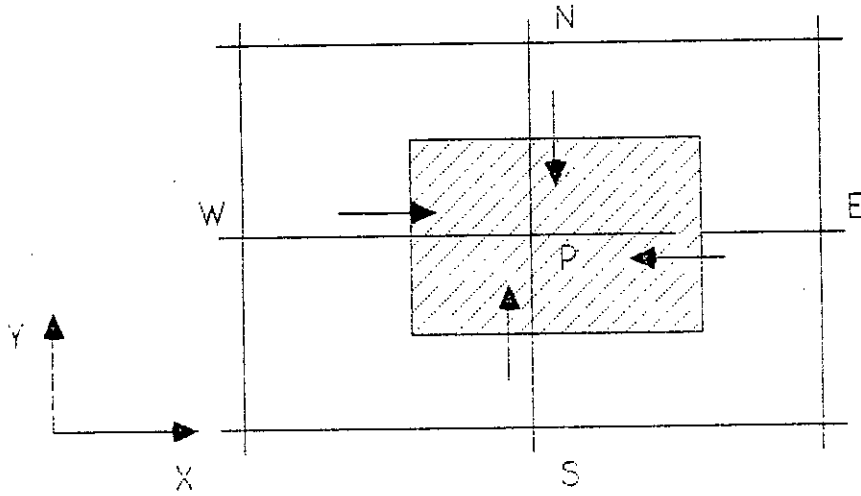$$a_P P_P' = a_E P_E' + a_W P_W' + a_N P_N' + a_S P_S' + b \qquad (A.14$$

Fig. A.3 : Control volume for continuity equation
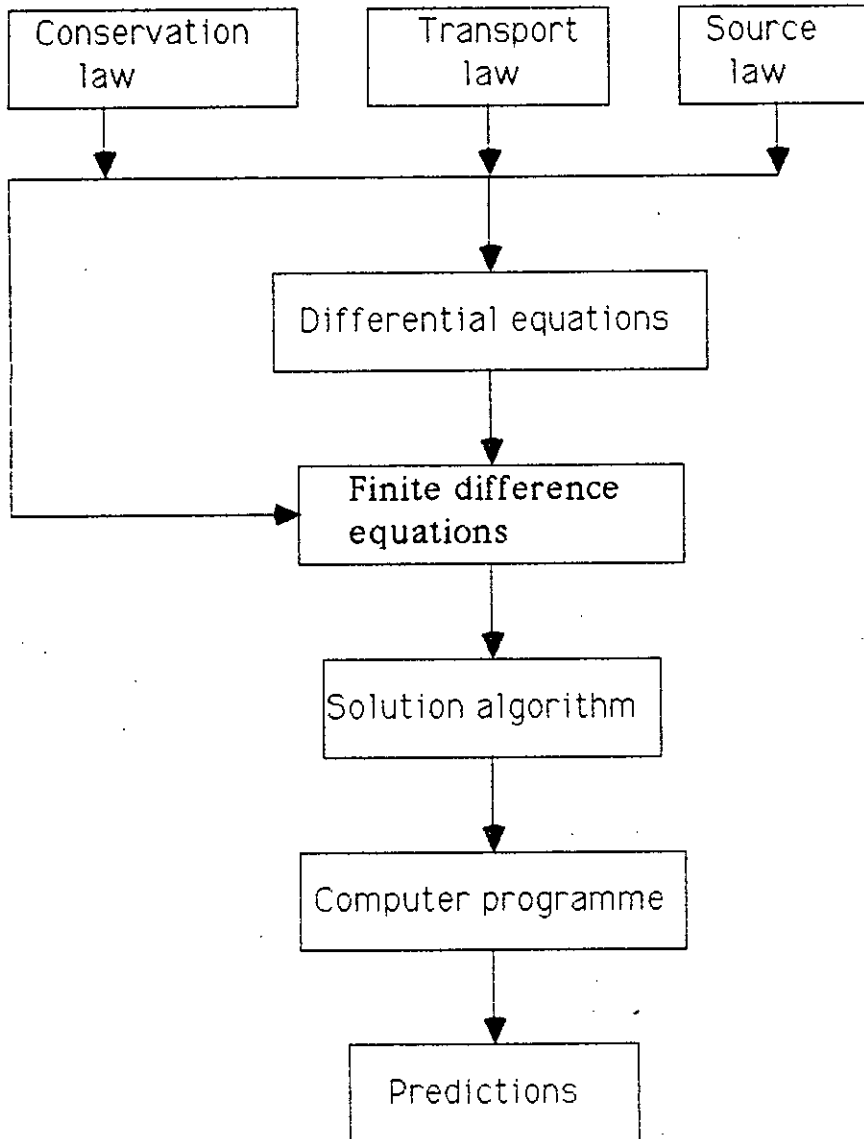
APPENDIX – B

SOLUTION PROCEDURE

For the calculation of the flow field, the algorithm used in the entire solution is SIMPLE (Semi-Implicit Method for Pressure-Linked Equations). The important operations, in the order of their executions are :

(1)   Guess the pressure field P^*

(2)   Solve the momentum equations to obtain U^*, V^*

(3)   Solve the $P^/$ equation

(4)   Calculate P by adding $P^/$ to P^*

(5)   Calculate U, V from their starred values using the velocity-correction formula

(6)   Solve the discretization equation for other variables (such as turbulence quantities) if they influence the flow field through fluid properties, source term etc.

(7)   Treat the corrected pressure P as a new guessd pressure P^*, return to step (2) and repeat the whole procedure until a converged solution is obtained.

APPENDIX - C

Structure of the Mathematical foundation

APPENDIX – D

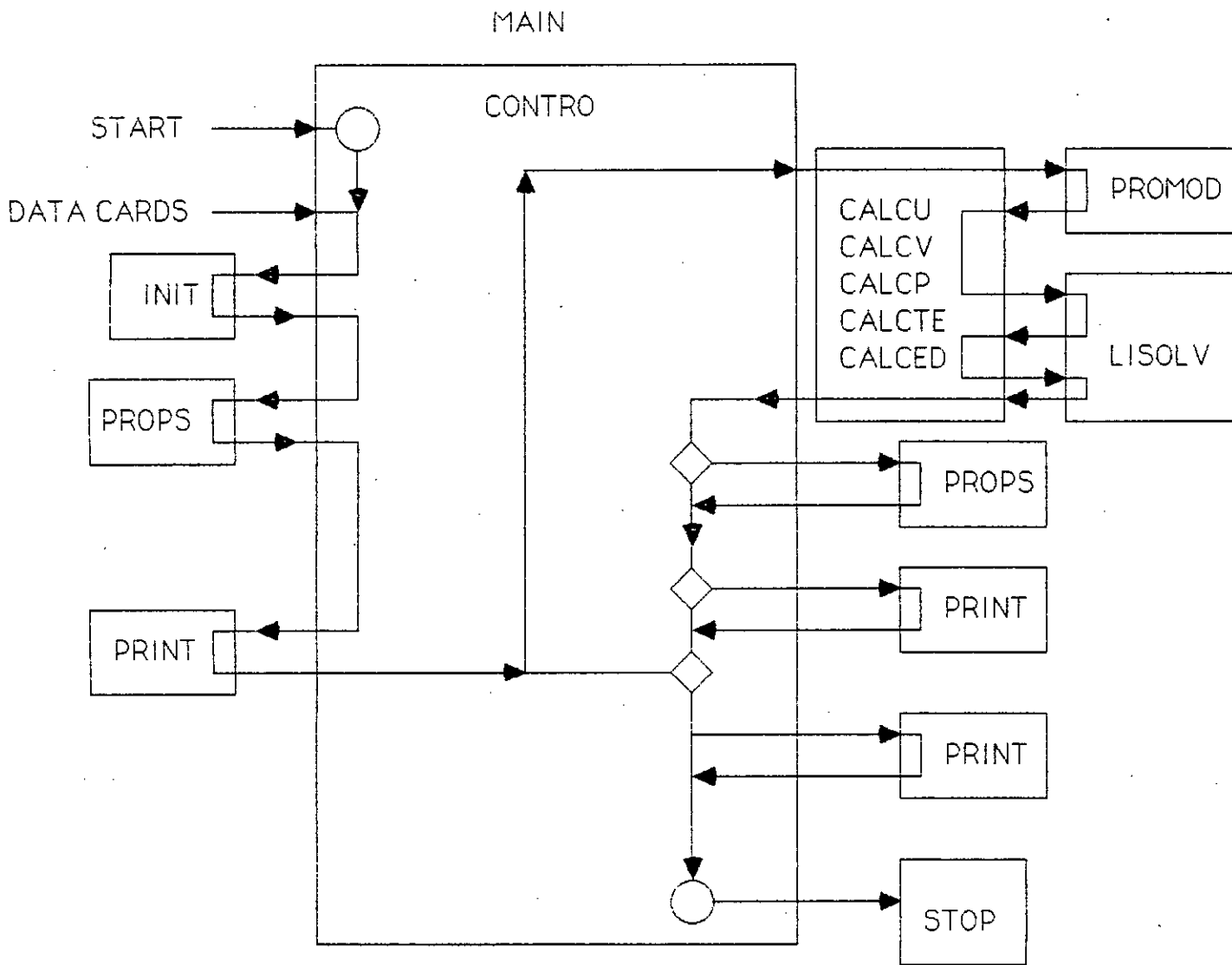## The overall structure of TEACH – T

TABLE 4.1

THE CONSERVATION EQUATIONS

Equations \Cofficients	ϕ	$\Gamma\phi$	$S\phi$
Mass	1	0	0
U - Momentum	U	μ	$-\dfrac{\partial P}{\partial x}+\dfrac{\partial}{\partial x}(\mu_t\dfrac{\partial U}{\partial x})+\dfrac{\partial}{\partial y}(\mu_t\dfrac{\partial U}{\partial y})$
V - Momentum	V	μ	$-\dfrac{\partial P}{\partial y}+\dfrac{\partial}{\partial x}(\mu_t\dfrac{\partial V}{\partial x})+\dfrac{\partial}{\partial y}(\mu_t\dfrac{\partial V}{\partial y})$
Turbulent kinetic energy	k	$\mu_{eff}/\sigma k$	$G-\rho\in$
Dissipation rate of energy	$\in$	$\mu_{eff}/\sigma\in$	$\in/k\,[\,c_{\in1}\,G\,-c_{\in2}\in\rho\,]$

TABLE 5.1

Authors	Cylinder size	Turbulent intensity	Reynolds number	C_D
Present prediction	50mm x 50mm	3%	2.87×10^4	1.46
Mosharaf 1991	50mm x 50mm	0.17%	6.05×10^4	2.33
A.C.Mondal 1975	30mm x 30mm	0.4%	5.46×10^4	2.10
B.E.Lee 1975	165mmx165mm	4.4%	1.76×10^5	1.99
B.E.Lee 1975	165mmx165mm	12.5%	1.76×10^5	1.53
Davis & Moore 1982	–	0.05%	250 1000	1.77 2.05

5.1 Variation of drag co-efficient of the present prediction with other researchers at various Reynolds number with different turbulent intensity.